Rehabilitation of One-Way Slabs Using Pre-stressed Concrete Prisms

by

Saeed Gerami

A Thesis submitted to the Faculty of Graduate Studies of

The University of Manitoba

in partial fulfilment of the requirements of the degree of

MASTER OF SCIENCE

Department of Civil Engineering

University of Manitoba

Winnipeg

This page intentionally left blank

Abstract

The main objective of this research study is to investigate the performance and efficiency of steel pre-stressed concrete prisms (PCPs) as strengthening material for reinforced concrete one-way slabs under both service and ultimate load levels. Six 3000 mm long, 600 mm wide and 200 mm deep one-way slabs were cast at the University of Manitoba's structures lab. The slabs were tested under monotonically increasing load till cracking, and then rehabilitated with PCPs. The rehabilitated slabs were consequently tested until failure. It was concluded that PCPs performed satisfactorily in this rehabilitation scheme by arresting the existing cracks. Overall, available pre-stress force in the PCPs reduced the crack width and deflection of the slabs.

Acknowledgements

I would like to acknowledge the guidance provided by my advisor, Dr. Dagmar Svecova throughout my graduate research. Her insight and support were most valuable. I would also like to acknowledge my dear brother Hamid who helped me through the whole research process especially at the structures lab.

I thankfully appreciate the W.R. McQuade Structures Laboratory technical staff, Dr. Chad Klowak, Mr. Brendan Pachal and Mr. Grant Whiteside for their efforts throughout the course of this project.

Help of fellow graduate students and friends, especially Mr. Shervin Khalili Ghomi, Mr. Rushang Kumar Dave, Ms. Sarah Boila and Mrs. Maha Ghaib is greatly appreciated.

I also need to express my gratitude to my friends Sarah Stevenson, Matthew Lynch and David Amorim. Thanks for all the warm memories you guys made for me in #A244.

This page intentionally left blank

This Thesis is dedicated to

My Mother Marzieh Jannat

A strong and gentle queen who taught me to trust in myself, believe in hard work and that so much could be done with little

My Father Ali Gerami

For earning and honest living for us and for supporting and encouraging me to believe in myself

My Brothers Hamid and Hamed

Brother, a person who is there when you need him, someone who picks you up when you fall, a person who sticks up for you when no one else will, a brother is always a friend

My Wife

She lends her pen

to thought of him

that flow from it

in her solitary

For she is his poet

and he is her poetry

Thank you all

This page intentionally left blank

Table of Contents

List of Figures

List of Tables

Chapter 1

Introduction

1.1 General

Regardless of their nature, whether they are made of concrete or steel, all structures are susceptible to environmental effects and increased loads due to traffic. This is a common issue among all aging structures around the world. The most important concerns for engineers are thus to improve durability and lifespan, as well as reduce maintenance costs. Maintenance includes all aspects required to keep a structure performing satisfactorily, in terms of load-carrying capacity, serviceability and durability. Low-quality maintenance will naturally lead to greater and quicker degradation. Reinforced concrete structures are designed and constructed to serve during their service life for almost 75 years which justifies the time and cost required during the construction process. Over time, however, their load-carrying capacity, performance, and use may be changed. As a result, reinforced structures are often required to undergo rehabilitation and strengthening.

Due to the sheer number of concrete structures worldwide, the demand for repairing and strengthening outdated structures is increasing. It is not always applicable and economical to substitute a current failing or dysfunctional structure with a new one. Therefore, engineers and researchers are always looking for the most appropriate methods for retrofitting structures. Sometimes, strengthening an existing structure can be more complex compared with the construction of a new one, since structural elements are already in place. In addition, weak joints

that need to be rehabilitated are often not accessible. Some of the traditional strengthening techniques to improve performance of concrete structures during their service life are as follows (Carolin 2003, Nordin 2003):

- Application of overlays
- Increasing the number of supports to reach shorter spans for flexural members
- Shotcrete and post-tensioning
- Using external steel / FRP plates

The most feasible strengthening methods for existing concrete structures are externally bonded reinforcement (EBR) and near surface mounted (NSM) reinforcement. In EBR, steel or fiber-reinforced polymer (FRP) plates, bars, laminates, or strips are bonded to the external surface of a compromised concrete member to enhance both shear and flexural capacity. The main obstacle to using EBR is the appearance of premature failure, which shows itself as debonding failure in longitudinal laminates and delamination. On the other hand, when steel is used for strengthening, the corrosion of externally bonded materials can be another barrier to the application of this method, since the strengthening system will lose efficiency. These insufficiencies may not permit a structural element to develop its ultimate flexural capacity (Hawileh, R.A. et al., 2014). Furthermore, in EBR systems, externally bonded materials are exposed to thermal, environmental, and mechanical destruction. To eliminate these prevalent difficulties with EBR mechanisms, the NSM technique was developed, and used for the first time in Finland in 1940s to strengthen a bridge deck slab (Asplund, S, 1949). In NSM, FRP and steel bars or straps are embedded in surrounding concrete to protect against thermal, environmental and mechanical damage. Other advantages of NSM method include improved durability and more optimized stress-sharing mechanism and fatigue performance. Grooves are sawed in concrete elements at a depth that would

inhibit any damage to the main internal flexural reinforcements. After the grooves are cleaned, epoxy is injected into them before the installation of the NSM, which involves steel or FRP products, or pre-stressed concrete prisms (PCPs). PCPs are a combination of high strength concrete and reinforcement bars that are pre-tensioned by steel or FRP tendons. After placing the PCPs, the grooves are again filled with epoxy, and supplementary epoxy is aligned with the surface of concrete. In this way, the PCP is protected by epoxy throughout the coverage area of the concrete element. NSM can also be used for strengthening of negative moment areas, where steel or FRP plates are bonded on the top surface of concrete members and thus threatened by corrosion; PCPs can also be ideal for this technique. In addition, unlike EBR, NSM grooves do not require to be manufactured before installation.

1.2 Problem Definition

Cracking is inevitable in concrete and happens as a result of its low tensile strength when subjected to load. Generally, reinforced concrete structures experience some cracking under service load except for cracking due to shrinkage and temperature changes (Piyasena 2002). When loads higher than service loads are applied, visible and wider cracks start to be appeared. Large cracks affect aesthetics of structure and stimulate adverse criticism. When this occurs, steel reinforcement inside concrete members is at risk of corrosion, and the concrete can delaminate at the location of the reinforcement. In addition, flexural stiffness of reinforced concrete members reduces which will lead to excessive deflection. Reinforced concrete slabs designed to stay under traffic at service load even with very limited cracking.

When concrete is subjected to harsh weather and chemicals, it starts to rapidly deteriorate. When this occurs, steel reinforcement inside concrete members is at risk of corrosion, and the concrete

can become delaminated at the location of the reinforcement. Due to additional volume resulting from rust formation on the surface of the steel reinforcement, cracking and spalling of concrete may occur. Almost 30 percent of the bridges in the United States (581,000) suffer from structural deficiencies that had affected their performance (US DOT, 1997). The majority of these bridges are conventionally reinforced or pre-stressed concrete structures that need rehabilitation to be able to serve traffic during their service life. The situation is similar in the United Kingdom, with more than 10,000 concrete bridges needing retrofitting. Overall, the European Union's department of transportation expects total annual budget of $600 million to repair concrete structures due to internal reinforcement corrosion (Tann and Delpark, 1999). In Canada, strengthening only concrete garages will require $6 billion (Benmokrane and Wang, 2001) while rehabilitation of bridges with poor physical condition requires $11 billion. (Canadian Infrastructure Report, 2016).

1.3 Objectives and Scope

The main objective of this research study is to investigate the performance and efficiency of steel PCPs for repair of cracked reinforced concrete one-way slabs. The effect of using these prisms on serviceability behavior of reinforced concrete slabs, specifically deflection and crack width will be of main relevance to the findings of this research.

The scope of the present research is restricted to the short-term behavior of one-way slabs rehabilitated with steel PCP under monotonic loading. There will be two main variables in the program: the size and pre-stressing level of the prisms.

1.4 Outline of The Thesis

This thesis is divided to five chapters as follows:

Chapter One - Introduction

- Introduction of the research project, in addition to classification of study program objectives and scope

Chapter Two - Literature Review:

- Literature Review conducted on the strengthening of concrete structures by application of PCP, as well as the mechanical properties of High Strength Concrete (HSC)

Chapter Three - Research Program:

- Representation of test specifications and instrumentation
- Details of test schemes and setup

Chapter Four - Experimental Results and Analysis:

- Experimental results of the behavior of one-way slabs rehabilitated with PCPs
- Discussion of experimental results and data analysis

Chapter Five - Summary, Conclusion and Future Recommendations:

- Summary of the research program
- Conclusions
- Recommendations for future work

Chapter 2

Literature Review

This chapter provides an overview of the literature review on topics related to the current project. Specifically, a historical background of strengthening and rehabilitation of concrete structures, pre-stressed high-strength concrete prisms, and the mechanical properties of high-strength concrete (HSC) will be discussed.

2.1 Introduction

Steel reinforced concrete slabs are common for short span bridges. Primarily, cracking is the most critical factor that affects bridge deck durability. Although the problem has been studied substantially in the past, cracking remains of importance in old and new concrete bridges alike. Cracks appear in bridge decks due to different reasons such as cyclic loading of passed vehicles. Crack spacing and width both are affected by concrete area around the rebar and size of steel reinforcement (Soltani et al. 2013). A total of 71 newly constructed concrete bridge decks were inspected for Utah Department of Transportation (Linford and Reaveley, 2004). They state that 70 of the 71 bridges suffered from various cracking. In their report, bridges were ranked according to a Cracking Severity Index Number (CSIN). They reported the prevalence of 87% of diagonal cracking near abutments. Transverse cracking due to shrinkage was found on 67% of bridges while only 11% of bridges experienced longitudinal cracking. Cracking is a crucial issue that has to be

addressed prior to initiating serious consequences. They provide avenues for detrimental and corrosive materials to enter concrete, which deteriorate steel reinforcements.

According to previous research studies use of near surface mounted PCP has the potential to improve the serviceability of structures, and reduce susceptibility to corrosion (Bishara and Almeida, 1970, Bishara et al., 1971, Mawal, 1979 Chen and Nawy, 1994, Nawy and Chen, 1998, Svecova and Razaqprur, 2000).

2.2 Classification of Cracks in Reinforced Concrete Members

Cracks in reinforced concrete member are classified in three categories:

- Cracks dependent on applied loads:
    - Flexural cracks
    - Inclined shear cracks
- Cracks independent of loading:
    - Plastic shrinkage
    - Autogenous shrinkage
    - Drying shrinkage
    - Thermally induced shrinkage
- Cracks according to orientation:
    - Transverse cracks
    - Longitudinal cracks
    - Diagonal cracks
    - Map or pattern cracks

Cracks due to loading and oriented cracks are two more prevalent types of cracks which might occur in a concrete bridge deck (NCHRP Synthesis 333, 2004).

2.2.1 Longitudinal Cracks

These types of cracks are along the longitudinal axis of the bridge deck. They mostly will be created due to restrained shrinkage, inadequate structural design or construction details (Frosch et al., 2002). Schmitt and Darwin (1995) reported that longitudinal cracks mainly happen on solid and hollow bridge decks. On the other hand, (Curtis and White, 2007) proposed that these types of cracks possibly will develop in the area close to steel stringer beams.

2.2.2 Transverse Cracks

Transverse cracks are principal kind of cracking in any concrete bridge deck. They are roughly perpendicular to the longitudinal axis of bridge deck. They usually appear during the first days after casting. According to (Ramey et al., 1997), transverse cracks arise mostly after setting and widen during time. They cover whole depth of bridge deck and are located each 3-10 feet (Krauss and Rogalla, 1996). The main factor in case of transverse cracks is their location which is responsible for service life and maintenance cost. They facilitate penetration of detrimental chemical materials to the steel reinforcement inside the bridge deck since they occur usually above transverse bars.

2.2.3 Diagonal Cracks

Diagonal cracking ordinarily is found under sharp angles especially in skewed bridge decks (Fu et al., 2007). The most important reason for formation of diagonal cracking is restraint which is provided by abutments and piers. Shrinkage on the other hand can also be a factor.

2.2.4 Map or Pattern Cracks

This type of cracking generally initiates at the bottom of the deck moving towards deck surface (Curtis and White, 2007). Inappropriate curing after casting is the primary factor that causes map pattern cracking. Comparing to other kinds of cracking, they would be narrower. (Schmitt and Darwin, 1995) announced that map pattern cracking does not have significant effects on the bridge durability while they lead to delamination and concrete spalling.

2.2.5 Flexural Cracks

When applied tensile stresses in tension zone overpass the tensile flexural capacity of concrete, a flexural cracks emerge and propagate in flexural members like beams and slabs. Generally, it will be presumed that cracks distribute between tension face and location of neutral axis of the cross-section. The most impressive way to restrict crack widths within the allowable values is to control the strain of steel reinforcements. The other main factors that affect flexural crack widths are concrete cover, dimension of steel reinforcement and distribution of steel bars in tension zone.

2.3 Crack Width

Crack width under service load should satisfy allowable limits suggested by national codes to minimize their detrimental effect on reinforced concrete structures. The cracking of conventional RC slabs does not affect the appearance of the structure and leads to corrosion of embedded steel reinforcements. Table 2-1 provides permissible crack width based on the environmental condition according to ACI 224 report.

Table 2-1 Permissible Crack Width in Reinforced Concrete Member (ACI 224R-01)

Environment Condition	**Permissible Crack width (mm)**
Dry Air	0.41
Humidity	0.3
Deicing Chemicals	0.18
Sea Water	0.15
Water Retaining Structures	0.15

It should be noted that values in Table 2-1 are not definitive and engineers are highly recommended to account for their judgment and experience as well.

Both CSA A23.3-14 and ACI 318 proposed the following equation (Eq. 2-1) which is known as Gergely-Lutz approach to estimate maximum crack width on the tension face of a reinforced concrete member (Ralph J, et al. (2003)):

$$w_{max} = 11 f_s \beta \sqrt[3]{d_c A} \times 10^{-6} \qquad \text{Eq. (2-1)}$$

Where:

w_{max} = maximum crack width (mm)

f_s = stress in the reinforcement at specified load (MPa)

$$\beta = \frac{\text{distance from neutral axis to extreme tension fibre}}{\text{distance from neutral axis to the center of tensile reinforcement}} \text{ (mm)}$$

d_c = concrete cover (mm)

A = effective tension area of concrete surrounding the flexural tension reinforcement and having the same centroid as the reinforcement, divided by the number of bars (mm^2)

Another well-known crack width predictive equation was suggested by Kaar-Mattock which is expressed in Eq. 2-2. Like Gergely-Lutz equation, Kaar and Mattock developed their crack width relationship according to statistical analysis of experimental data. It predicts width of flexural cracks at the tension face of a reinforced concrete flexural member as:

$$w_{max} = 11.5\, f_s \beta \sqrt[4]{A} \times 10^{-4} \qquad \text{Eq. (2-2)}$$

Frosch discovered that Gergely-Lutz and Kaar-mattock equations considerably have shortcoming to predict crack width of reinforced concrete section due to the fact that they are based on statistical analysis on experimental data. Indeed, he noticed that only three test specimens had concrete cover greater than 66 mm. Therefore, Frosch developed the following simple equation (Eq. 2-3) for anticipation of crack width regardless of the value of concrete cover:

$$w_{max} = 2\frac{f_s}{E_s}\beta\sqrt{(d_c)^2 + \left(\frac{s}{2}\right)^2} \qquad \text{Eq. (2-3)}$$

Where:

s = reinforcement bar spacing (mm)

E_s = modulus of elasticity of steel reinforcement (MPa)

AASHTO endorsed Gergely-Lutz model for controlling flexural cracking but in a slightly rearranged form. The crack width factor w_{max} and β were merged into a single q-factor and equation was written in terms of allowable stress. Using an approximate limiting crack width of

0.041 mm and an average β factor of 1.2 resulted in the current equation found in the AASHTO LRFD specifications as Eq. 2-4:

$$f_{sa} = \frac{q}{\sqrt[3]{d_c A}} \leq 0.6 f_y \qquad \text{Eq. (2-4)}$$

Where:

f_{sa} = allowable reinforcement stress (MPa)

f_y = yield strength of steel reinforcement (MPa)

q = 170 for moderate exposure conditions,

= 130 for severe exposure conditions,

= 100 for precast box culverts,

= $\frac{155}{\beta}$ for cast-in-place box culverts

On the other hand, CSA A23.3-14 does not require crack width calculation directly. In other words, similar to AASHTO, CSA postulates the so-called z parameter to be restricted to specified values to comply with crack width limitations under various conditions. Eq. 2-5 indicates z parameter provided in CSA A23.3-14 as follows:

$$z = f_s (d_c A)^{1/3} \qquad \text{Eq. (2-5)}$$

Where z is a quantity that limits the distribution and amount of flexural reinforcement. CSA recommends that z should not exceed 30 000 N/mm for interior exposure and 25000 N/mm for exterior exposure.

In addition, CEB-FIP recommended the following equation for anticipation of average crack width at any load level from product of the strain in reinforcement and average crack spacing:

$$w_m = \frac{\Delta_m}{n} = \varepsilon_{sm} s_m \qquad \text{Eq. (2-6)}$$

Where:

w_m = average crack width

Δ_m = elongation of the member after first cracking

n = number of cracks

ε_{sm} = average strain in reinforcement

s_m = average crack spacing

Moreover, CEB-FIP proposed Eq. 2-7 for average crack spacing (s_m) as follows:

$$s_m = 2\left(c + \frac{s}{10}\right) + k_1 k_2 \left(\frac{d_b}{\rho_{eff}}\right) \qquad \text{Eq. (2-7)}$$

Where:

c = concrete cover

s = reinforcement spacing

d_b = bar diameter

ρ_{eff} = effective reinforcement ratio

k_1 = coefficient account for bond properties = $\frac{f_{cr}}{\tau_{ave}}$

k_2 = coefficient account for distribution of strain across the section equal to 0.25 for pure tension

f_{cr} = tensile strength of the concrete

τ_{ave} = average bond stress

2.4 Rehabilitation Techniques for Concrete Decks and Slabs

2.4.1 Introduction

Structural elements of a bridge are exposed to fatigue, wear and tear from vehicular loads during service life. Some other factors such as overloading and exposure to harsh environmental conditions will also contribute to their destruction. Post-tensioned bridges may suffer from loss of pre-stressing force over time, leading to lower load carrying capacity of the damaged member. Moreover, poor quality of construction process and lack of proper maintenance are the two most important factors that lead to major rehabilitation of bridges. Typically, deficiencies in concrete structures are revealed as excessive deflection, cracking-spalling of concrete and corrosion of steel reinforcements. It should be noted that bridge rehabilitation process includes restoration of numerous problems and there is no single method to propose a complete solution. Hence, addressing each problem individually with the most convenient method will result in a quality retrofit.

2.4.2 Historical Background

Research throughout the last few decades have been trying to find an optimized method for strengthening concrete structures and extending their service life. Because of the many financial restrictions for most rehabilitation projects, this goal has proven to be very challenging. Klaiber

classified various strengthening procedures in his research, such as external pre-stressing, injection methods, shot concrete, hand-applied repairs with concrete mortar, and the application of different concrete castings (Klaiber et al. (1987)).

Beginning in the mid-1960s, due to financial concerns, the most popular technique for retrofitting concrete was the utilization of external materials as an attachment to cracked members. The bonding of steel plates to concrete with epoxy or anchors is one of the most common methods. The installation of steel plates to concrete using epoxy has been a common repair method for the last 30 years, despite advancements in technology (Beber et al., 2001). The first use of external steel plates as a reinforcement for concrete beams was conducted in France by L'Hermite and Bressson (1967). This method received widespread use by other researchers around the world in Japan (Raithby, 1980), United Kingdom (Jones et al., 1988), Israel (Lerchental, 1967), Sweden (Taljsten, 1994), Switzerland (Lander, 1983), United States (Klaiber et al., 1987), Germany (Kaiser, 1989) and Australia (Palmer, 1979). In addition, simulated lab-scale specimens of externally bonded steel plates on site in Belgium were tested by Van Gemert (1980). Similar to the previous small-scale project, Brosens and Van Gemert carried out a strengthening project on a concrete bridge deck above the Nete Canal in Lier, Belgium (Brosens and Van Gemert, 2001).

Although this method has limitations in field applications due to the weight of the steel plates, it demonstrates a quite solid technical performance. However it has been shown in literature that a common problem can occur: corrosion on the interface between the steel and epoxy (He et al., 1997). To help provide a better bond mechanism between the steel and concrete, it is recommended by manufacturers to exert external pressure on the plate during the epoxy curing period. Moreover, apart from the high cost of steel products worldwide, high stiffness is the leading issue that makes steel an unsuitable strengthening material for some applications, such as for curved surfaces.

Considering the above-mentioned reasons, engineers and researchers have been investigating the application of new materials, specifically non-metallic composite materials, as an alternative to steel.

2.4.3 Reinforced / Pre-stressed Concrete Bridges

The techniques for rehabilitation of reinforced concrete members and reinforced concrete bridge decks are approximately similar. Table 2-2 provides different rehabilitation and repair methods of bridge decks. In addition to all proposed solutions, external post-tensioning and FRP retrofit may also be suitable for pre-stressed concrete structures.

Table 2-2 Different Repair and Strengthening Techniques of Concrete Bridge Decks

Repair Techniques	➢ Crack injection with low viscosity epoxy ➢ Patch repair with polymer modified mortar ➢ Patch repair with non-shrink grout
Rehabilitation Techniques	➢ Steel plate bonding ➢ Steel plate bonding ➢ FRP (strengthening) ➢ External Post-Tensioning ➢ Near Surface Mounted techniques (NSM)

2.4.3.1 Steel Plate Bonding

In this technique, a steel plate with a specified thickness will be bonded with adhesives and anchored to the existing concrete member to improve stiffness and strength. Steel plates enhance the moment of inertia of the composite cross section (concrete-steel) however, they operate as

externally bonded reinforcement as well. This method is more effective to boost flexural and shear capacity of bending members such as beams and slabs and compression capacity of columns.

Steel plate technique requires a really hard process like hacking and drilling of the current concrete member. Moreover, steel plates are heavy to lift and need to be anchored properly on the member. On the other hand, steel plates are in threat of corrosion over time and final surface finish in not pleasant.

2.4.3.2 FRP Strengthening

A Fiber Reinforced Polymer (FRP) is made of high strength fibers and a matrix. The three most common types of FRPs are manufactured using Aramid, Carbon and Glass fibers. FRPs can be bonded to the external surface of the deficient concrete member to improve its shear, flexural and compressive capacity. The FRP materials for the purpose of structural strengthening are produced in three forms consisting of *wet lay-up* (fibre sheets or fabric saturated in site), *pre-preg* (pre-impregnated fibre sheets of fabrics off site) and *pre-cured* (composite sheets and shapes manufactured off-site). Table 2-3 provides mechanical properties of different types of FRP systems.

Table 2-3 Typical Mechanical Properties of FRP Laminates (Yogesh Chhabra, 2004)

FRP System	**Tensile Strength (MPa)**	**Elastic Modulus (GPa)**	**Ultimate Elongation (%)**
Aramid + Epoxy (High performance)	700-1725	48-68	2.0-3.0
Carbon + Epoxy (High Strength)	1025-2075	100-145	1.0-1.5
E-Glass + Epoxy	525-1400	20-40	1.5-3.0

Utilizing FRP strengthening to rehabilitate reinforced and pre-stressed concrete structures unlike steel plates bonding is a quick and neat technique with a pleasant final surface finish. Furthermore, it offers better strength to self-weight ratio in comparison with steel plates and will not corrode.

2.4.3.3 External Post-Tensioning

Loss in pre-stress force might happen due to different reason during the service life of a pre-stressed concrete member. Post-tensioned bridges can be strengthened with external post-tensioning method to offset for pre-stress loss or increase in wheel load. In this strengthening technique, pre-stressing tendons are positioned on the external surface of the concrete member, anchored at the ends and post-tensioning force will be applied using a hydraulic jack. This method is quite effective however, it requires adequate reserved strength in current concrete member to transfer pre-stress force. On the other hand, pre-stressed tendons and anchorages need proper protection system against corrosion.

2.4.3.4 Near Surface Mounted Techniques (NSM)

The NSM technique was initially introduced in the 1940s in Lapland, Finland, where it was selected as a retrofitting method to strengthen a concrete bridge deck at the negative bending moment (Asplund, 1949). In this project, steel bars were located in the grooves in the top concrete cover, which was exposed to the negative bending moment and bonded with cement grout. Steel bars can also be externally fastened to concrete members with shotcrete. One of the drawbacks for these types of repairing methods is the difficulty maintaining a sufficient bond between strengthening materials and original structure. During the 1960s, the production of high quality adhesives for construction industry advanced this method substantially by placing steel bars internally in the sawed grooves in the concrete cover. However, to prevent corrosion issues that threaten steel reinforcement, an additional concrete cover is required for protection. Various studies have proven that the utilization of NSM steel bars has not shown to offer better performance, compared with FRP-NSM (Shehab Monir SOLIMAN, 2008). Obstacles such as corrosion are eliminated when FRPs are implemented using NSM, which meet the requirements for having a thick concrete cover.

In contrast to the externally bonded (EB) FRP method, NSM-FRP system protects reinforcement bars in the concrete cover from environmental conditions. In addition, both methods can be combined together in a specific layout with a desired concrete cover for grooves. By contrast, slots in NSM do not need any surface preparation, which facilitates the execution of this method. To prevent debonding in NSM, bars can be anchored to the adjacent member. Applying a pre-stress force using NSM is more effortless than with EB, which improve workability of the former method. In addition, NSM will not change the aesthetic features of concrete structural members,

as a cover would be applied over top of the reinforcements. Thus, based on these advantages, NSM method is preferred over EB.

In practice, the following steps are taken to comply with the NSM method (Sika Canada 2006):

1. Cutting the groove with a concrete saw
2. Adding the adhesive material to the groove
3. Locate the strengthening reinforcement in the groove
4. Apply additional adhesive to fill the groove

2.5 Pre-stressed High-Strength Concrete Prisms

Pre-stressed concrete prisms (PCPs) are high strength concrete rectangular members concentrically pre-tensioned by steel or FRP tendons. A common model of pre-stressed concrete prism is presented in Figure 2-1.

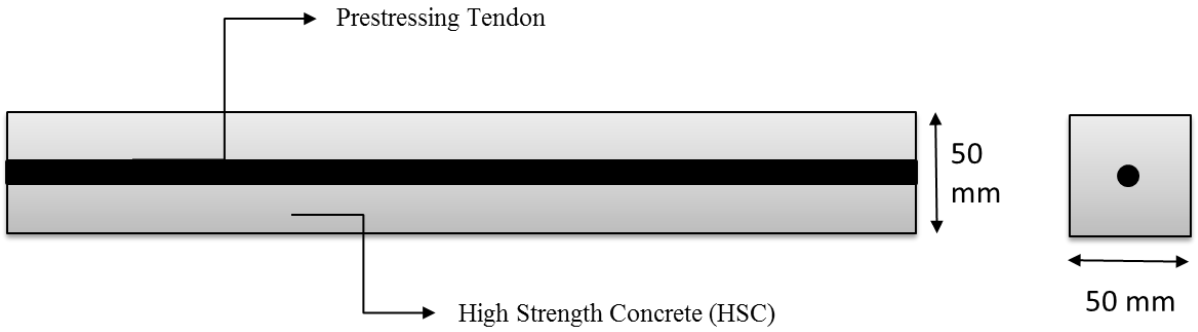

Figure 2-1 Pre-stressed Concrete Prism (PCP)

To prevent any camber or cracking under pre-stressing load, the tendons are to be located at the center of the prisms to minimize the effects of eccentricity. On the other hand, high-strength concrete is used to provide sufficient tensile capacity against high forces at the time of pre-stressing release.

2.5.1 Steel Pre-Stressed Concrete Prisms

Steel PCPs are the most widely used form of prisms, and have been developed over 60 years ago. They were used as reinforcements for concrete pavements in Germany (Dyckerhoff and Widman (1963)), or for strengthening water-storage tanks (Mikhailov (1958)). Hoppe compared the behavior of conventional concrete, pre-stressed concrete, and PCP reinforced concrete (Hoppe 1963).

The bond connection between concrete and pre-stressed prisms was examined by (Evans and Parker (1955)). They found that if the joint location between concrete and PCPs is rough enough, an adequate bond connection would be achieved to prevent any slippage. Additionally, cracks are more prone to appear in reinforced and pre-stressed concrete than PCP reinforced concrete. Similarly Ozell found good bond mechanism between pre-stressed prisms and cast-in-place concrete to tolerate all shear forces before cracking load (Ozell (1957)). Both studies specified rough surface between PCP surfaces and cast-in-place concrete as a requirement for a sufficient bond mechanism and monolithic action. Additionally, Ozell presumed following assumptions (Ozell (1957)):

- Elastic behavior would be valid for composite sections
- The actual and theoretical moment of inertia are equal
- Deflection can be calculated based on theoretical moment of inertia

Steel pre-stressed prisms were implemented by Mikhailov for the first time as reinforcement for water-storage tanks (Mikhailov 1958). He reported late formation of cracks in PCP reinforced tanks with a slow spread rate of cracks. He also confirmed that cracks started to get wider after strain of about 0.0003 in concrete, and deformation initiated after the failure of PCPs.

Evans and Kong (1964) perceived maximum tensile strain of 0.0001 for concrete before the beginning of cracks, while on the other hand (Kajfasz and Rowe (1961)) reported high strain value of 0.0004 in the concrete beam reinforced with PCPs. Pre-stressed concrete prisms have the ability to be implemented as different types of reinforcement with various performances. Hoppe (1963) classified the application of PCPs as a longitudinal reinforcement in pre-stressed concrete pressure pipes, as a vertical reinforcement for tanks, and as a transverse reinforcement for roads and floors. He cast 2.75-meter-long prisms with a 50-mm^2 cross-section (for an entire length of 39,624 meters) in the mid-1960s as a longitudinal reinforcement for pre-stressed pressure pipes.

Another research study was done by Burns on continuous slabs using 50 x 50 mm pre-stressed prisms for strengthening slabs under negative moment and improving cracking patterns (Burns (1966)). Different kinds of specimens were reinforced with bars, PCPs and combination of the two. Those slabs reinforced solely with PCPs cracked only when load went over 50% of the ultimate capacity. In addition, their collapse mechanism was a complete formation of fully plastic joints under individual positive and negative moments. He also mentioned that after unloading, the cracks closed and there were no symptoms of serious deflection. They thus concluded that pre-stressed concrete prisms are able to reduce the level of cracking in concrete structures by a significant rate.

Hanson (1969) compared the cracking behavior of seven T-beams with three different cross sections reinforced with deformed bars, a combination of bars and PCP, and a combination of bars and pre-stressed steel. All seven beams were tested at the center support under a negative bending moment. He observed that the negative bending moment increased in specimens with pre-stressed concrete prisms, before the formation of cracks. The flexural behavior changed after the appearance of the initial cracks and applied moments resulted in slender cracks. On the other hand,

beams reinforced with PCPs demonstrated better deflection behavior compared with the other specimens. The majority of research studies conformed that the general application of PCPs and direct prestressing has similar effects. The bond mechanism between concrete prisms and beams was acceptable, and no bond failure was reported by (Hanson (1969)).

Bishara and Almeida (1970) tested groups of rectangular simply supported beams to study their serviceability and ultimate capacity. The beams were reinforced with different sets of steel reinforcement and PCPs. The prisms had a 38x68 mm cross-section and a length of 3280 mm. Since the prisms were pre-tensioned, stronger concrete with a strength of 58.6 MPa was used to test against releasing force, compared to the beam's concrete with a strength of between 42 to 44.5 MPa. All beams experienced the same load level for cracking; the only difference assigned to the beams with PCPs was that the cracks were shorter compared to others. Moreover, beams with PCPs benefitted from a smaller maximum crack width and fewer cracks overall. However, beams with PCPs at ultimate load level had a larger maximum crack width. According to their test results, the implementation of PCPs in tension areas as a reinforcement can affect flexural rigidity. Cracks started to close when the load was removed, and an overall reduction in deflection was observed after the concrete cracked under the same load level, compared to the beam without PCPs. On the other hand, PCP-reinforced beams had lower ultimate compressive strain, curvature, and total hinge rotation. They did not report any bond failure among PCP and in-situ concrete for beams.

Bishara et al. (1971) compared flexural rigidity, crack behavior and development, moment redistribution and plastic hinge rotation in rectangular continuous beams with two equal spans of 4.5 m reinforced with PCPs and steel bars. The beams differed in terms of their tension reinforcement ratio, which is determined either by the PCPs or steel bars. The PCP-reinforced beams performance was better than the steel-reinforced beams, which demonstrated more narrow

cracks. Further, the cracks did not exceed the PCPs level. Beams with a higher rate of PCPs experienced smaller rate of deflection, and considering non-prestressed reinforcement in the section also will support this action. The failure pattern for all beams was the crushing of concrete, which confirms a sufficient rotational capacity for all beams for full moment redistribution. Due to the almost full action of moment redistribution in PCP-reinforced beams over intermediate support, their ultimate moment capacity decreased by 40%. Moreover, by increasing the number of PCPs, the total ultimate rotational capacity decreased. Bishara et al. (1971) deduced that implementing PCPs as reinforcement will lead to higher performance of beams under service load without affecting moment redistribution capacity.

Another research study was performed by Mirza et al. (1971) on the performance of simply supported beams strengthened with PCPs under static and fatigue loads. A total number of nineteen beams were analyzed, two under static loading, nine under fatigue loading less than cracking load of PCPs, and eight under fatigue loading over the cracking load of PCPs. The standard concrete strength of 37 MPa was used for the 50x50 mm prisms in the study. Nearly 1 million cycles of loading were carried out on the beams without any sign of fatigue or failure for loading value less than $0.7P_{cr}$ ($\text{almost } 0.3\ P_u$). However, fatigue failure occurred before 1 million loading cycles for loads between $1.7P_{cr}\ to\ 2.0P_{cr}$. At the load equal to beam cracking, beam stiffness did not change, while at the load equal to the cracking for prisms, stiffness decreased. Mirza et al. (1971) reported that the advantage of substituting steel reinforcements with PCPs to keep continuity is a 52% higher cracking moment capacity.

Zia et al. (1976) used PCPs with 50x75 mm cross-sections, with a compressive strength of 42 MPa to 55 MPa in simply supported and continuous T-beams to determine their static and fatigue performance. T-beams were reinforced with three PCPs and two number-15 steel bars as tensile

reinforcement in their flange area. During testing under fatigue loading, for less than cracking loads they did not report any failure, even after 1 million loading cycles. They also reported nearly 35% of moment redistribution for continuous beams under static loading. As well, by using a combination of steel bars and pre-stressed prisms, the endurance limit was increased to $1\ P_{cr}$, compared to the $0.7\ P_{cr}$ when PCPs are only used. They mentioned that beams reinforced only with PCPs demonstrated less deflection and narrower crack width under similar loading conditions, compared to specimens reinforced solely with steel bars. The only factor that affected flexural rigidity of beams was cracking of prisms, which lead to lower level of rigidity, while cracking of in-situ concrete did not change stiffness of beams. The main difference between the static and fatigue tests was the issue of cracking, as beams under fatigue loading developed one major crack, whereas those under static loading conditions displayed uniformly smaller and distributed crack patterns.

Chen and Nawy (1994) worked on thirteen rectangular simply supported beams reinforced with prisms. Both beams and prisms were cast with high-strength concrete with a compressive strength of 84.4 to 98.5 MPa. The prisms were 38.1x76.2 mm, 38.1x101.6 mm and 76.2x76.2 mm, and pre-stressed with one 9.5 mm steel strand; the last set had a cross-section of 114.3x76.2 mm with two 9.5 mm steel strands. Although conventional concrete-reinforced beams have a trilinear load-deflection behavior, PCP-reinforced beams indicated a bilinear performance. Therefore, PCP-reinforced beams did not present any deviation from the original slope in their diagram. The bilinear behavior increased cracking moment capacity and flexural rigidity. The cracking of prisms considerably changed the behavior of reinforced concrete beams: right after cracking, flexural cracks were distributed, which led to a lower flexural rigidity, and the load-deflection diagram experienced a substantial deviation in slope. Crack widths in PCP-reinforced beams meet the

conditions in ACI 318-02, while regular reinforced beams had wider cracks under identical loading conditions. Based on the final results, the application of prisms did not increase cracking capacity of beams, but the pre-stressing of prisms resulted in a higher cracking capacity compared to the concrete cover, which was proportional to prestressing level. They also reported a full plastic rotation capacity for all beams, accompanied by flexural failure without any sign of shear failure. The maximum compressive strains of 0.00305 to 0.00533 were recorded for beams, and the effective pre-stress level in steel tendons was a criterion which governed the reserve strength $\left(\frac{M_u}{M_y}\right)$ of the beams. In addition, higher effective pre-stress levels led to smaller reserve strengths.

Following their previous research study, Nawy and Chen (1998) studied the behavior of four continuous concrete T-beams under flexure, reinforced with steel pre-stressed prisms. All beams had a length of 5,791 mm, with two equal, separate spans of 2,743 mm. The prisms fit each span, since they were 2,743 mm long with 50x50 mm cross section. Both beams and prisms were cast with high-strength concrete with a strength variation of between 84 and 94 MPa, and 9.5 mm diameter steel strands with an upper capacity of 1862 MPa in the prisms. They were pre-stressed with 1200 MPa, with an approximate prestressing loss between 23% to 34%. Comparing results with simply supported beams under identical loading and testing conditions, cracking did not have a considerable effect on the flexural stiffness of T-beams, and the load-deflection curve confirmed the ductile behavior of the beams. According to the results, all four beams demonstrated full moment redistribution over loading points and interior support location with the full establishment of plastic hinges. Their findings supported earlier research results that PCPs postpones cracking in the flange region in the negative moment zone in the middle support. The flange area over the middle support cracked under higher load levels at faster rates, compared to the loading point locations after the cracking of PCPs. Furthermore, a non-linear relationship was detected between

the maximum crack width and applied load because of moment redistribution. The ultimate recorded compressive strain for concrete varied from 0.00461 to 0.00845, which was significantly higher than the value of 0.0035 recommended by the CSA A23.3-94. On the other hand, as proven in the same research study, an increase in the effective pre-stress level results in a decrease in ductility and reserve strength.

In the literature up to date PCP were never used to repair cracked reinforced concrete decks. Considering the effects of embedding the prisms in new structures, it is assumed that similar benefits will be associated with using PCP as repair material. This will be studied in this research.

2.6 Stress-Strain Relationship of PCP

This section provides information regarding the behavior of pre-stressed concrete prisms when they are subjected to axial loads. Figure 2-2 represents a conceptual model of a PCP under an axial load; as can be seen, strains derived from axial loads are distributed uniformly over the whole cross-section.

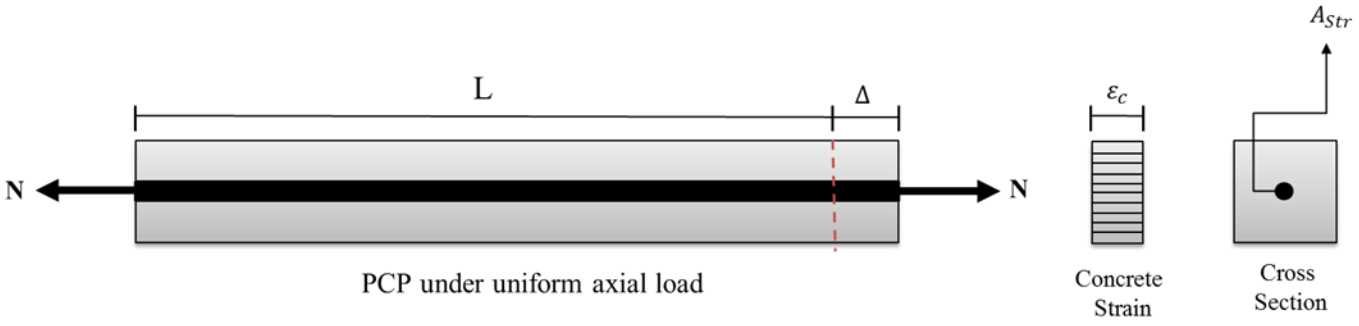

Figure 2-2 Pre-stressed Concrete Prisms Subjected to Axial Load

In this study 9-mm 7-wire strands with an ultimate tensile strength of 1860 MPa and modulus of elasticity of 190 GPa were used for pre-stressing the PCPs. Since high tensile strength for concrete is required to tolerate large pre-stressing force distributed over small cross-sectional area at release,

it is assumed that highly compressive concrete with a strength of 90 MPa is used for casting the PCPs. Prisms are presumed to have a cross-section of 50x50 mm to provide sufficient cover for the pre-stressed strand and prevent cracking when the pre-stress force is released. Finally, the load-strain relationship for the pre-stressing force of 20 kN is provided here in Figure 2-8. This pre-stressing rate applies a uniform stress of 8 MPa over the entire PCP cross-section.

Since PCP in this thesis works as a tension reinforcement, a positive branch is plotted in Figure 2-3.

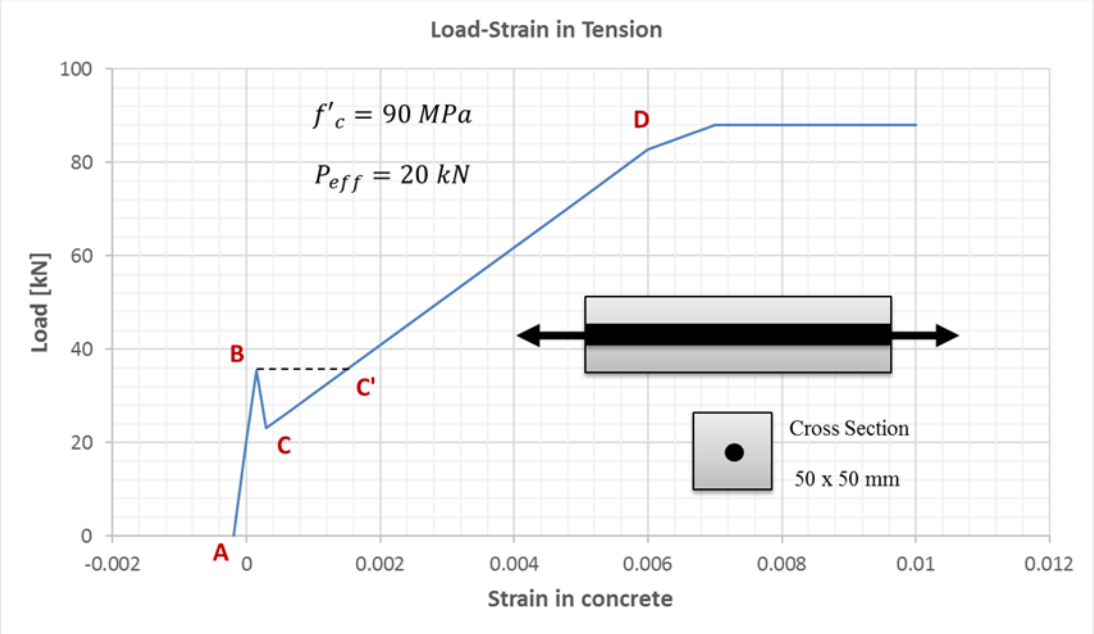

Figure 2-3 Load-Strain Relationship of PCP in Tension

It should be noted that commonly tensile strains and stresses would be assumed positive during the calculation for PCPs when exposed to axial loads. After releasing of prestressing force, the entire cross section of prism will rapidly be subjected to the uniform compressive strains. Moreover, it should be pointed out that the graph in Figure 2-3 only covers the short-term behavior

of the prisms. When the moment-curvature of beams reinforced with the prisms is calculated, the load-strain relationship of the prisms will be used.

As indicated in Figure 2-3, prisms have an elastic behavior before concrete cracking, as shown by line AB. The sudden jump at point B to point C demonstrates the cracking of the prism. If a load control tensile test was conducted on the prisms, the load would not represent a drop as shown; rather, the strain would increase sharply under the identical load level magnitude as plotted by dotted line BC'. It is important to remember that the main objective behind using PCPs is to prevent cracking under service loads. The cracking of prisms will not lead to a sudden failure of the PCP, since the internal steel strand will take over the tensile force due to the reserved strength still available in the pre-stressing tendon, as indicated by line CD in Figure 2-3. However, by increasing the applied axial load as it reaches the maximum tensile capacity of steel strand, failure is inevitable when internally applied strand ruptures (Point D). Throughout the test, the percentage difference between the ultimate load capacity and cracking load of pre-stressed concrete prisms might be considered as a safety margin.

There are several factors that affect the load-strain relationship of PCP and their axial stiffness (EA):

- Pre-stressing level
- Properties of the pre-stressed bar
- Concrete strength
- Stress-strain behavior of concrete in terms of tension and compression
- Concrete cover

Chapter 3

Research Program

3.1 Introduction

This study investigates the feasibility of using near surface mounted PCP as repair technique for cracked concrete bridge decks. This research study covers the construction and static testing of six one-way slabs pre-cracked and then retrofitted with near surface mounted PCPs.

3.2 Test Specimens

Six 3000 mm long, 600 mm wide and 200 mm deep one-way slabs and forty eight 2000 mm long PCPs were cast at the University of Manitoba's structures laboratory to study the effects of the presence of PCPs on arresting existing cracks in concrete slabs. The PCPs were 35 x 35 mm or 50 x 50 mm in cross section and were cast using high strength concrete. A pre-stressing load in the range of 30 kN to 45 kN was applied to the prisms at jacking. A detailed description of all cast and tested specimens is presented in the subsequent sections.

3.3 Pre-stressed Concrete Prisms (PCP)

3.3.1 Casting of the Prisms

The prisms were cast in two groups with the following cross-sectional dimensions: 35 x 35 mm and 50 x 50 mm. They were concentrically pre-stressed using one 9 mm diameter seven-wire steel strand. High-strength concrete (HSC) with an average compressive strength f'_c of 100 MPa was

used to cast the prisms, to diminish the possibility of cracks during the pre-stress release. A wooden formwork structure was built and installed on top of the flange of a W920x420 steel girder as a pre-stressing bed. The width of the girders was wide enough to accommodate two rows of prisms and also provided space for the pre-stressing of three specimens in a line, for total of six prisms per casting. It was ensured that steel bulkheads had adequate stiffness to tolerate the applied force. The application of the load throughout the pre-stressing process was monitored using a load cell, embedded between a hydraulic jack and the bulkhead and recording the strain gauges applied on the surface of the steel tendon. Load cell and strain gauge readings were tracked using strain indicator boxes.

A set of wooden plywood forms were attached to the bottom of pre-stressing bed, which were supported by a total of five threaded rods in each side. The rods were connected to the top surface of the steel girder by sets of bolts and nuts, which simplified the adjustment of the steel strand to the center of the prisms without any eccentricity. It is important that prisms are concentrically pre-stressed to avoid any camber that may interfere with placement of the elements in the slabs. For PCPs with 35 x 35 mm and 50 x 50 mm cross section L127x127x9.5 and L203x203x130, steel angles were assembled concentrically around the pre-stressed steel strand to create sides of the formwork. Figure 3-1 shows the pre-stressing bed details and dimensions, and Figure 3-2 outlines the pre-stressing setup.

During the pre-stressing process, elongation of the steels strand due to applied load was measured using a 2 mm strain gauge, which was attached to the surface of the steel strands and connected to a data acquisition (DAQ) system.

CSA A23.3-04 prescribes a maximum of $0.6f'_c$ as the permissible concrete stress in extreme fibre in compression, and a maximum of $0.8f_{pu}$ as the admissible tensile stress in prestressed steel

tendons at jacking. Therefore, the maximum theoretical allowable force for a seven-wire strand with an ultimate tensile strength of 1860 MPa is 82 kN. As a result, pre-stressing force of 35, 40 and 45 kN were applied to the prisms at jacking using a hydraulic jack. After pre-tensioning, the end points of the angles were marked, and remaining strain gauges were attached. High strength concrete was cast and cured for 14 days to provide sufficient time to develop tensile strength of the concrete before pre-stress release. The steel tendon was cut and effective forces after losses were 20, 25 and 30 kN.

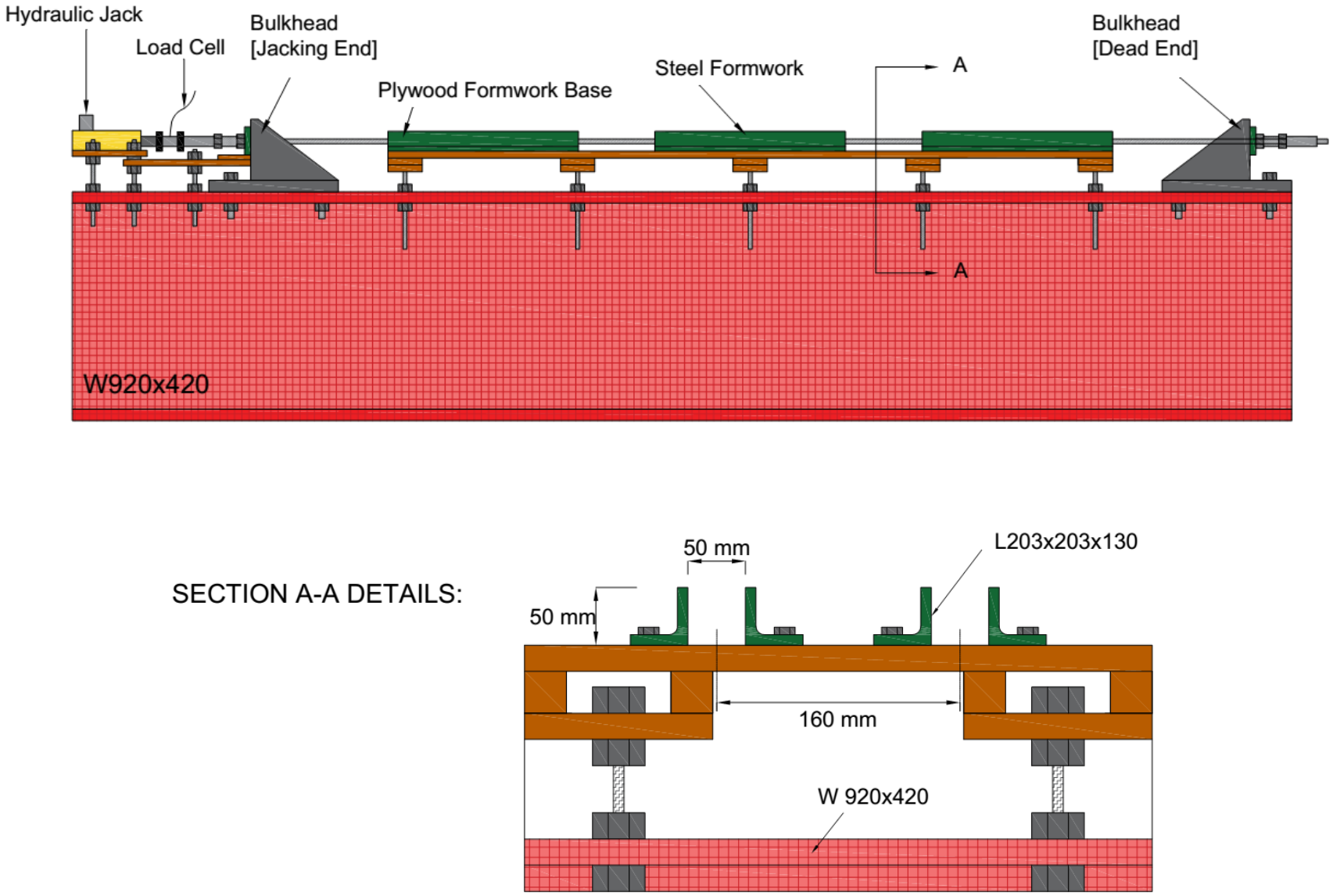

Figure 3-1 Pre-stressing Bed Details and Dimensions


Figure 3-2 Pre-stressing Setup

The 35 x 35mm prisms are referred to as small prisms (SP) and 50 x 50 mm prisms are referred to as large prisms (LP). The level of effective pre-stressing in the prisms is denoted at the end of the prism's nomenclature. For instance, a prism with 35 x 35 mm cross section and 20 kN effective pre-stressing force is named SP-PCP-20, and prism with 50 x 50 mm cross section and 30 kN effective pre-stressing force will be called LP-PCP-30, where the first two characters signify the dimension and the last two digits signify the effective pre-stressing force in the prisms. Table 3-1 presents comprehensive details of the prisms. Experimental and calculated pre-stress losses are tabulated in Table 3-2 in the following sections.

Table 3-1 Types of Pre-stressed Concrete Prisms (PCPs)

Batch No	**Prism**	**Jacking Load (kN)**	**Effective Pre-stress (P_{eff}) (kN)**	**f'c (MPa)**	**Length (mm)**	**Dimension (mm)**
1	SP-PCP-20	30	20	100	2000	35 x 35
2	SP-PCP-25	35	25	98		
3	SP-PCP-30	45	30	102		
4	LP-PCP-20	30	20	95		50 x 50
5	LP-PCP-25	35	25	104		
6	LP-PCP-30	45	30	98		

High tensile strength concrete with a minimum tensile strength of 6 MPa was used to prevent the PCP cover from splitting after release of pre-stressing. To keep track of tensile strength development over time, concrete cylinders were tested in compression and tension, at ages (3, 7, 14 and 28 days) after casting. Almost all cylinders reached a tensile strength of 6 MPa within a week. The pre-stressing force was released two weeks after casting the concrete. The load was released gradually by loosening the nuts and bolts attached between the steel chucks and bulkheads, not by cutting the steel strands, to prevent the application of a sudden high force on the PCPs. The releasing mechanism is displayed in Figure 3-3.

Figure 3-3 Pre-stress Release Mechanism

3.3.2 Pre-stress Losses

The loss throughout the application of pre-stress load and afterwards was tracked using strain gauges applied to the surface of the steel strands. A strain indicator was used to measure the strain until the testing of the slabs. Pre-stress losses were computed on the basis of CSA-S6-06 and compared to experimental values, as summarized in Table 3-2. The geometrical properties of the PCPs, such as the cross-section dimension and the diameter of the seven-wire steel strand, were used to calculate the pre-stressing loss levels, including short-term losses due to elastic shortening according to CSA-S6-06. Figure 3-4 displays a variation of strains versus time. From the strains shown in Figure 3-4 there is an evident drop in strain after the release of pre-stressing force, which is assumed to be elastic shortening.

Table 3-2 Estimated and Measured Pre-stress Losses in PCPs

Type of Loss	LP-PCP-20	LP-PCP-25	LP-PCP-30	SP-PCP-20	SP-PCP-25	SP-PCP-30
Elastic Shortening (ES) [MPa]	54.93	64.08	82.40	112.10	130.78	168.15
Short term Relaxation (REL1) [MPa]	1.43	1.43	1.43	1.43	1.43	1.43
Shrinkage (SH) [MPa]	43.50	43.50	43.50	43.50	43.50	43.50
Total (Theoretical) [MPa]	***99.86***	***109.01***	***127.33***	***157.03***	***175.71***	***213.08***
Total (Experimental) [MPa]	***84.20***	***157.70***	***186.90***	***111.20***	***159.10***	***226.6***
Experimental Pre-stress loss (%)	15.40	24.70	25.60	19.10	23.60	27.6

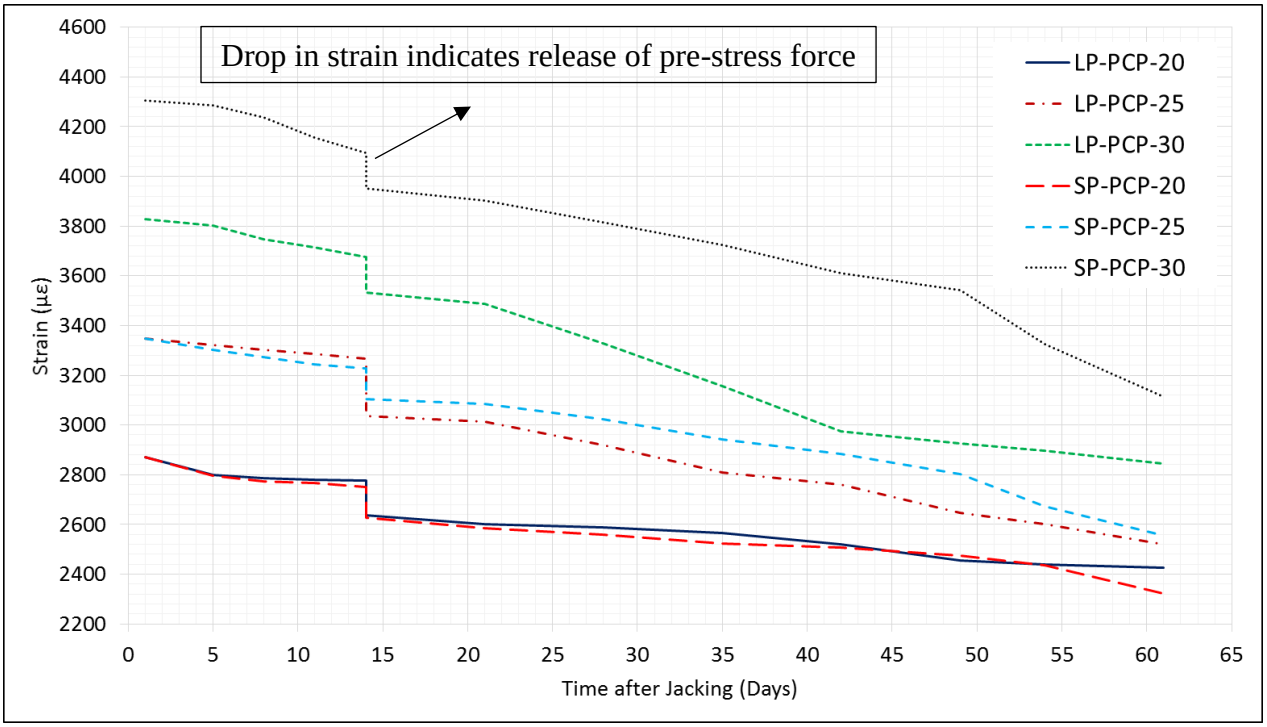

Figure 3-4 Pre-stress Losses in PCPs

3.4 Slabs Nomenclature

As mentioned above, three of the one-way slabs were reinforced with 35 x 35 mm PCPs, while three others were reinforced with 50 x 50 mm PCPs, with effective pre-stress forces of 20, 25 and 30 kN, respectively. All slabs had similar dimensions and geometry, with a total length and clear span lengths of 3,000 and 2,800 mm, respectively, and an effective depth of 132 mm. All six slabs were designed to have equal ultimate capacity before applying PCPs. Figures 3-5 and 3-6 display cross-section views of the PCP-repaired slabs. Table 3-3 provides the reinforcement details of the slabs. As could be seen reinforcement ratio due to application of steel strands increased about 27 % after rehabilitation which still less than balanced ratio of 3.44 %. The first two characters in the slab label identify the dimension of the PCPs installed in the slab. “SP” for small prisms (35 x 35 mm) and “LP” for large prisms (50 x 50 mm). The third character “S” stands for slab. Finally, the last two digits indicate level of effective pre-stress force in the prisms in kN. This naming convention resulted in six one-way slabs: SP-S-20, SP-S-25, SP-S-30, LP-S-20, LP-S-25 and LP-S-30.

To our knowledge, no research has been completed to date on using PCPs for concrete bridge deck or slab rehabilitation.

Table 3-3 Reinforcement Details of the Slabs before and after Rehabilitation

Specimen	28 days Concrete Strength (MPa)	Longitudinal Reinforcement	Transverse Reinforcement	$A_S(mm^2)$	$\rho_1(\%)$	$\rho_2(\%)$
SP-S-20	42	4 No 15	9 No 15	800	1.01	1.28
SP-S-25	44					
SP-S-30	45					
LP-S-20	41					
LP-S-25	42					
LP-S-30	43					

- $\rho_1(\%)$: Reinforcement ratio BEFORE rehabilitation
- $\rho_2(\%)$: Reinforcement ratio AFTER rehabilitation

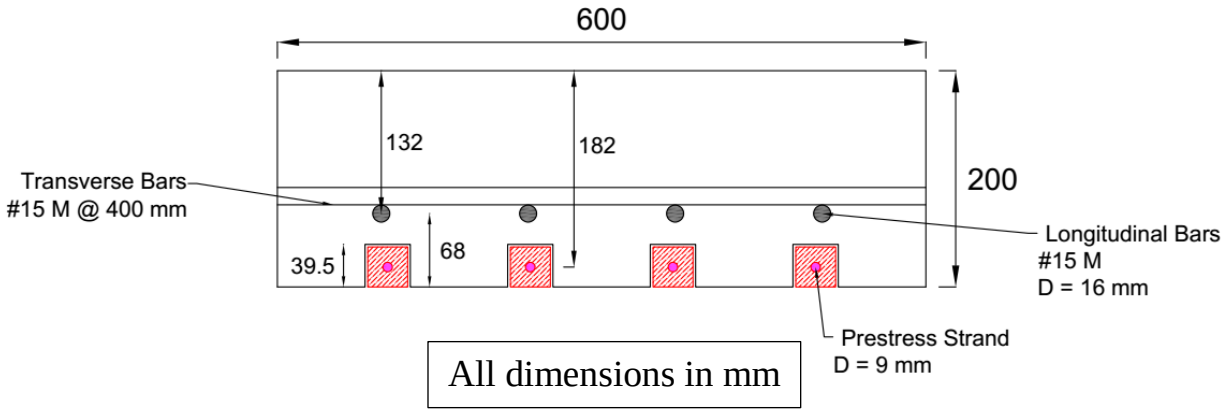

Figure 3-5 Cross-Section View of Slabs Repaired With 35 x 35 mm PCPs

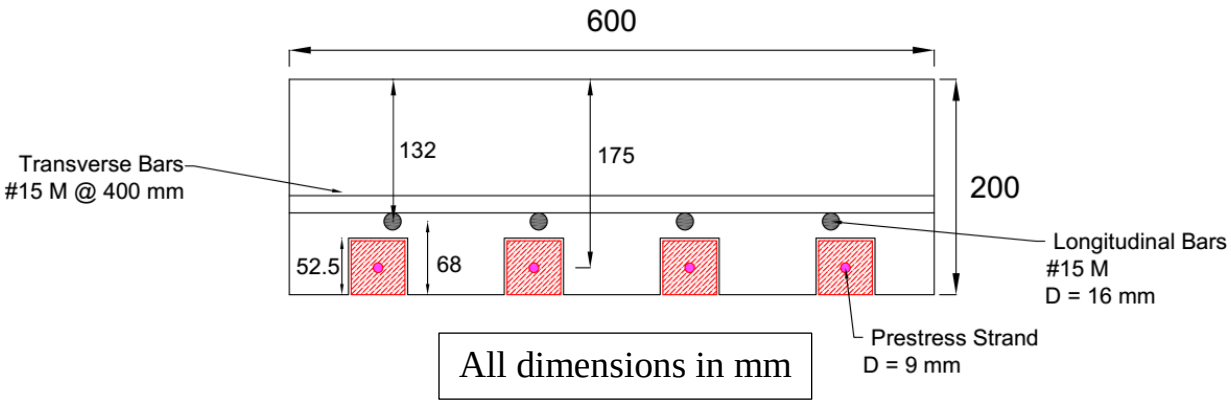

Figure 3-6 Cross-Section View of Slabs Repaired With 50 x 50 mm PCPs

3.5 Fabrication of the Slabs

Formwork and steel reinforcement cages were constructed and assembled prior to the casting of the slabs. Thereafter, surfaces were prepared on the steel bars to place strain gauges in desired locations, and steel reinforcement cages were positioned on plastic chairs inside the formwork, as shown in Figure 3-7. The inner surfaces of the formwork were coated with release agent to facilitate the removal of the plywood after the concrete was cast and cured. An electrical vibrator was used during the casting to enhance compaction. It was essential in this step to prevent concrete segregation due to extra compaction and prevent any damage to the strain gauges. A total of 50 cylinders with dimensions of 100 x 200 mm and 150 x 300 mm were cast using plastic molds; they were used to track the compressive and tensile strength development of the concrete, respectively. All cast slabs and cylinders were cured with burlap and plastic sheets to ensure the maximum compressive strength. Figure 3-8 illustrates the casting process of the slabs. A group of four

Styrofoam prisms was used for each slab to keep the location hollow for future insertion of the PCPs.

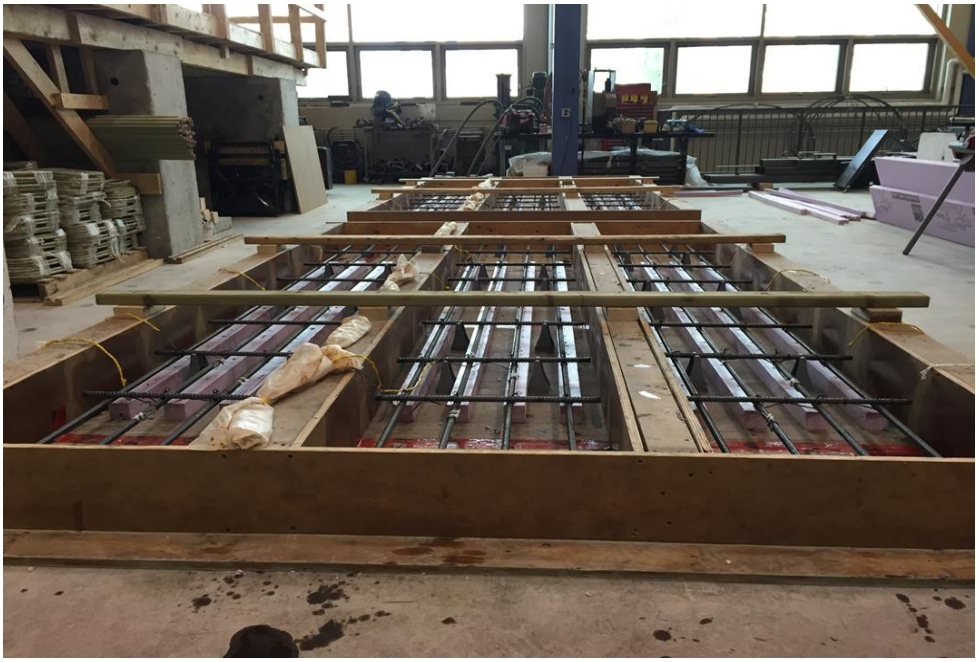

Figure 3-7 Positioning of Steel Reinforcement Grids in the Form Prior to Casting of Concrete

Figure 3-8 Casting of Slabs

3.6 Material Properties of Slabs

All six slabs were cast using ready-mixed, normal-strength concrete with a compressive strength of 40 MPa after 28 days. The maximum aggregate size was 10 mm to ensure all voids around the reinforcements were filled, and a slump of almost 150 mm was obtained during the casting for all slabs. Standard cylinder compressive tests were performed according to ASTM C39/C39M-14a on cylinders at 3, 7, 14 and 28 days after casting to track the progression of strength gain of the concrete. The average compressive strength varied between 41 and 45 MPa on the day of flexural testing, as shown in Table 3-3.

Grade 400 deformed steel bars with a modulus of elasticity of 200 GPa were used as longitudinal and transverse reinforcements for all six slabs. A total of three steel bars were tested according to

CSA/G30.18-09 to detect the mechanical properties of steel bars used in the specimens, and are summarized in Table 3-4.

Table 3-4 Mechanical Properties of Steel Reinforcements

Bar type	**Nominal Diameter (mm)**	**Area (mm^2)**	**Modulus of Elasticity (GPa)**	**Nominal Yield Strength (f_y) (MPa)**	**Experimental Yield Strength (f_y) (MPa)**	**Nominal Yield Strain (ε_y)**	**Experimental Yield Strain (ε_y)**
No. 15 M	16	200	200	400	460	0.002	0.0023

3.7 PCPs Material Properties

The seven-wire steel strand grade 1860 MPa with a nominal diameter of 9.53 mm (conforming to ASTM A416M-16 guidelines) was used to pre-stress the PCPs. Table 3-5 shows the published mechanical properties of the seven-wire strands used in this study.

Table 3-5 Mechanical Properties of the Seven-Wire Strands (ASTM-A416), (CSA G279)

Tendon type	**Grade (f_{pu}) (MPa)**	**Nominal Diameter (mm)**	**Nominal Area (mm^2)**	**Nominal Mass (g/m)**	**Yield Strength at 1.0% extension (kN)**	**Yield Strength at 1.0% extension (f_{py})(MPa)**
Seven wire strand	1860	9.53	55	432	92.1	1675

High-strength concrete was used to more effectively absorb forces during the releasing process, and increase the cracking load as well as the axial stiffness of PCPs. Subsequently, the higher tensile strength ensures that the stresses due to the lateral expansion during pre-stress release are not exceeded.

All PCPs were cast at the structural laboratory using an HSC mix that was prepared at the University of Manitoba using a mix design provided by PCA research and Development Bulletin RD104T (1992) and according to research by Berg and Ost (1994). The mix design features a high value of silica fume to minimize chloride permeability and water absorption, especially in environments that are susceptible to deterioration. Further, due to the low water-cement ratio, a High Range Water Reducer (HRWR) is required to improve the workability of concrete. In addition, to provide sufficient time for the casting of PCPs and maintain workability, a retarder was used in mix design. The mix design is listed in Table 3-6, which presents the dry weight of silica fume. The maximum size of aggregates in the mix was restricted to 10 mm to facilitate their placement between the pre-stressed strand and formwork.

The concrete was mixed using a 200-litre horizontal drum mixer. 100 x 200 mm and 150 x 300 mm plastic moulds were used to cast the cylinders. The concrete was then placed and compacted in the moulds according to the ASTM C192-16 guidelines. All moulds were removed after 48 hours, and the cylinders were moist cured for 24 hours before testing.

Table 3-6 High-Strength Concrete (HSC) Mix Design

Parameters (/m^3)	**Quantity**
Cement Type I (kg)	564
Silica Fume (kg)	89
Coarse Aggs SSD [1] (kg)	1068
Fine Aggs (kg)	593
HRWR Type F (L)	20.11
Retarder Type D (L)	1.46
Water (kg)	144
Water-Cement Ratio	0.26

1. Coarse aggregates are required to be in a Saturated Surface Dry (SSD) condition.

The concrete cylinders were tested regularly to find the compressive strength, splitting tensile strength and modulus of elasticity of HSC, according to ASTM C39/C39M-14a, C496/C496M-11 and C469/C469M-14, respectively. The test setup is illustrated in Figures 3-9 (a) and 3-9 (b).

(a) Compressive Strength, **ASTM C39/C39M-14a**

(b) Tensile Strength, **ASTM C496/C496M-11**

Figure 3-9 Cylindrical Concrete Test Setup

The loading ratio was kept as close as possible to 14.4 ± 6 MPa/min for all compressive tests, and 1.05 ± 0.35 MPa/min for all tensile strength tests. As permitted by ASTM standards and observed during tests, a continuous reduction was seen in the loading ratio during the final test stages due to the creation and progression of internal cracks in the samples. The development of internal cracks leads to a gradual loss in stiffness due to material non-linearity.

Three cylinders with a diameter of 100 mm and a height of 200 mm were tested at 3, 7, 14 and 28 days after casting to determine the compressive strength of all batches of HSC. All specimens were kept dry 24 hours before testing since any remaining water in pores can develop transverse stresses, which substantially affect compressive strength (Li (2004)). The average compressive strengths between the three cylinders for all six batches of PCPs are presented in Table 3-7 and Figure 3-10. It can be seen in Figure 3-10 that the SP-PCP-20 batch of prisms shows a higher compressive strength in comparison with other batches. This batch was cast in the structural lab with the doors open during the summer, when the temperature was near 30^{o} C, while other batches were cast in the fall and winter at room temperature, around 23^{o} C. It is highly possible that during the summer the water content of the first batch was diminished, thereby increasing the compressive strength of the concrete. The results represent a significant connection between the water content in the concrete mix and the resulting compressive strength.

Table 3-7 High Performance Concrete Strength Development with Time

Age (Days)	Compressive Strength (f'_c) (MPa) – ASTM C39/C39M-14a					
	SP-PCP-20	**SP-PCP-25**	**SP-PCP-30**	**LP-PCP-20**	**LP-PCP-25**	**LP-PCP-30**
3	83.10	N/A	76.30	80.90	79.80	82.70
7	108.30	92.40	86.40	104.60	N/A	109.80
14	120.20	105.80	102.40	119.40	108.50	118.70
28	125.60	110.30	107.60	122.30	113.30	123.20

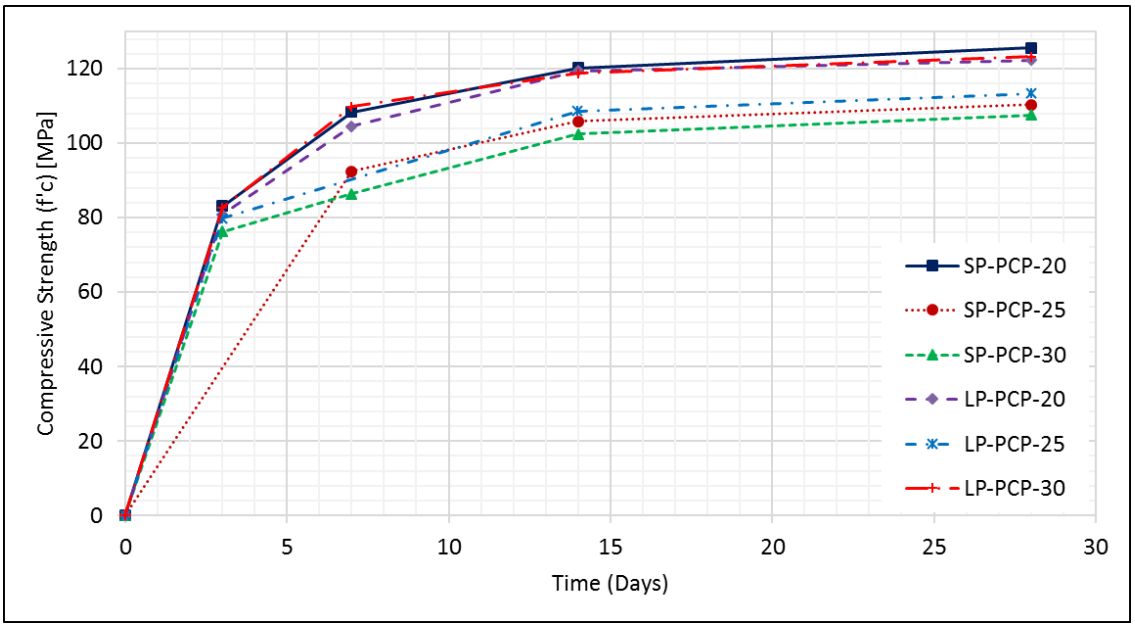

Figure 3-10 High Performance Concrete Strength Development with Time

Procedures similar to the ones for compressive strength testing were followed for tensile strength testing. The results are collected in Table 3-8 and demonstrated in Figure 3-11. It is observed that approximately 80% of the splitting tensile strength for HSC was obtained during first week after casting. The values after 28 days showed only a 5% improvement. Therefore, values for ages more than 8 months can be assumed equal to those at 28 days. It can also be concluded that in high-

strength concrete as compressive strength increases, splitting tensile strength also experiences such an incremental increase.

Table 3-8 Tensile Strength Development in High Performance Concrete

Age (Days)	Splitting Tensile Strength (MPa) – ASTM C496/C496M-11					
	SP-PCP-20	SP-PCP-25	SP-PCP-30	LP-PCP-20	LP-PCP-25	LP-PCP-30
3	5.80	5.60	5.10	5.30	5.10	5.20
7	6.20	N/A	5.30	6.10	5.90	N/A
14	N/A	6.20	5.80	N/A	N/A	6.30
28	6.80	6.40	6.20	6.50	6.30	6.90

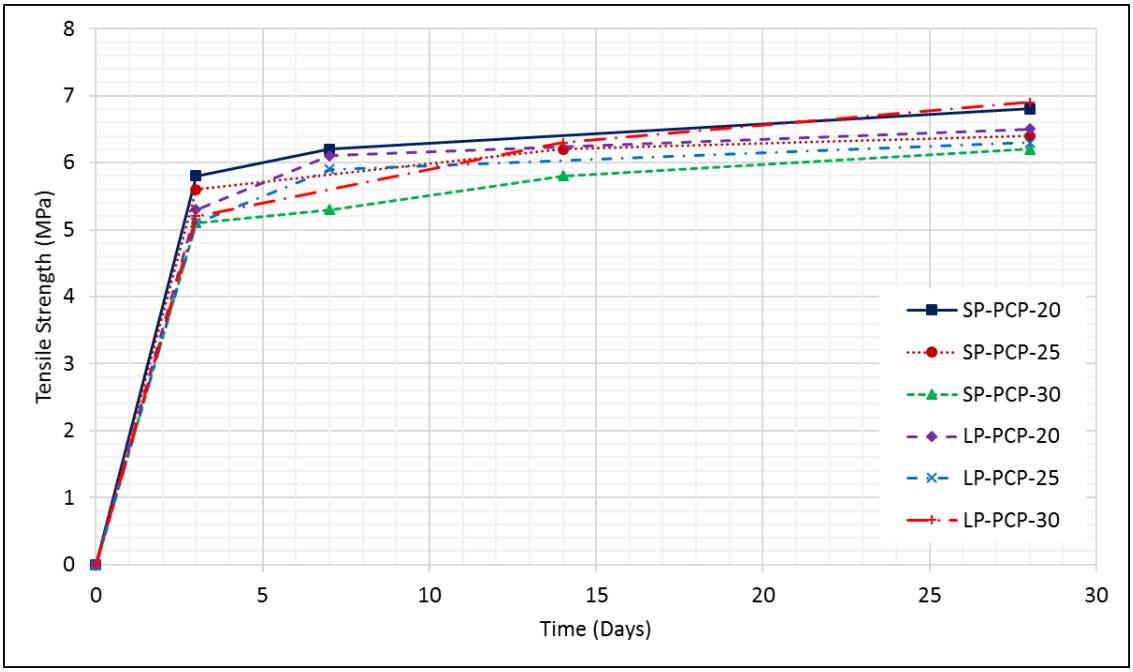

Figure 3-11 Tensile Strength Development in High Performance Concrete

3.8 Installation of PCPs

In bridge deck, a saw cut method would be used to create grooves for installation of PCPs. Saw cutting is a hard and time consuming method especially when it requires to be performed overhead. Therefore, to expedite and facilitate research project, styrofoam was used before casting inside formwork to keep the location where PCPs were to be inserted hollow. Styrofoam was removed after casting and grooves were cleaned and sand blasted prior to the installation of PCPs. Figure 3-12 and 3-13 demonstrate removal of styrofoam and slab prepared for PCP installation respectively.

Figure 3-12 Removal of Styrofoam

Figure 3-13 Ready Grooves for PCPs Installation

3.9 Testing Procedure

Slabs were painted with rectangular grids to track the cracking propagation during the testing procedure. The slabs were pre-loaded until cracking load and the cracks were marked and their widths were measured. Afterwards, the load was removed and PCPs were installed inside grooves, using adhesive. The prisms were installed in overhead position. The grooves were sand-blasted prior to the application of the prisms to provide a rougher surface area and a better bond mechanism between the concrete and adhesive. All slabs were tested to failure seven days after the installation of the PCPs to allow sufficient time for the adhesive to be cured. Figure 3-14 to 3-15 present the installation of the prisms in the slabs.

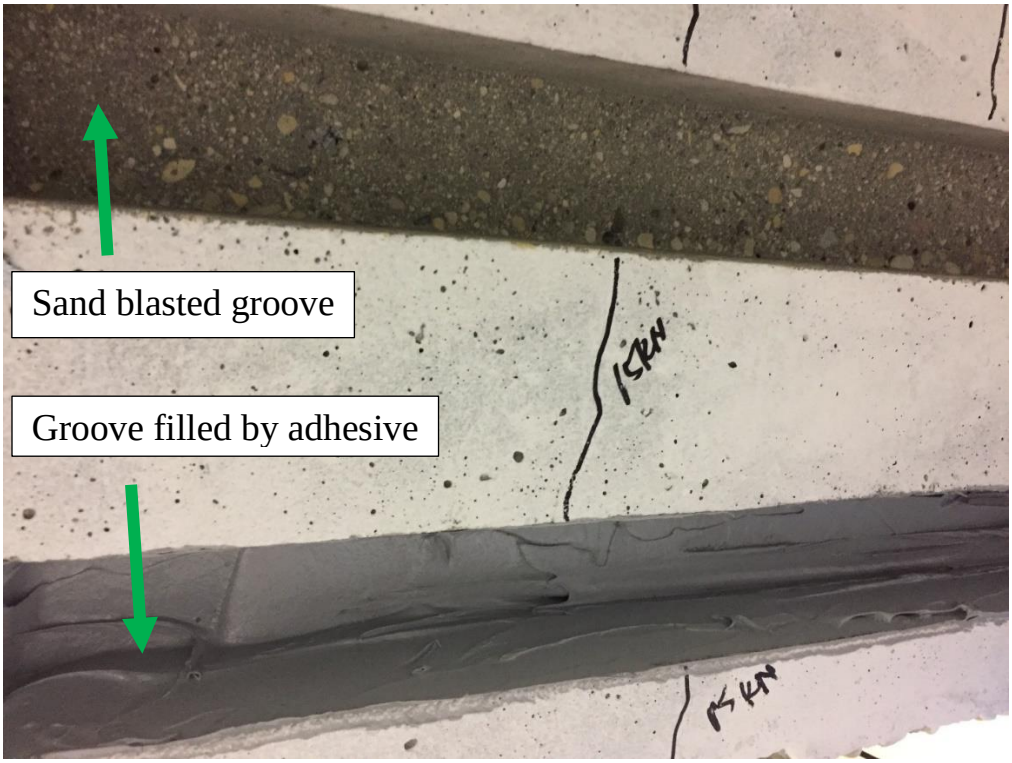

Figure 3-14 Applying Adhesive to the Grooves

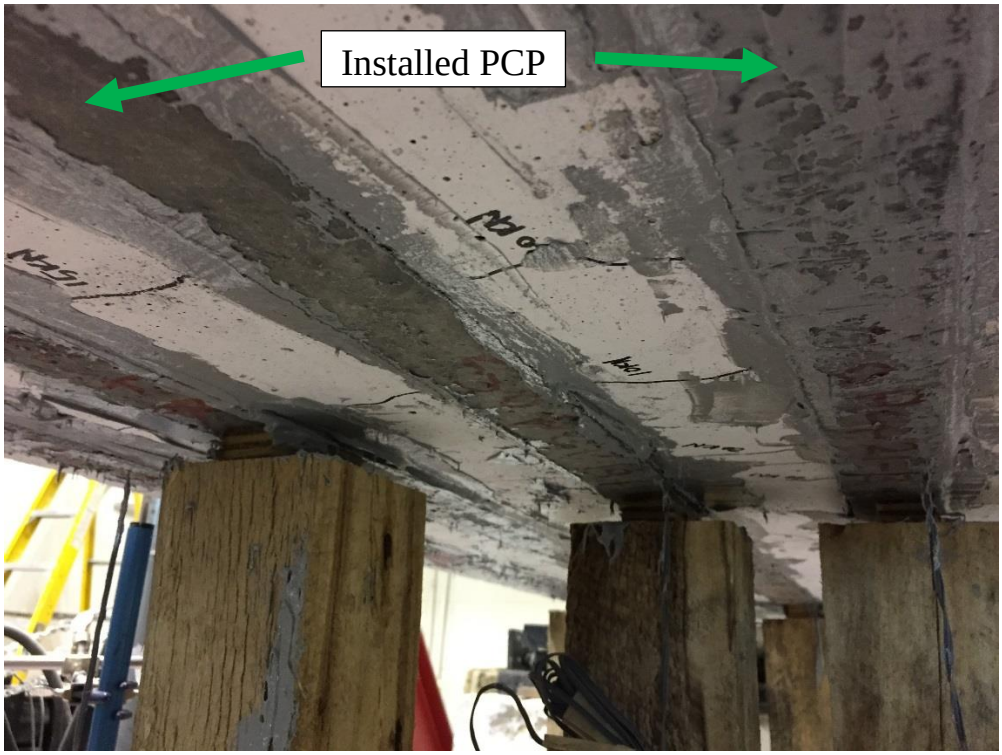

Figure 3-15 Installation of PCPs Inside the Grooves

3.10 Slab Test Setup and Instrumentation

A precise equipment and instrumentation system is required to record all values during the testing of the slabs. Throughout this research study, all readings were collected using a data acquisition (DAQ) system. The following subsections provide details of the loading procedure and instrumentation employed to record the test data such as deflection, strain, and crack-width.

3.10.1 Loading Condition

All slabs were initially pre-cracked to a cracking load of 20 kN, and after the installation of PCPs they were tested under center-point loading until failure. The load was applied monotonically based on the displacement control, at a rate of 0.5 mm/min. During testing, loading was paused frequently at different loading steps to take photos and mark the propagation of cracks. The point load was applied at the mid span of a simply supported slab using a 1000 kN MTS machine. The load from the actuator was transmitted to a steel beam to facilitate uniform loading distribution across the slab cross sections. Moreover, a thin layer of neoprene strips was placed under the steel beam to maintain a smooth, uniform surface between the loading plate and concrete. In addition, plaster bags were utilized at the contact surface between slab and support to level specimens. Figure 3-16 shows test setup that was used for all specimens.

Figure 3-16 Test Setup

3.10.2 Instrumentation Details

During the testing process, the applied load was measured using a load cell attached to an actuator. A total of four linear variable displacement transducers (LVDTs) were used to measure the deflection of slabs at different sections. Two LVDTs were placed at mid-span under the point load on both sides of slabs to measure possible rotation in addition to measuring deflection. Two more LVDTs were positioned at quarter span points. To ensure that LVDTs provide accurate results, they were calibrated prior to testing. The LVDTs at quarter span were mounted using steel angles and clamps. The two at the mid points were positioned using steel magnets. Figure 3-17 illustrates the placement of the LVDTs.

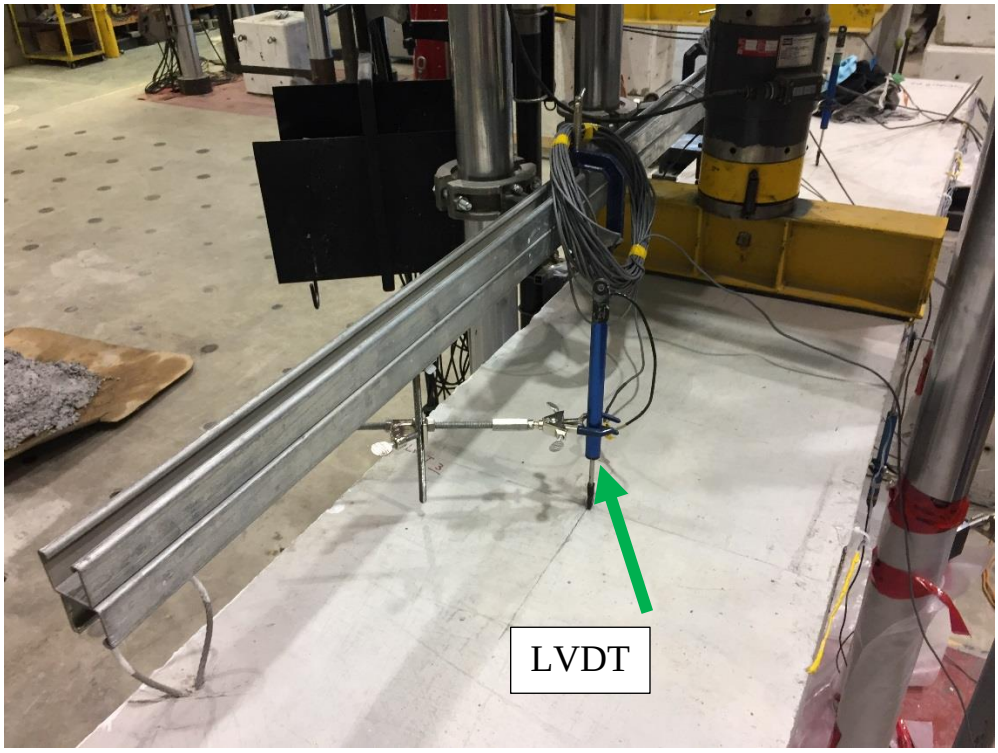

Figure 3-17 Installation of LVDTs

For each slab, a total of six 6 mm -120 Ω electrical strain gauges (ESGs) were mounted on the longitudinal steel reinforcements at mid span, quarter span, eighth span, and at the start of the PCPs. Strain gauges were used to measure strain due to applied load and will be used to establish the moment-curvature relationship for each slab. One ESG was also installed on the concrete surface at mid span, in the compression zone. In addition, there is one ESG with size of 2 mm -120 Ω located at the midspan of the seven-wire steel tendon in each PCP. All ESG were applied according to proper procedures dependent on the substrate.

Figures 3-18 and 3-19 show the installation of the ESGs on the seven-wire steel strand and concrete, respectively.

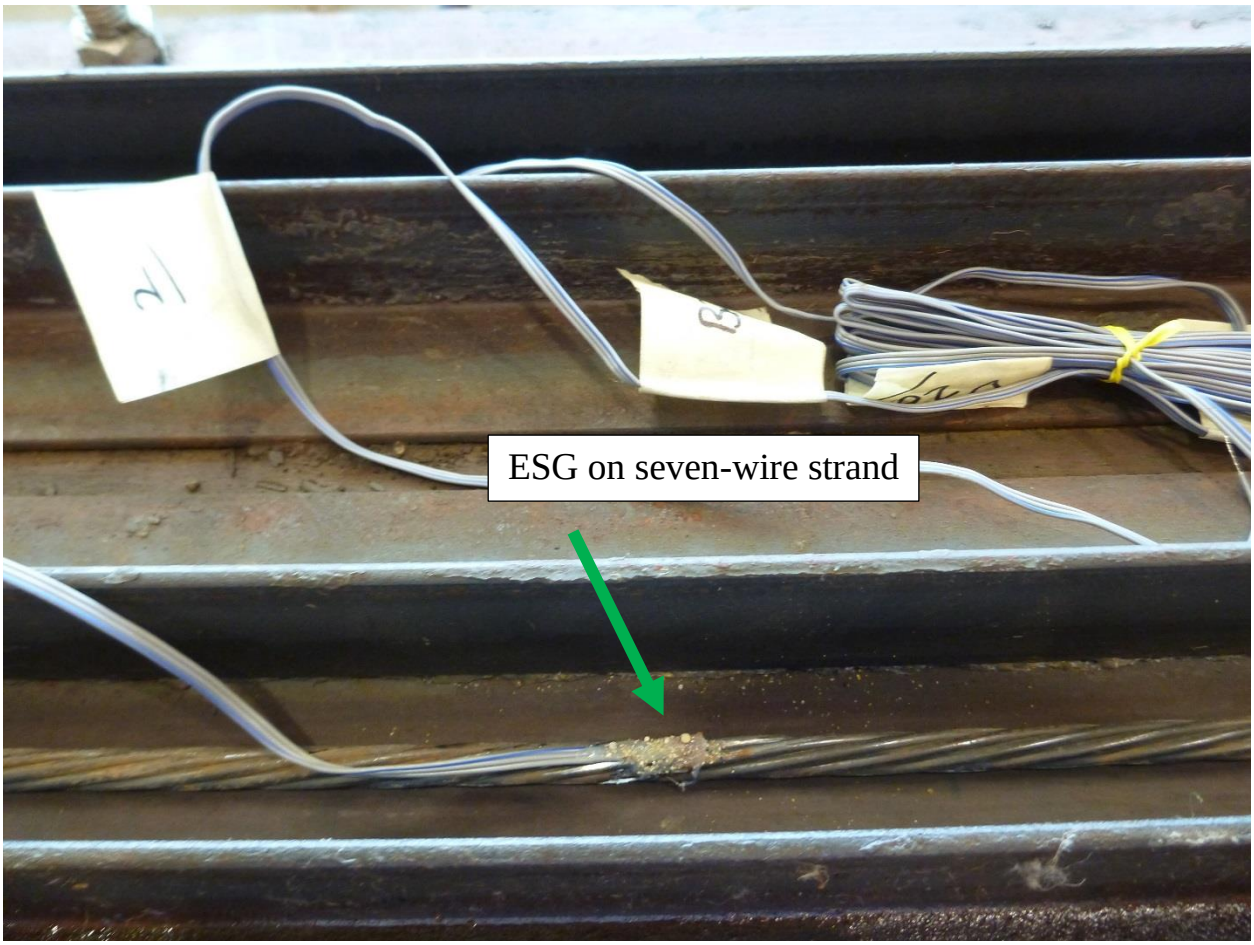

Figure 3-18 ESG on Seven-Wire Steel Strand

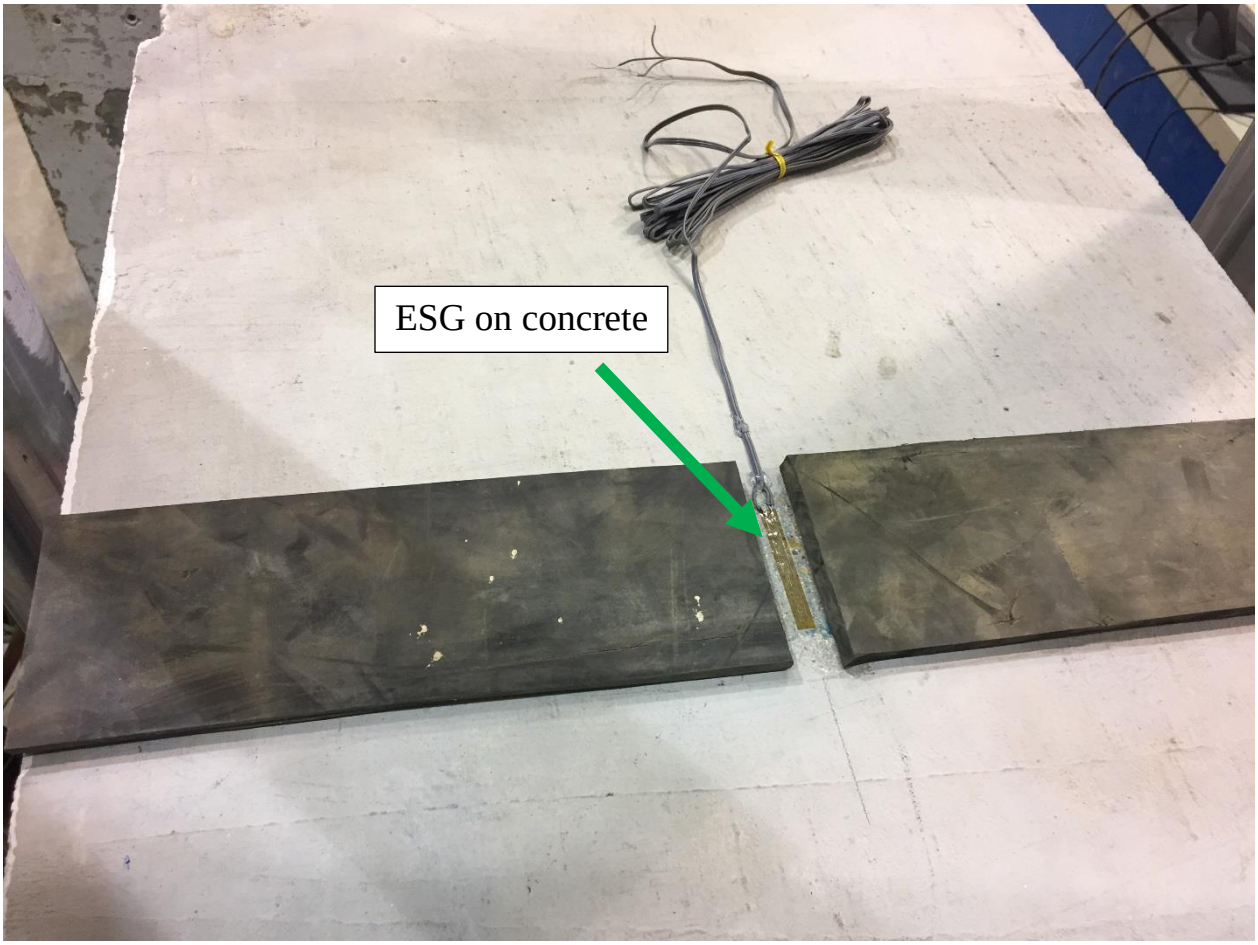

Figure 3-19 ESG on Concrete

200 mm PI gauges were used to monitor the concrete strain and measure crack-width throughout the test. One PI-gauge was installed 20 mm underneath the top compression fiber of the concrete to determine the strain in the concrete surface across the depth of the slab. Another PI-gauge was mounted 20 mm from the bottom of the slab to measure crack width, as demonstrated in Figure 3-20. Both PI-gauges were positioned at the mid span of the slabs, where the bending moment is highest, and calibrated prior to testing for accurate measurement. The measured strain values were used to plot a strain profile of the mid span along the depth of slabs. Variations in crack width were also plotted along with changes in the applied load.

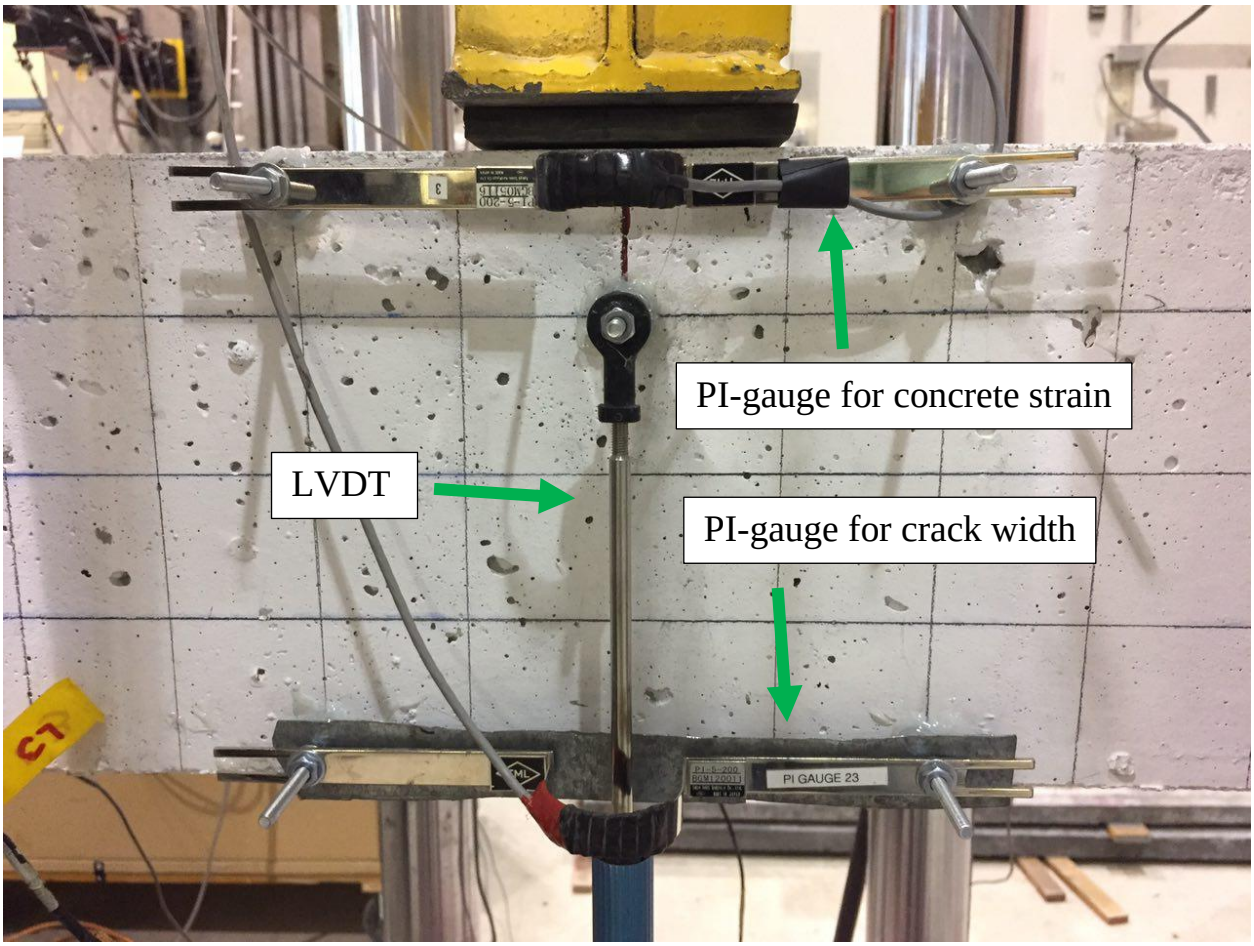

Figure 3-20 PI-Gauge Setup

Figure 3-21 represents detailed location of all censors attached to the specimens.

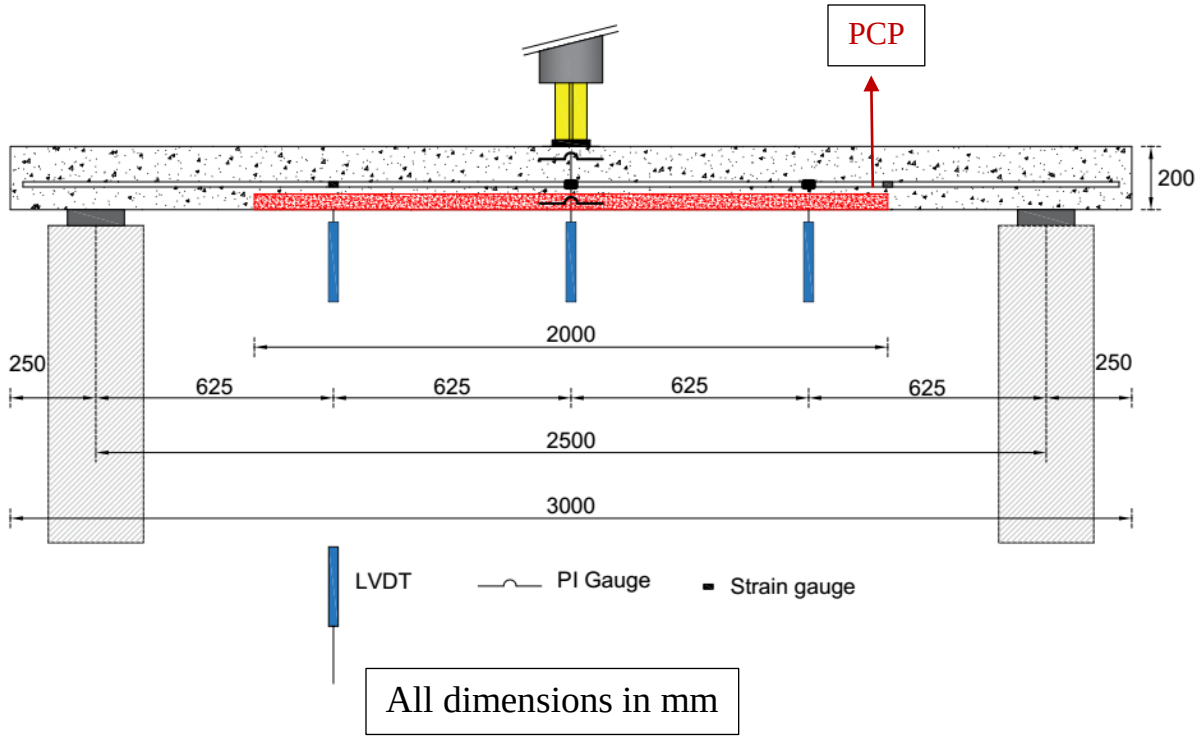

Figure 3-21 Detailed Location of All Censors Attached to the Specimens

The DAQ shown in Figure 3-22 was used to read the data from all strain gauges, PI-gauges, LVDTs and the MTS machine.

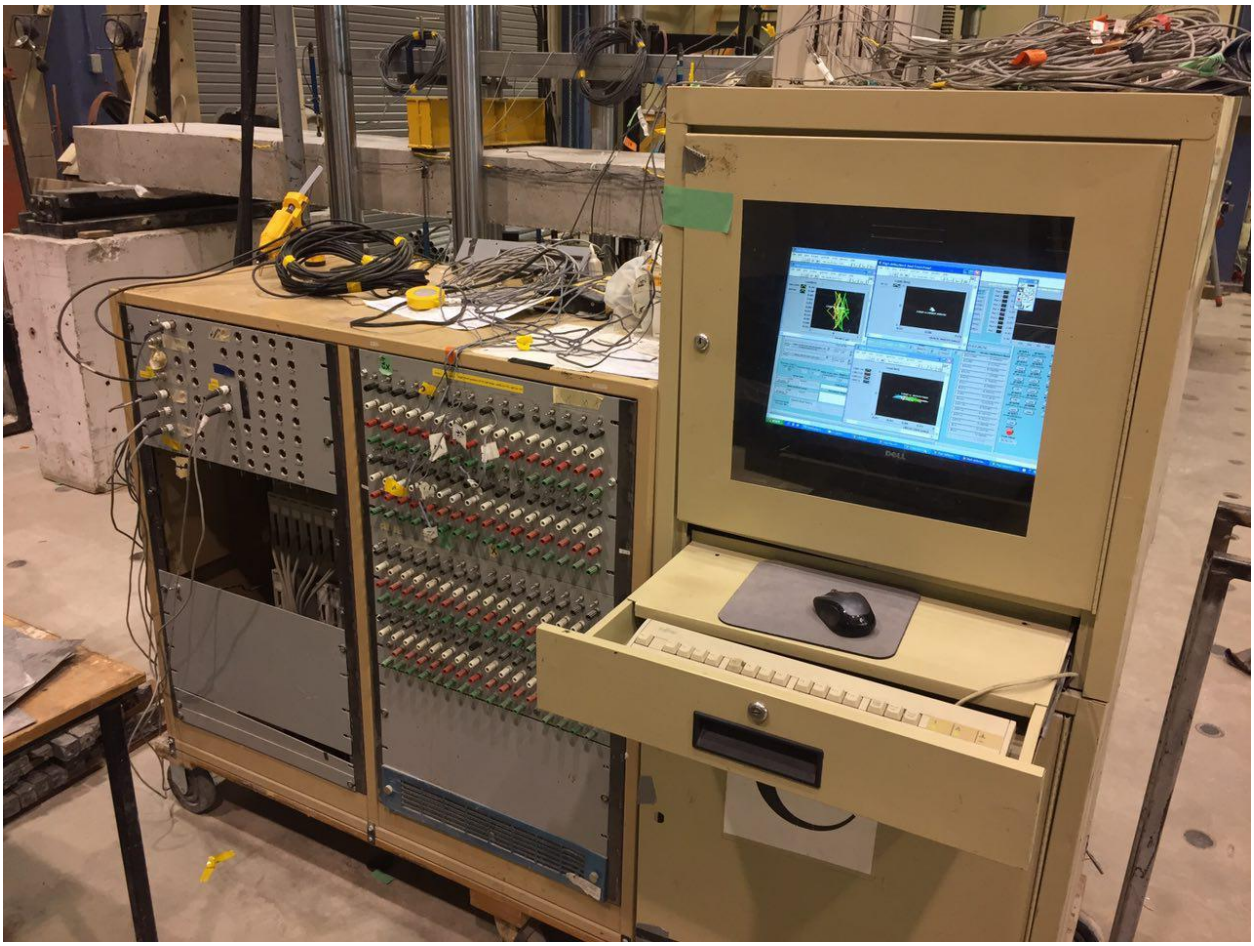

Figure 3-22 Data Acquisition System (DAQ)

Chapter 4

Experimental Results and Analysis

4.1 General

This chapter provides test results of all six slabs rehabilitated by PCPs. As mentioned earlier all slabs were simply supported and 3,000 mm long. The slabs were subjected to monotonic loading until failure and performance of all slabs will be described in detail at service and ultimate load conditions. Throughout the entire test, crack initiation and propagation was marked and modes of failure was recorded. Furthermore, strains in concrete and longitudinal reinforcement as well as crack width in critical regions and deflection of slabs were monitored and recorded.

According to the experimental observations and performance of slabs, variation in crack widths, strain and deflection in different sections along the length of slabs were observed. The load – deflection and moment – curvature relations were used to study ductility of all specimens. Finally, the effect of each test variable presented above on slab performance will be discussed.

4.2 Cracking Phase

In order to assess the efficiency of PCPs in rehabilitation of cracked structural concrete members, slabs were loaded until the cracking load and all cracks were marked. Afterwards load was removed and the PCPs were installed inside grooves, using epoxy adhesive. The grooves were sand-blasted prior to the application of the prisms to provide a rougher surface area and a better bond mechanism between the concrete and adhesive. All slabs were tested seven days after the

installation of the PCPs to allow sufficient time for the epoxy adhesive to be cured. In the second step, all slabs were tested until failure. All slabs had the same reinforcement details, therefore results including load-deflection and moment-curvature response during this loading phase will be illustrated only for one of the tested slabs. Remaining plots can be found in Appendix B.

4.2.1 Load-Deflection Response

The load-deflection behavior of the slab at mid-span just under the load point in cracking phase is depicted in Figure 4-1. Early stage hairline cracks initiated at mid-span (under load point at around 10 kN) followed by cracking at quarter span. Slabs had a bilinear behavior in the cracking phase with a change of stiffness at concrete cracking. Once tiny crack formed at around 10 kN at mid-span, the deflection experienced a rapid increase. The loading procedure stopped at 20 kN which was the theoretical cracking load of all slabs. There were two LVDTs on both sides of the slab at mid span, it can be seen in Figure 4-1 that there is a good agreement between deflection readings on both sides. Finally, the permanent deflection of approximately 2.0 mm was observed at the termination of the cracking phase.

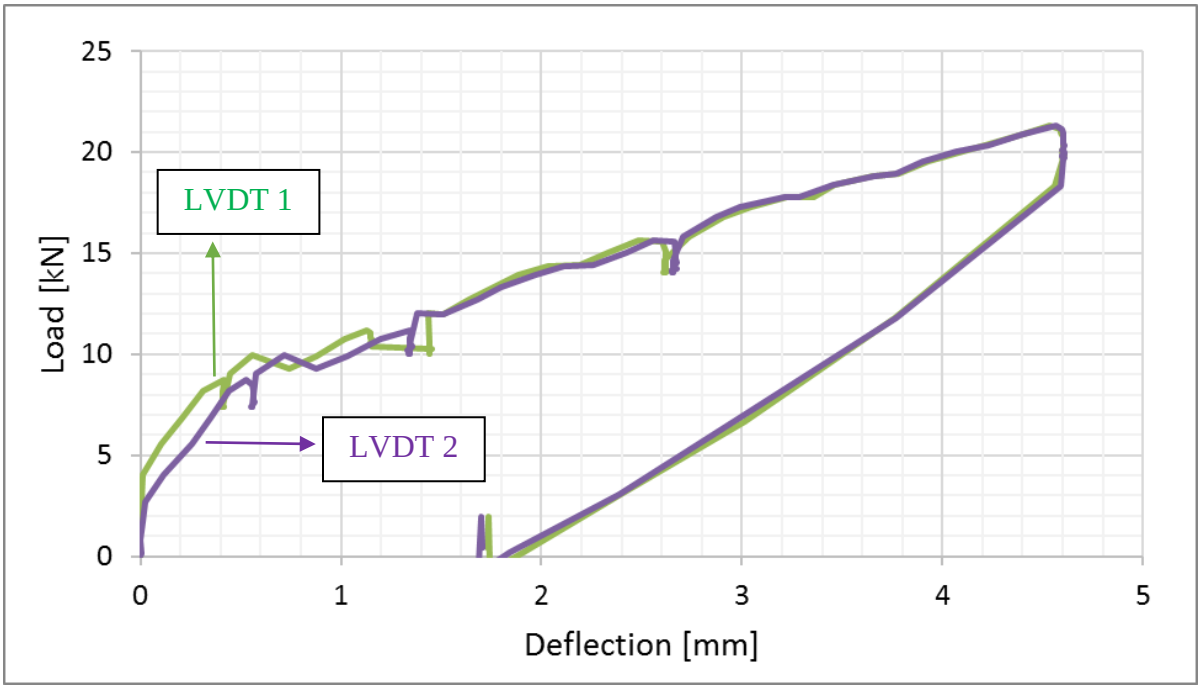

Figure 4-1 Load – Deflection at Mid-Span During Cracking Phase (Slab LP-S-30)

4.2.2 Moment-Curvature Response

The slope of the strain profile represents the curvature in that section. Therefore, the slopes of strain profiles at various load levels will be used to develop moment-curvature diagrams. Trend lines were employed for all strain values recorded by strain gauges and PI-gauges at various heights of the sections. The slope of trend lines represents values of the curvature at those sections. The values of curvature at mid span are illustrated in Figure 4-2 for slab LP-S-30 during the cracking phase. Two strain gauges were mounted on the surface of the steel reinforcement at mid span. As can be seen from Figure 4-2, the moment-curvature relationship is linear before cracking of concrete at $M = 8\ kN.m$. Furthermore, flexural stiffness of steel reinforced slabs did not change remarkably after cracking of concrete. The average permanent curvature of $\emptyset = 2.5 * 10^{-6}$ was recorded ultimately at the end of cracking stage for all slabs.

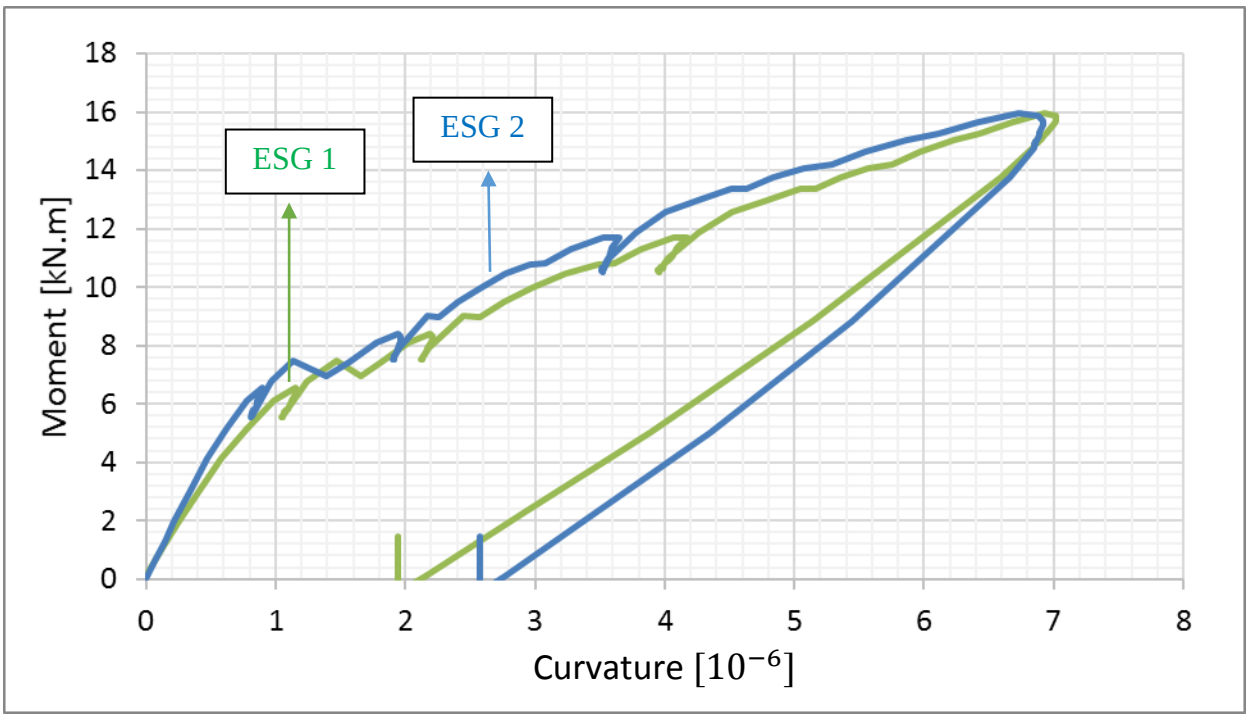

Figure 4-2 Moment – Curvature at Mid-Span During Cracking Phase (Slab LP-S-30)

4.3 Behavior of PCP Reinforced Concrete Slab

In this section behavior of concrete slabs repaired with PCPs will be investigated and compared with steel reinforced concrete slabs. For the current research program, in pre-cracking phase slabs were reinforced with four #15 mild steel reinforcement bars. Four PCPs were installed in these slabs after initial cracks appeared to improve serviceability of slabs and prevent crack propagation. To describe the behavior of these slabs, Figure 4-3 shows the strain and stress profiles of both slab types from the elastic stage to failure. Steel reinforced concrete slab is defined in Figure 4-3 as cross-section A, while the slab repaired with prisms is defined as cross-section B.

The ultimate moment capacity of the slab reinforced with PCPs will be calculated as follows:

$$M = T_{pcp}\left(d_2 - \frac{\beta c}{2}\right) + T_{st}\left(d_1 - \frac{\beta c}{2}\right) \quad \text{Eq. (4-1)}$$

Where:

T_{pcp} = resultant tension force in seven-wire steel strand at failure (N)

T_{st} = resultant tension force in mild steel reinforcement at failure (N)

d_1 = effective depth of mild steel rebar (mm)

d_2 = effective depth of seven-wire steel strand (mm)

β = concrete stress block parameter

c = neutral axis depth (mm)

To study flexural behavior of PCP reinforced slab, following assumptions are considered:

1. Plane sections before bending remain plane after bending
2. Stress-strain relationship of concrete is known
3. Force-strain relationship of PCP is known
4. Tensile strength of concrete is neglected

Figure 4-3 provides schematic view of stress and strain distributions for PCP and mild steel reinforced concrete slab cross-sections. The primary objective of using PCP for rehabilitation is to prevent reduction in stiffness of steel reinforced slabs after cracking and provide better crack control. Before cracking of concrete, behavior of both slabs is the same as PCPs installed after cracking. When cracks appeared and concrete behavior moved to inelastic stage, for the same $\varepsilon_b > \varepsilon_{cr}$, in the PCP reinforced slab, the high strength concrete which has higher tensile strength still provides contribution to tolerate tensile force in the section, whereas mild steel reinforced slab has lost all contributions of concrete in tension zone.

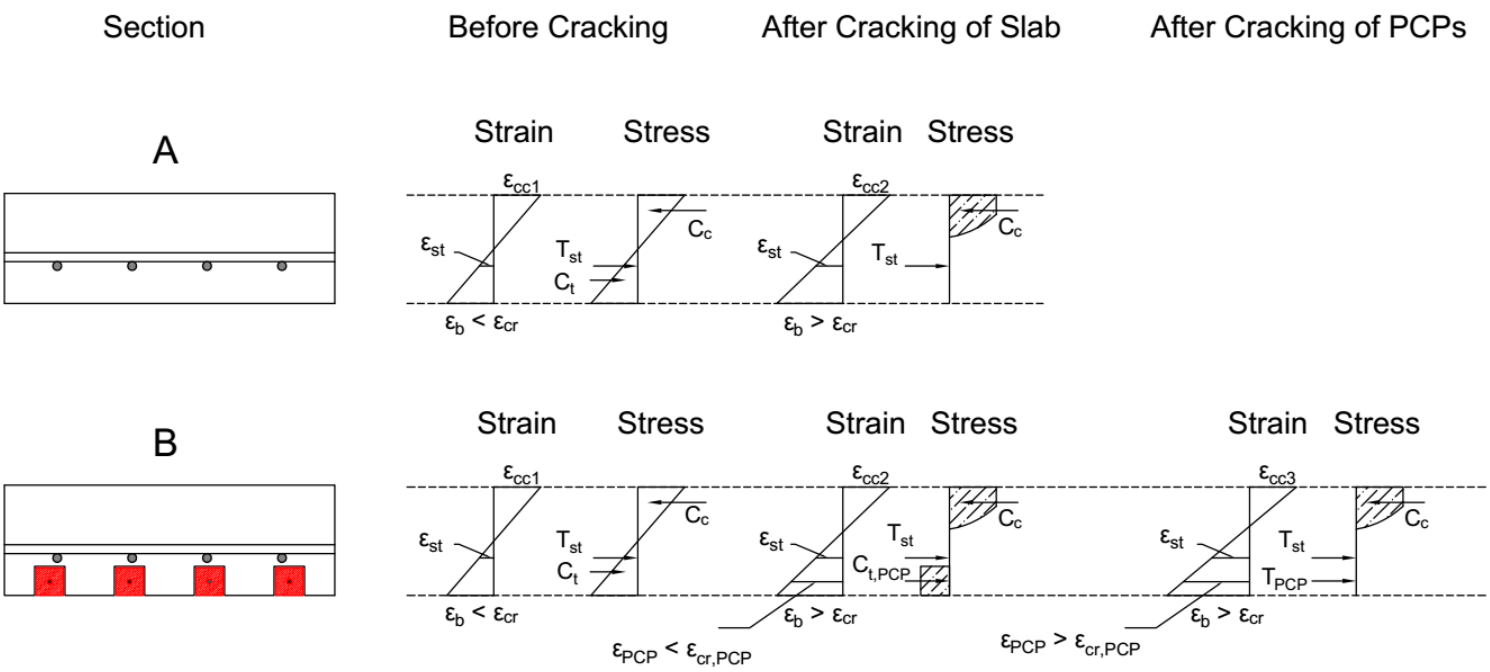

Figure 4-3 Stress and Strain Distribution in Slab Reinforced with Steel Rebar and PCP

A) Steel reinforced slab, B) Slab rehabilitated with PCP

For both load-deflection diagram (Figure 4-19) and moment-curvature diagram (Figure 4-22) as could be seen later, in a PCP reinforced concrete slab, cracking of prisms and yielding of mild steel reinforcement constitutes a change in stiffness while in a steel reinforced concrete slab stiffness is changed when concrete cracks and then when the steel yields only. Thus, PCP reinforced slab demonstrate higher stiffness compared to a mild steel reinforced concrete slab.

In summary, the idea of utilization of PCPs for concrete bridge and parkade rehabilitation is effective and practical. Serviceability limits can be met without increasing the reinforcement ratio for required strength that makes this method economical. The practical effects of using PCPs for bridge rehabilitation and serviceability behavior will be discussed in details in following sections.

4.4 Failure Phase

After installation of all prisms followed by 7 days of curing for the epoxy adhesive, the slabs were tested under center-point loading conditions until failure. The experimental results and analysis of the data for these tests are presented in this chapter.

4.4.1 Behaviour and Mode of Failure

Table 4-1 provides calculated and experimental ultimate loads for all slabs along with their modes of failures and strain in concrete and longitudinal reinforcements. Provisions of CSA A23.3-14 were used to calculate ultimate loads. All six slabs were designed to fail in flexure but experienced shear failure. This is believed to be caused by the reduction of the section of the slab in the vicinity of the slab support. The section was reduced, because the grooves that were prepared for installation of the prisms were longer than the prisms. The space that was left was filled with epoxy, and ultimately led to premature failure of the slabs. Therefore, concrete compressive strain at failure for all six slabs was below the ultimate strain of 0.0035 defined by CSA A23.3-14. Table 4-1 summarizes calculated and experimental failure load and modes of failure for all slabs.

Table 4-1 Calculated and Experimental Failure Load and Modes of Failure

Slab	Failure Load (kN)		P_{exp} / P_{cal}	Strain at Failure (10^{-6})		Mode of Failure
	exp	cal		Concrete	Steel	
SP-S-20	128.0	152.5	0.84	2010	11092	Shear Failure
SP-S-25	133.1	156.0	0.85	2907	8491	
SP-S-30	137.3	156.2	0.87	2935	4103	
LP-S-20	120.5	149.1	0.80	2299	3596	
LP-S-25	126.3	150.5	0.84	2382	2279	
LP-S-30	132.3	151.2	0.87	2620	2144	

Figure 4-4 shows similar cracking behavior in terms of initiation and propagation until failure in all tested slabs. Cracking started at load level of 50 kN to 65 kN for different pre-stressing load levels with the development of a few very fine vertical flexural cracks at the mid span. Early hairline cracks in the rehabilitated slab initiated at approximately 31, 37, 36, 33, 39 and 41 percent of the failure load for slabs SP-S-20, SP-S-25, SP-S-30, LP-S-20, LP-S-25 and LP-S-30, respectively. Subsequently, several inclined cracks widened in the area close to the section where PCPs were introduced in the cross section. As the cracks stabilized, one of the inclined cracks widened and extended towards the top of the slab, ultimately causing failure of the slab. Higher compressive strength of concrete at the time of test compared to assumed theoretical values in slabs SP-S-20 and SP-S-25, allowed steel reinforcement to enter its strain hardening phase. This is a brittle failure mode, and it occurred without warning shortly after the diagonal cracks developed. All slabs failed in the locations where PCPs were introduced in the cross-sections, close to supports. Immediate presence of inclined cracks at the locations where PCPs were introduced in the cross section caused the ultimate load in all slabs to be lower than calculated values.

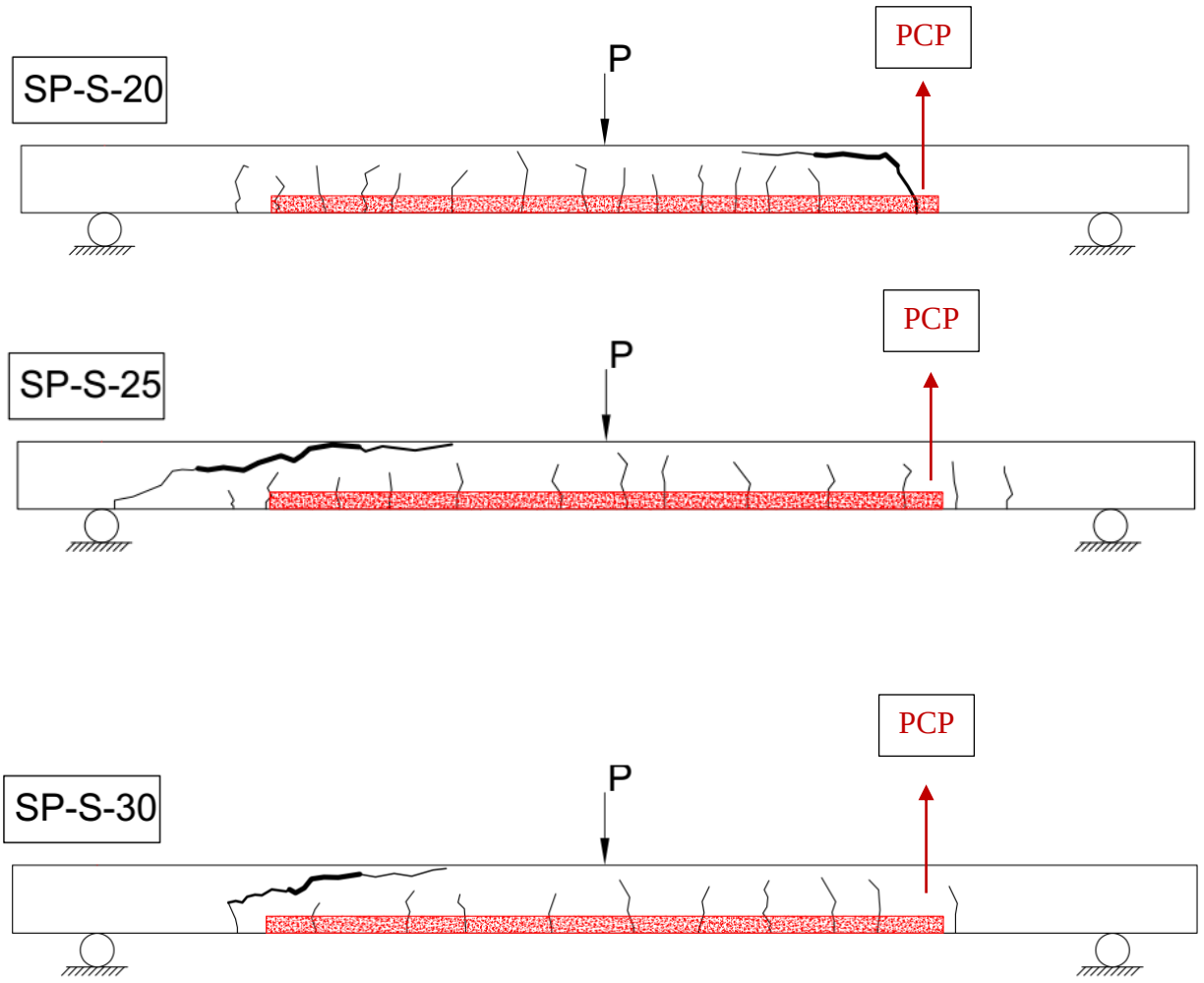
SP-S-20
P
PCP
SP-S-25
P
PCP
SP-S-30
P
PCP

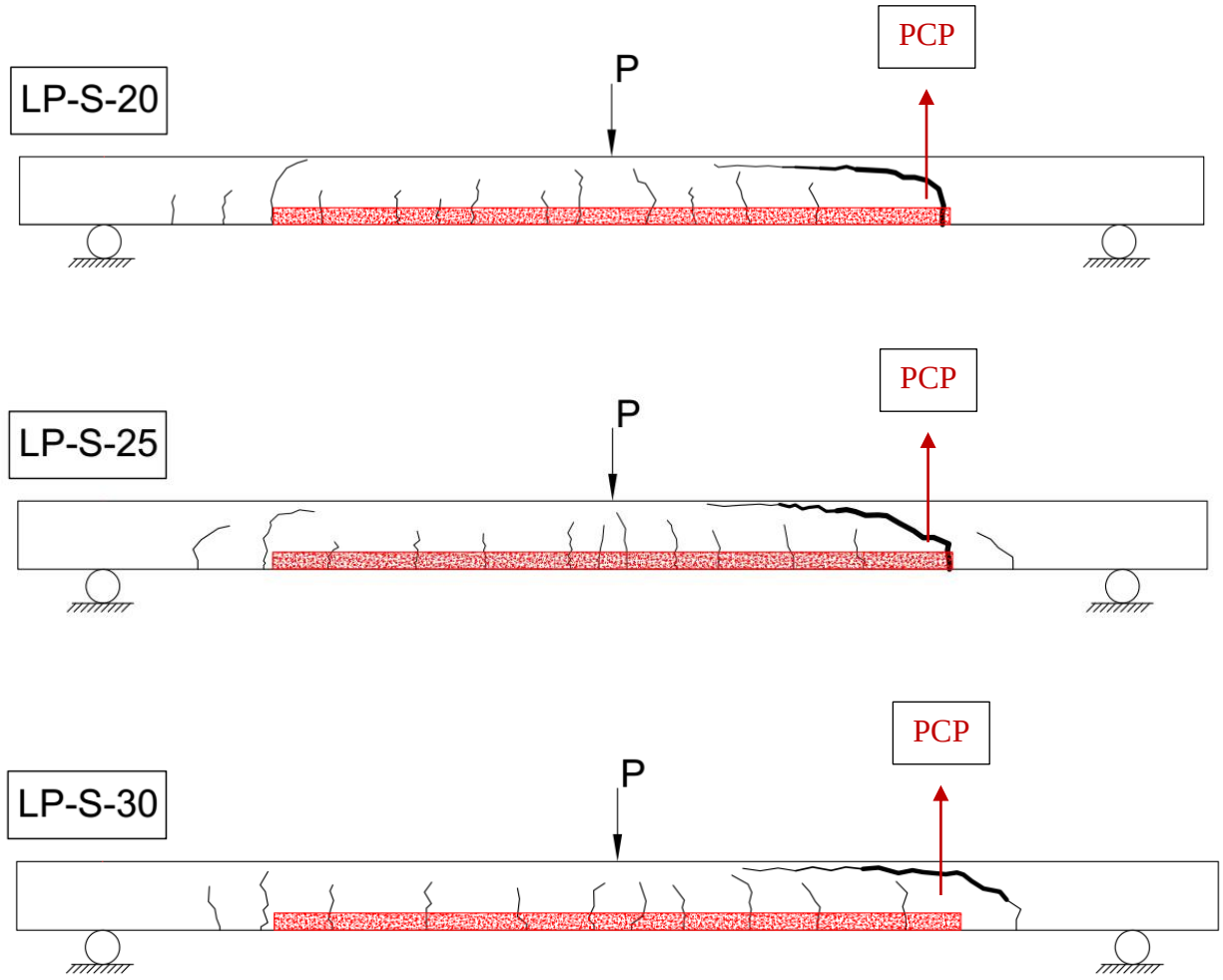

Figure 4-4 Cracking Patterns of Tested Slabs at Failure

Except in slabs LP-S-30 and LP-S-25, the mild steel reinforcement in four slabs yielded prior to the failure. Nearly 90% of the tensile capacity of steel strands inside the PCPs were utilized before failure took place.

No slip was observed between steel reinforcement, PCPs and concrete in any of the slabs. The larger curvature at ultimate and closer crack spacing at quarter span are visible in Figure 4-5 to Figure 4.10 which were extracted from recorded videos.

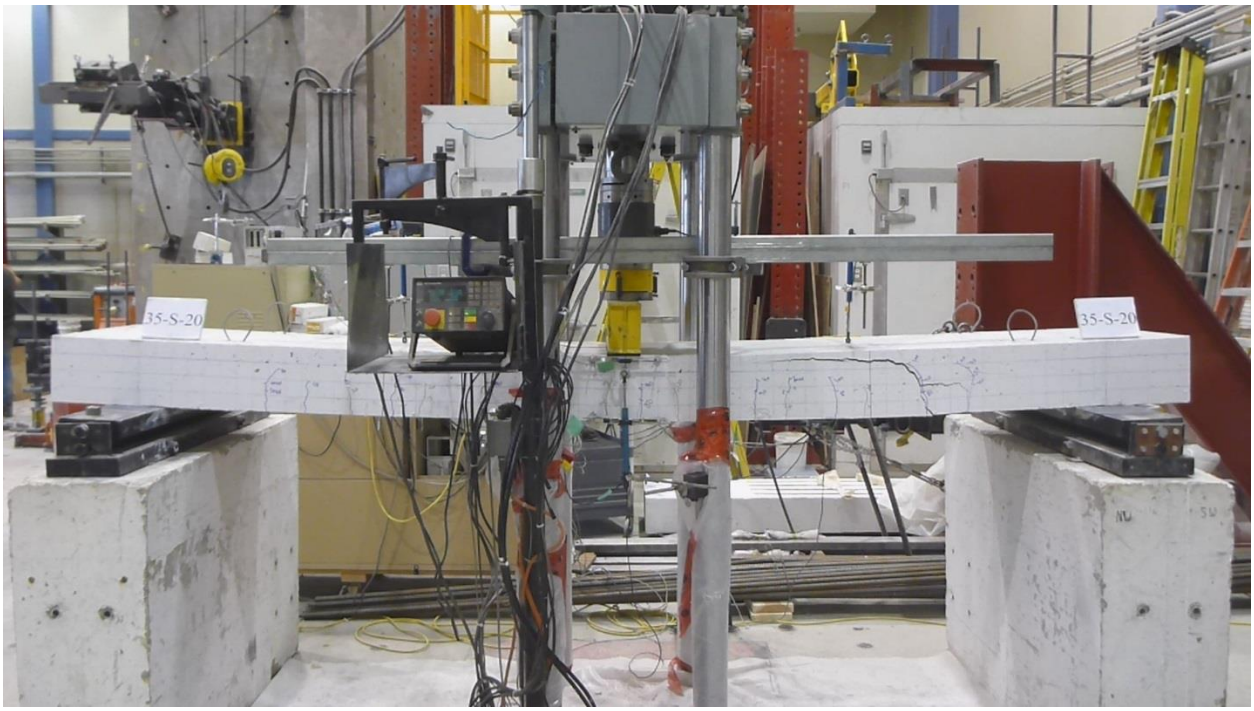

Figure 4-5 Modes of Failure and Condition of Slab SP-S-20 at Failure

Figure 4-6 Modes of Failure and Condition of Slab SP-S-25 at Failure

Figure 4-7 Modes of Failure and Condition of Slab SP-S-30 at Failure

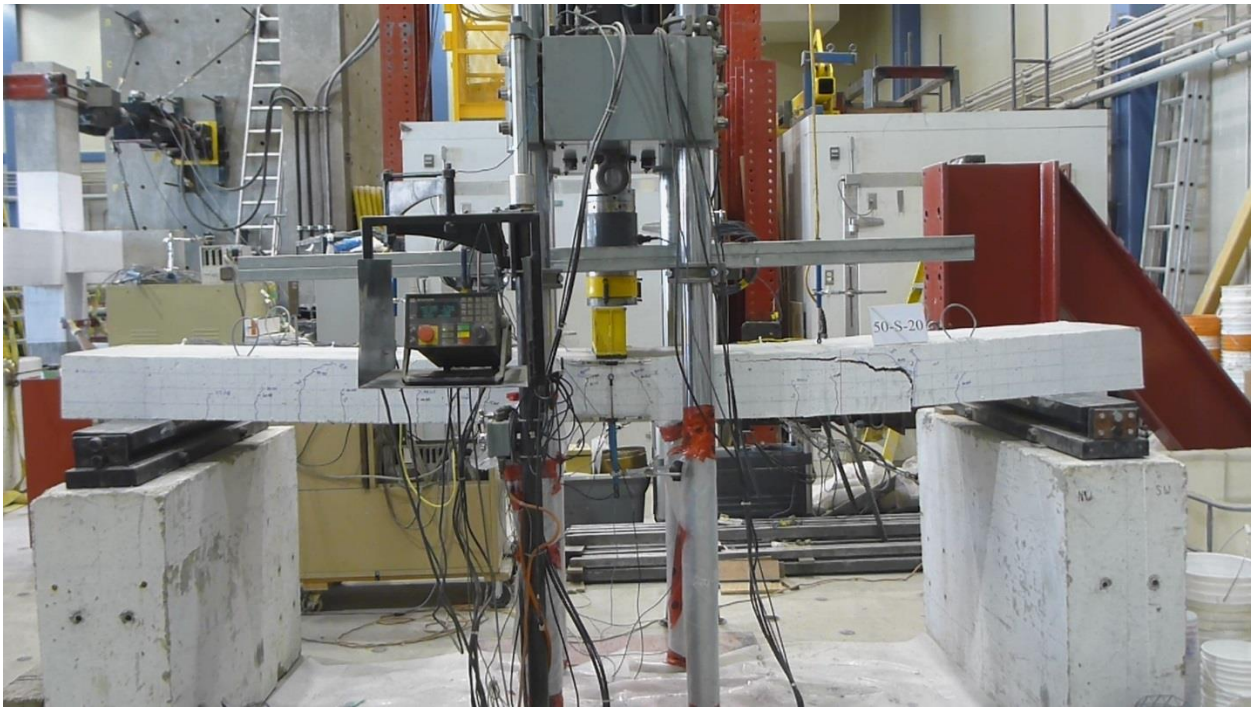

Figure 4-8 Modes of Failure and Condition of Slab LP-S-20 at Failure

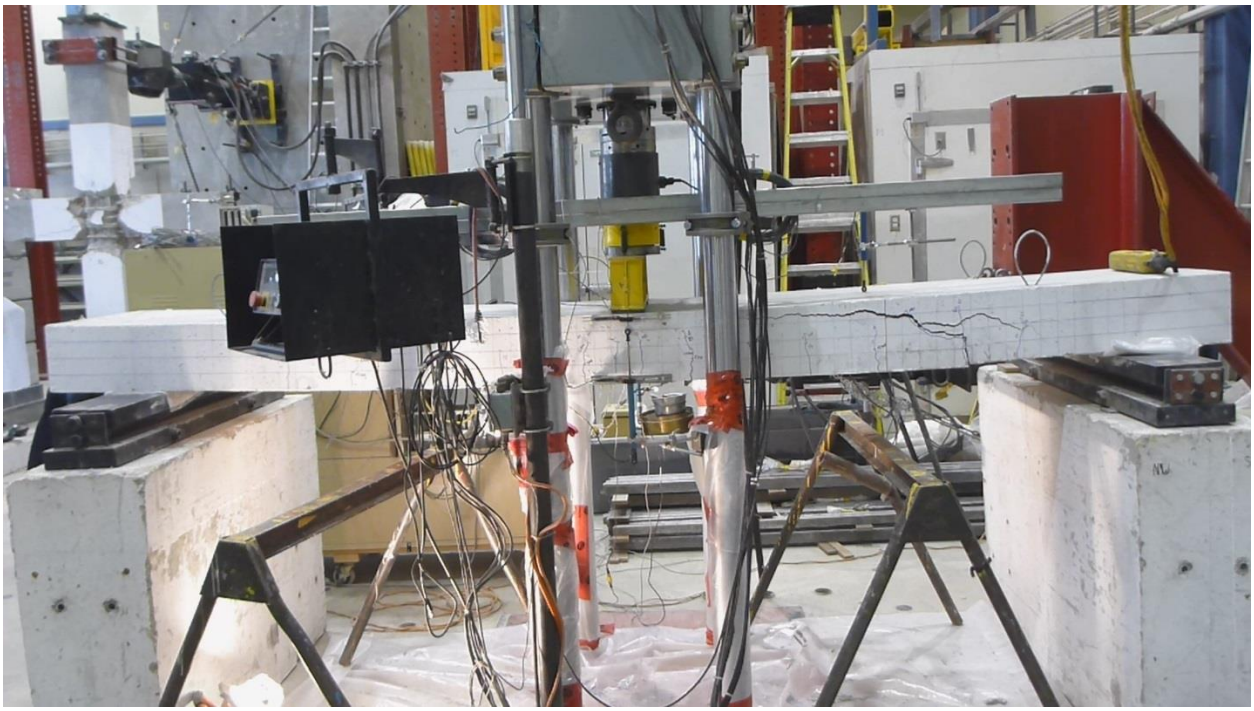

Figure 4-9 Modes of Failure and Condition of Slab LP-S-25 at Failure

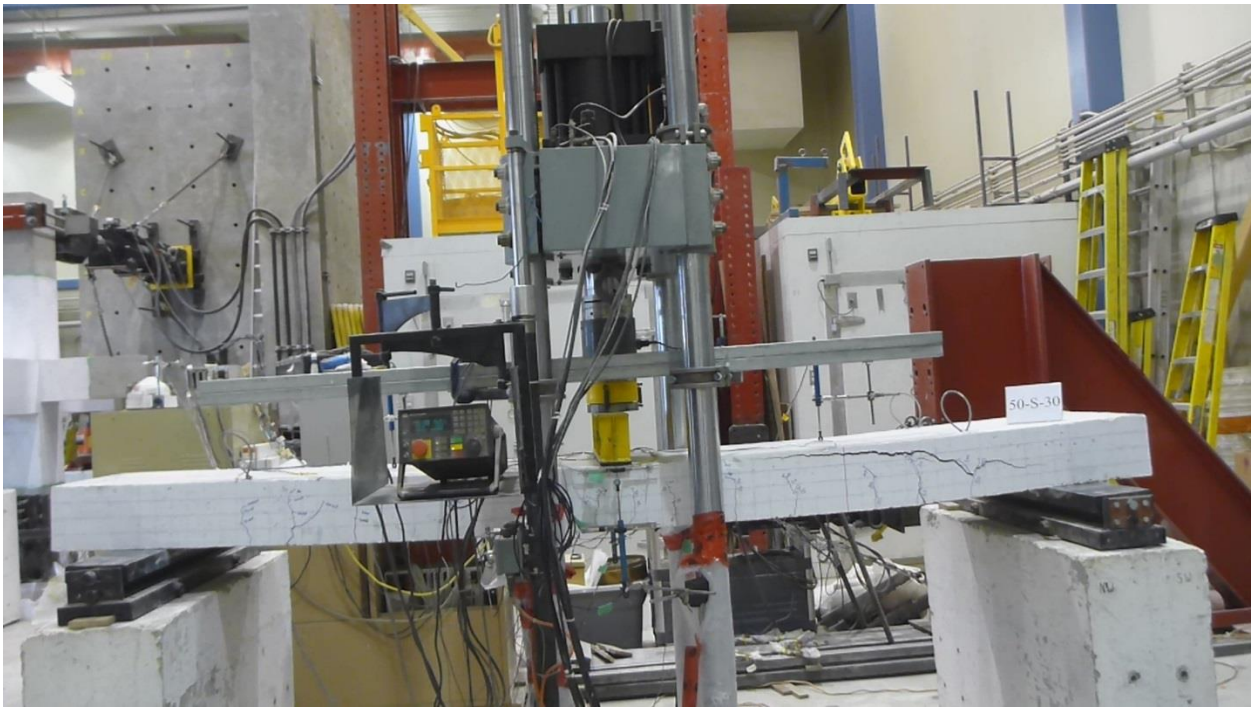

Figure 4-10 Modes of Failure and Condition of Slab LP-S-30 at Failure

4.4.2 Strain in Reinforcement and Concrete

The variation of strain in flexural reinforcement and concrete was measured by strain gauges at mid span under the point load. The recorded strains will be used to calculate moment-curvature behavior of all slabs, as will be presented in following section.

4.4.2.1 Strain in Flexural Reinforcement and Seven-Wire Strand

Figure 4-11 illustrates the strain in mild steel reinforcement for all tested slabs at mid span under the point load. This is the location of maximum bending moment and tension reinforcement is in the bottom of slabs.

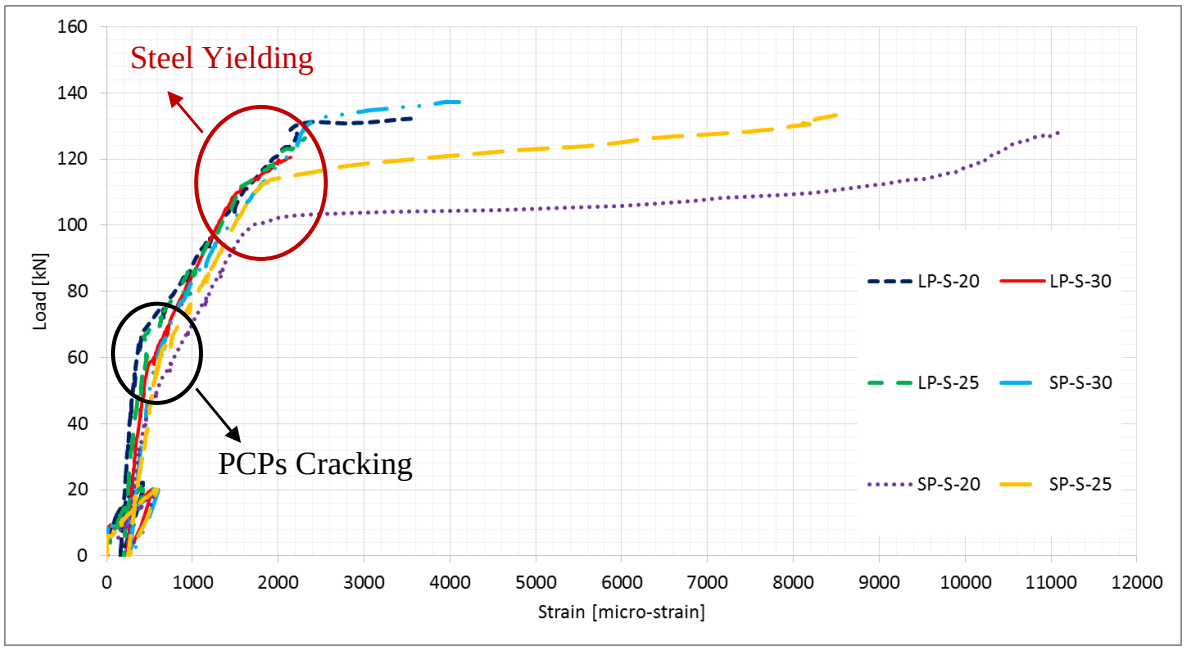

Figure 4-11 Strain in Steel Tension Reinforcement at Mid Span Under Load Point

Figure 4-11 indicates that strain in all slabs changed linearly with load up to the cracking loads of PCPs, which varied from 50 kN to 65 kN for different pre-stressing load levels. Strain values at this stage for all slabs are similar due to the fact that transformed cross-sectional properties of the slabs were comparable. When the prisms cracked, strain in flexural reinforcements experienced a

rapid increase with an approximately linear relationship and continued up to levels close to yielding load. When mild steel yielded at load levels around 100 kN to 139 kN depending on the level of pre-stressing in PCPs, strain changed considerably in mild steel bars with a very small change in load and a plateau was formed for most of the slabs. This increment in strain led steel bars to the strain hardening phase for slabs SP-S-20 and SP-S-25 at strains higher than 6000 micro strain. The yielding plateau in the strains of steel bars is representative of ductile behavior of the slabs. The longer the plateau is the larger strain, deflection, curvature and wider crack width were observed in the slabs.

Figure 4-12 demonstrates load-strain relationship for all four PCPs embedded in slab SP-S-30 at mid span. PCP 1 and PCP 2 were two middle interior prims while PCP 3 and PCP 4 were two external prisms along the sides.

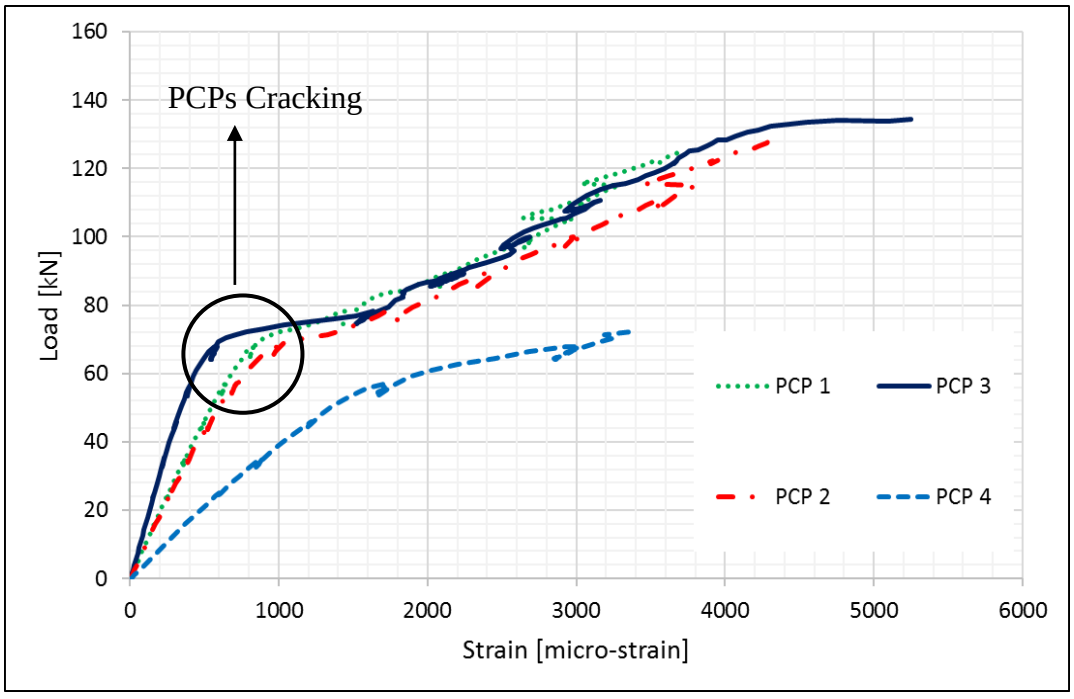

Figure 4-12 Strain in Seven-Wire Steel Strand of PCPs at Mid Span in Slab LP-S-30

As can be seen from Figure 4-12, strain in all PCPs changed linearly with load up to the cracking loads of PCPs which was 70 kN for all three PCPs (PCP 1, PCP 2 and PCP 3). PCP 4 was located at the exterior edge of the slab and cracked at load level close to 60 kN due to very small slippage and strain gauge readings were lost at 63 kN.

Furthermore, a pre-stressing strain of 2871, 2392 and 1914 micro strain is already imparted in PCPs on seven-wire steel strand with 30 kN, 25 kN and 20 kN pre-stressing force respectively on top of the strain due to applied external load. For the slab LP-S-30, the maximum total strain in the pre-stressing strands was 8070 micro-strains at failure. Therefore, about 75% to 82% of ultimate tensile strain of seven-wire steel strands was reached before failure. Strain values are proportionally related to the curvature, crack width and deflection. In the other words, higher strain means larger curvature and deflection as well as wider cracks. At service load level of 45 kN, the measured strains in slabs LP-S-30, LP-S-25, LP-S-20 and SP-S-30 were approximately 300 micro-strain, while slabs SP-S-25 and SP-S-20 demonstrated more ductile behavior and strain was about 500 micro-strain. On the other hand, for load levels lower than cracking of prisms, strain in reinforcement for all slabs roughly followed an identical trend with analogous values.

Strains in mild steels before and after rehabilitation were plotted in Figure 4-13 and 4-14 for slabs reinforced with large and small PCPs respectively. It is evident for all slabs that strain values reduced due to presence of PCPs. Lower strain will lead to smaller deflections and crack widths. The installation of PCPs helped slabs to retain their stiffness to the level as before cracking of concrete. Stiffness only changed at cracking loads of PCPs, which varied from 50 kN to 65 kN for different pre-stressing load levels and yielding of mild steel reinforcements.

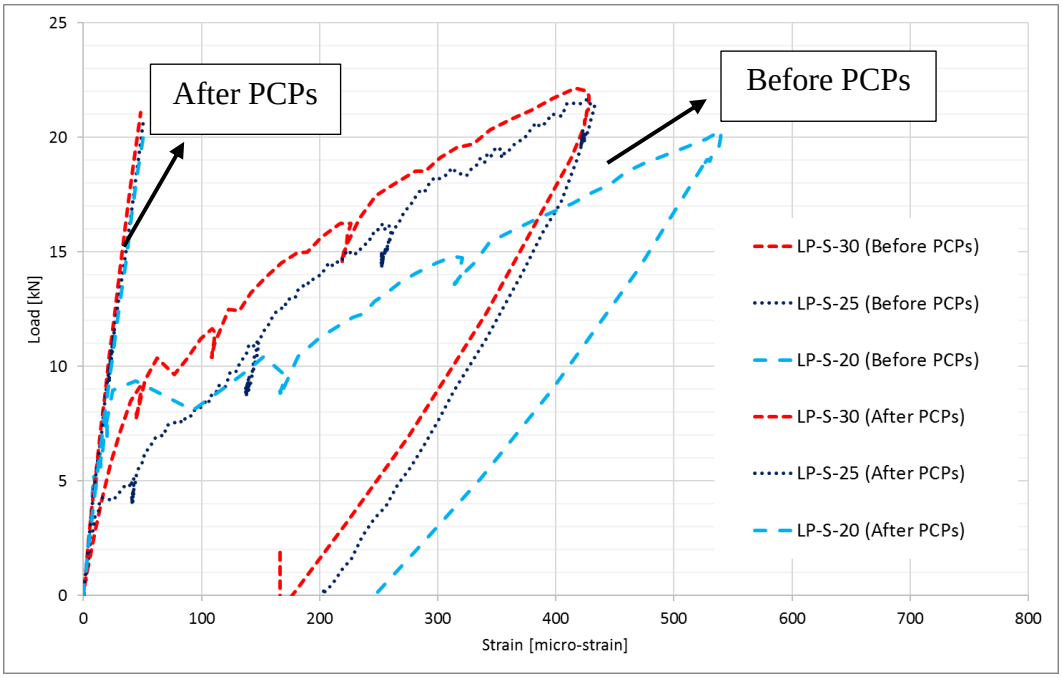

Figure 4-13 Steel Tension Reinforcement Strain Comparison for Slabs LP

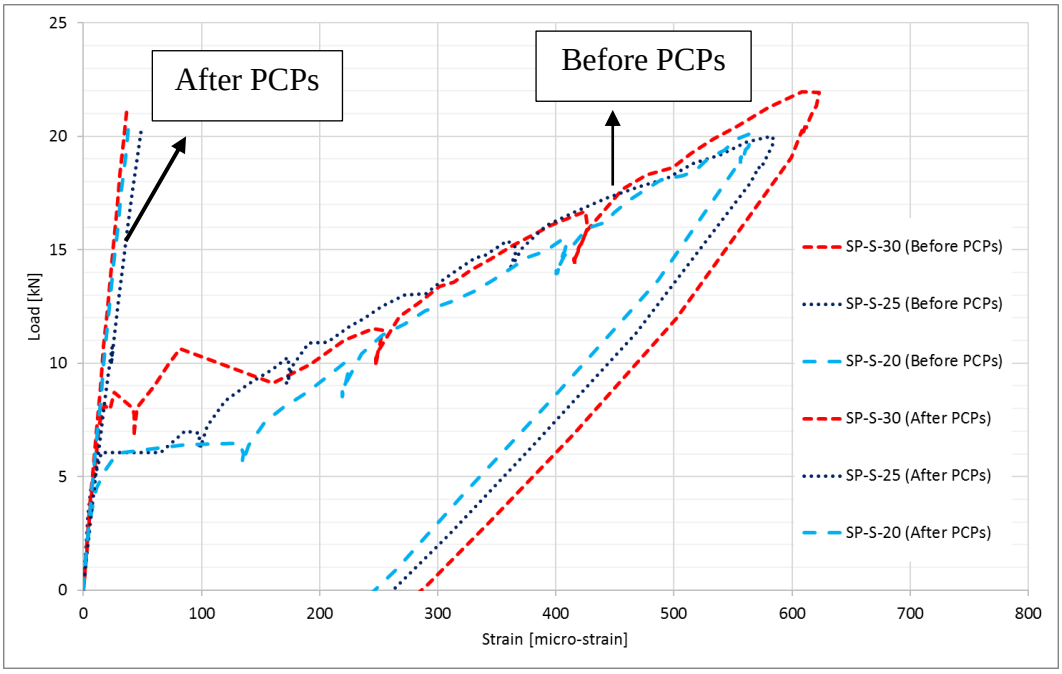

Figure 4-14 Steel Tension Reinforcement Strain Comparison for Slabs SP

4.4.2.2 Strain in Concrete

Strains in concrete were monitored in the extreme compression fiber of the concrete at mid span under load point where maximum bending moment occurs. Figure 4-15 represents concrete strain at the extreme compression fiber for all slabs at mid span. It can be seen clearly that concrete strain in slabs prior to the cracking of PCPs is linear and increases slightly with load. When tension cracks appeared on the tension face of slabs and PCPs, compressive strain of concrete changed with load more considerably up to load levels of 60 kN to 139 kN, close to the yielding point of mild steel. When steel reinforcement yields, concrete strain increases in a faster rate with applied load to maintain equilibrium and compensate for the reduction of concrete area in compression due to shift of the neutral axis. The smaller values of strain for slabs LP strengthened with larger prisms compared with slabs SP indicate higher stiffness of slabs LP. Flexural stiffness is directly related to the moment of inertia (I) which is function of geometry and modulus of elasticity (E). The larger cross section of PCPs, the larger area with high strength concrete and modulus of elasticity (E) after cracking of surrounding slab.

At failure load, the ultimate compressive strain in concrete varied from 2000 to 3000 micro-strain which is less than ultimate strain of 3500 micro-strains suggested by CSA A23.3-14.

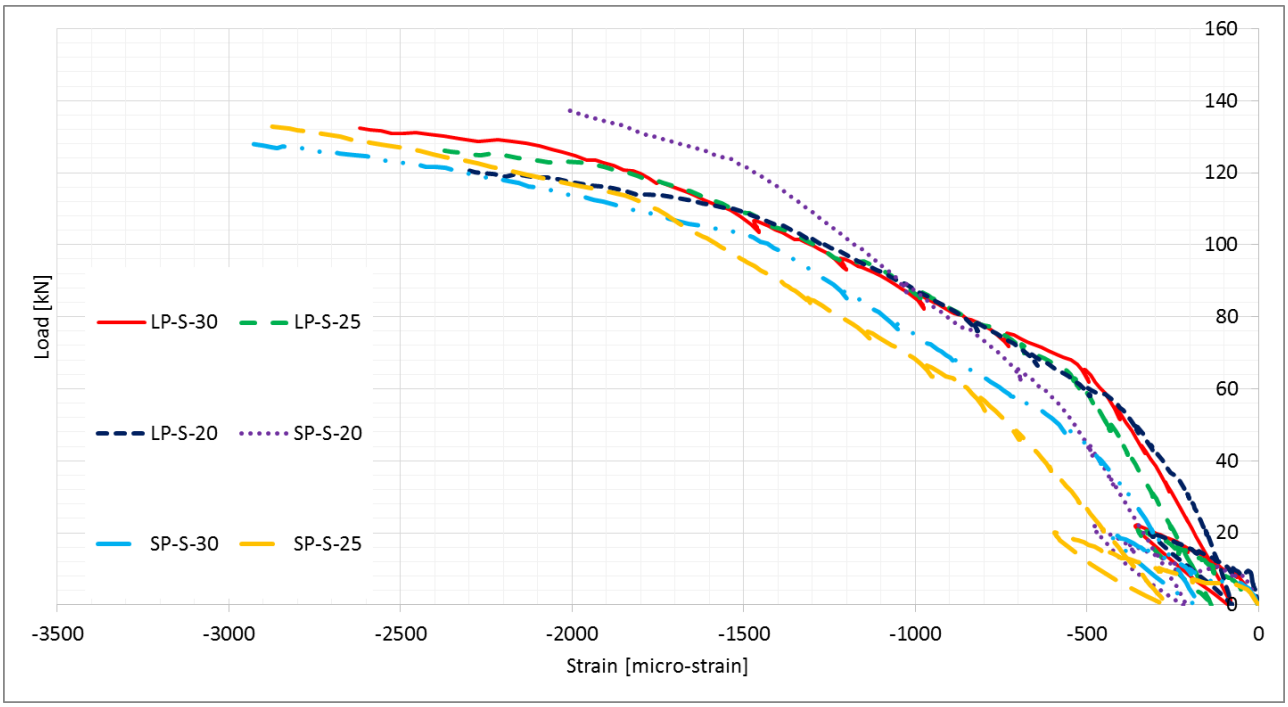

Figure 4-15 Compressive Strain in Concrete at Mid Span Under Load Point

4.4.3 Depth of Neutral Axis

Figures 4-16 to 4-18 show variation of depth of neutral axis with load in all slabs. It can be seen in all figures that the neutral axis is shifting towards the compression zone during cracking and ultimate failure phase. After installation of PCPs, prisms and internal pre-stressing forces helped slabs to maintain their stiffness after cracking of concrete which led to gradual relocation of neutral axis towards the tension zone. Finally when prisms cracked, the neutral axis again shifted towards the compression zone to keep equilibrium between tension and compression zones. Figure 4-16 represents change in the depth of neutral axis for slab LP-S-30. It can be seen during cracking phase that neutral axis shifted towards compression zone as load increased till cracking load of slabs at 20 kN. Neutral axis has moved towards tension zone after installation of PCPs due to increase in section area. However, application of PCPs could not compensate totally for cross-section cracks and did not bring neutral axis back to the first position before cracking of concrete.

Finally, after cracking of PCPs due to increase in applied load, neutral axis moved towards compression zone to keep equilibrium and concrete strain increased.

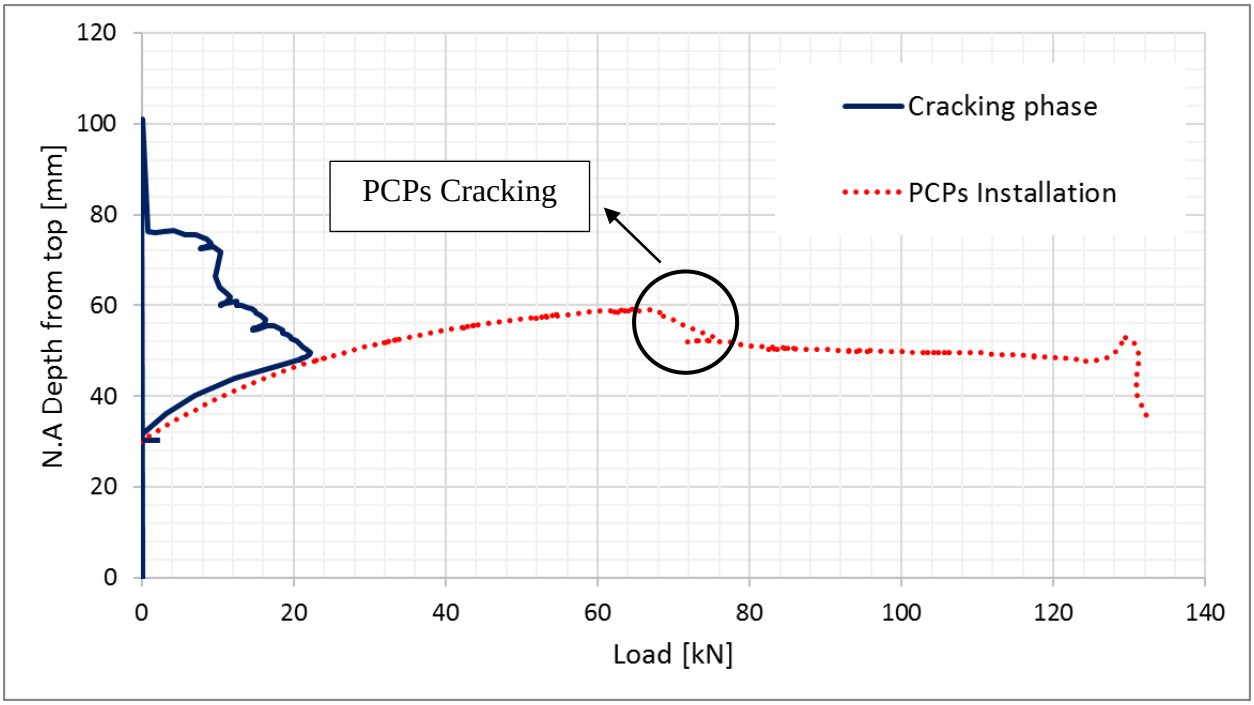

Figures 4-16 Change of Neutral Axis With Load in Slab LP-S-30

Figure 4-17 and 4-18 compare change in depth of neutral axis of slabs in two groups of slabs based on the dimension of PCPs. As can be seen in Figure 4-18 for slabs SP, the dramatic shift of neutral axis in the cracking phase is more visible in comparison to slabs LP due to the smaller cross section area provided by 35 x 35 mm prisms and consequently smaller area with higher modulus of elasticity of high strength concrete. This caused a considerable decrease in flexural stiffness of slabs repaired with small prisms which lead to larger deflection and wider crack widths as will be seen later. The neutral axis for slabs SP decreased rapidly after yielding of mild reinforcement. The drop in the depth of neutral axis that can be seen in Figure 4-18 for slab SP-S-20 at 100 kN corresponds to yielding of mild steel that is shown in Figure 4-11 for the same slab.

On the other hand, for both group of slabs, neutral axis shifted towards compression zone gradually after cracking of PCPs. It means the movement of neutral axis happened in two steps, one after cracking of concrete then after cracking of prisms. In addition, there was not a sudden change of neutral axis location after cracking of concrete and the transmission to next step where prisms cracked occurred gradually.

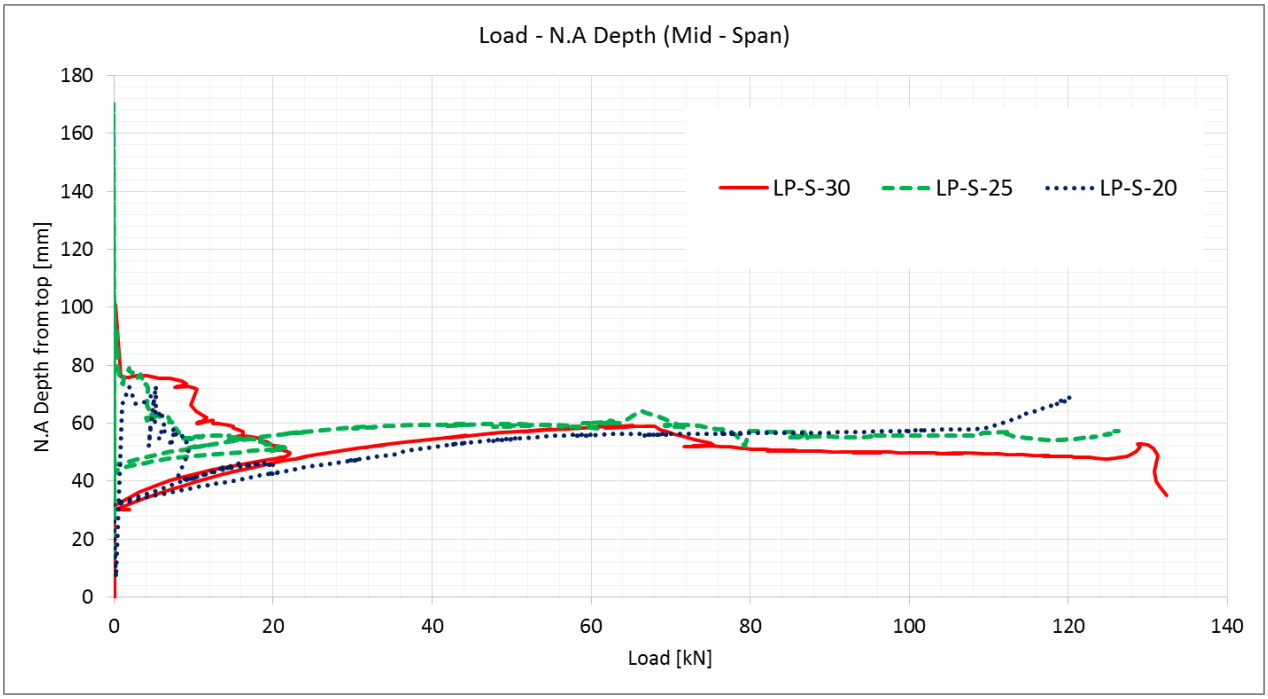

Figure 4-17 Change of Neutral Axis With Load in Slabs LP

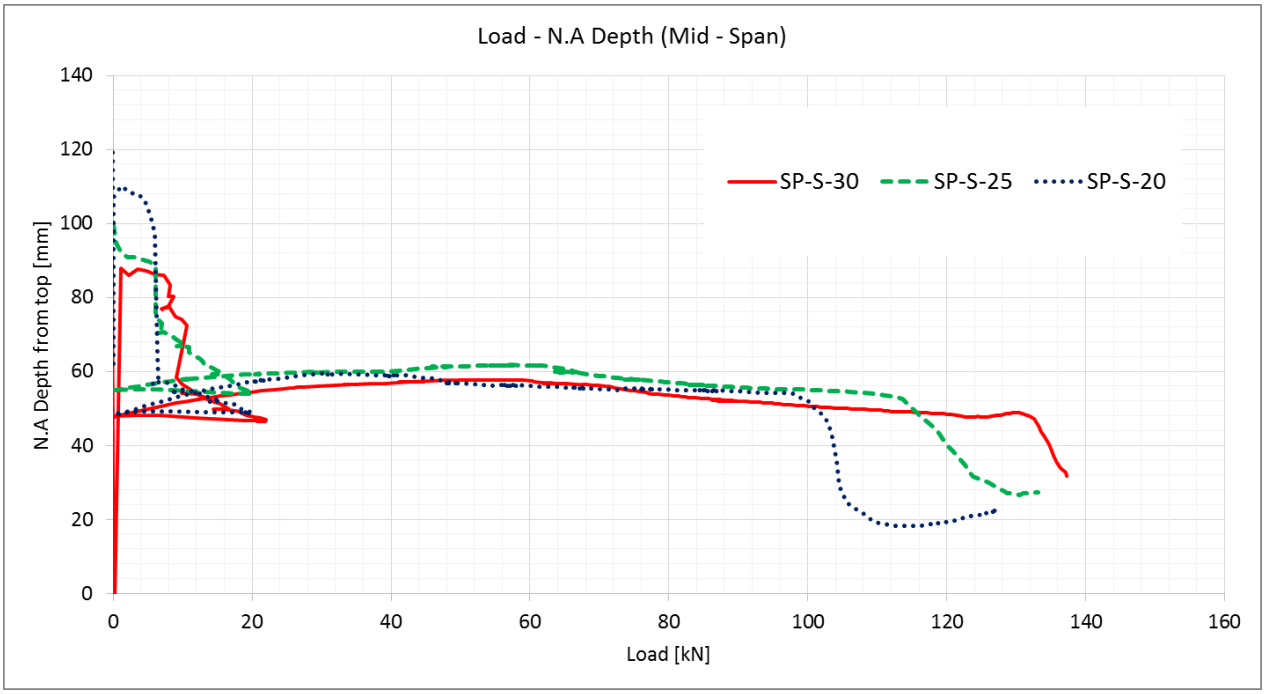

Figure 4-18 Change of Neutral Axis With Load in Slabs SP

4.4.4 Load-Deflection Response

Figure 4-19 provides load-deflection behavior for all slabs at mid span under load point and location of maximum bending moment. The figure contains the two loading stages of the slabs: the cracking phase before the installation of the prisms and the failure phase after installation of the prisms. It needs to be pointed out that prior to prism installation, the cross section of the slabs was 0.2% smaller, and as a result the original stiffness is smaller compared to the repaired slabs.

It can be seen that all slabs followed a general linear trend of load-deflection prior to cracking of concrete. After cracking of concrete and installation of PCPs, compared to the cracking phase, the initial stiffness increased due to the increase in the area of the slabs. For the slabs in group LP the effect of pre-stressing in the prisms can also be seen in the initial stiffness of the slabs. Load-deflection behavior remained linear after cracking of concrete at 20 kN without significant change of slope until cracking of the prisms at load levels of 50 kN to 65 kN. The non-linearity of the of load-deflection curve after cracking of PCPs is associated with the presence of mild steel reinforcement and their yielding at load levels from 100 to 139 kN for all slabs. Deflection increased at a faster rate after yielding of mild steel as a result of lower values of stiffness after prism cracking.

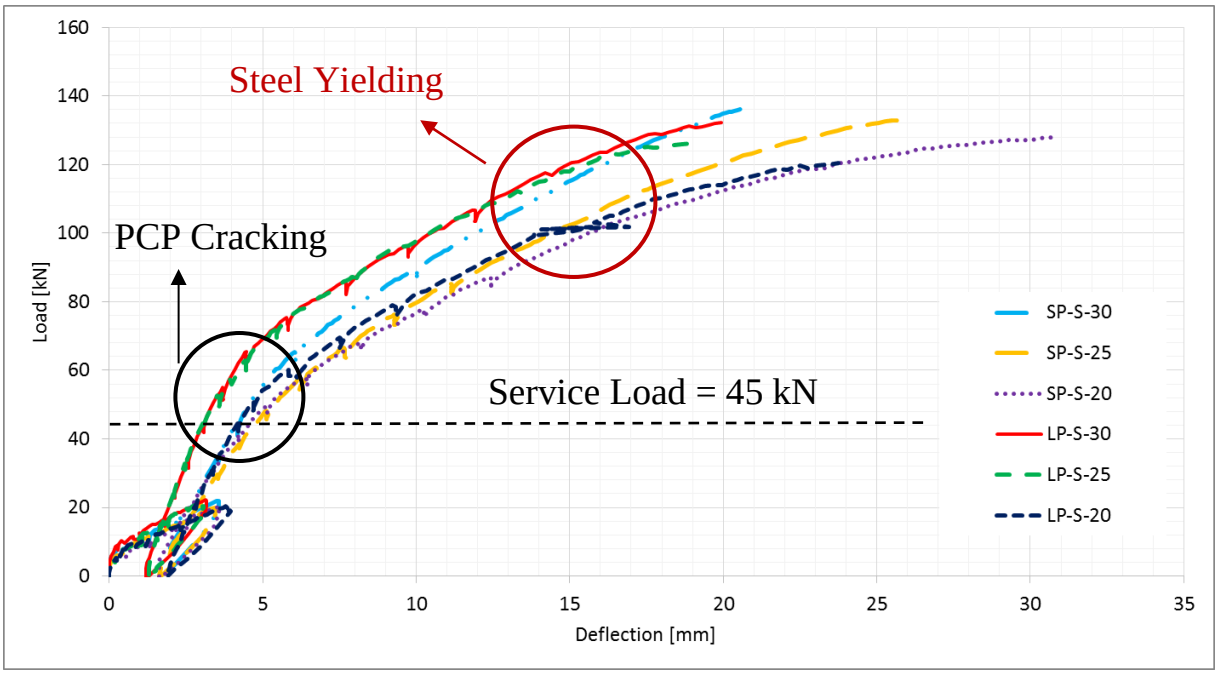

Figure 4-19 Load-Deflection at Mid Span Under Load Point

The yielding of steel reinforcement plays a main role for the non-linear relationship of load-deflection behavior after cracking of PCPs. The more ductile behavior of slabs SP-S-25 and SP-S-20 can be seen in the Figure 4-19 as steel reinforcement fully yielded in the two slabs and a plateau formed according to Figure 4-11. Table 4-2 summarizes the loads and deflections of the tested slabs at failure at mid span along with corresponding strain in the flexural reinforcement and extreme compressive strain in concrete.

Table 4-2 Ultimate Load, Deflection and Strain in Reinforcement and Concrete at Mid-Span

Slab	Failure Load (kN)	Deflection (mm)		Strain at Failure (10^{-6})	
		At Failure	At Service Load (45 kN)	Concrete	Steel
SP-S-20	128	30.78	4.63	2010	11091
SP-S-25	133.1	25.96	4.87	2907	8491
SP-S-30	137.3	21	4.28	2935	4103
LP-S-20	120.5	23.76	4.35	2299	3596
LP-S-25	126.3	19.23	3.06	2382	2279
LP-S-30	132.3	19.94	3.07	2620	2144

CSA A23.3-14 limits the maximum deflection of structural elements supporting or attached to non-structural elements likely to be damaged by large deflections to the value of $\frac{l_n}{480}$ where l_n is the clear span length. Based on the experimental results, deflection for all slabs needs to be below 4.8 mm to comply with restrictions provided by CSA A23.3-14. Except SP-S-25 which is slightly higher than the acceptable value of 4.8 mm, all other slabs have deflections that satisfy the CSA limit.

It is necessary to mention that in an elastic simply supported beam with point load at mid-span, the maximum deflection occurs under point load at mid-span at the location of maximum bending moment. This can be seen in Figure 4-20 to Figure 4-21 which demonstrates deflection profile of slabs strengthened using prisms with 30 kN pre-stressing level with respect to ultimate load.

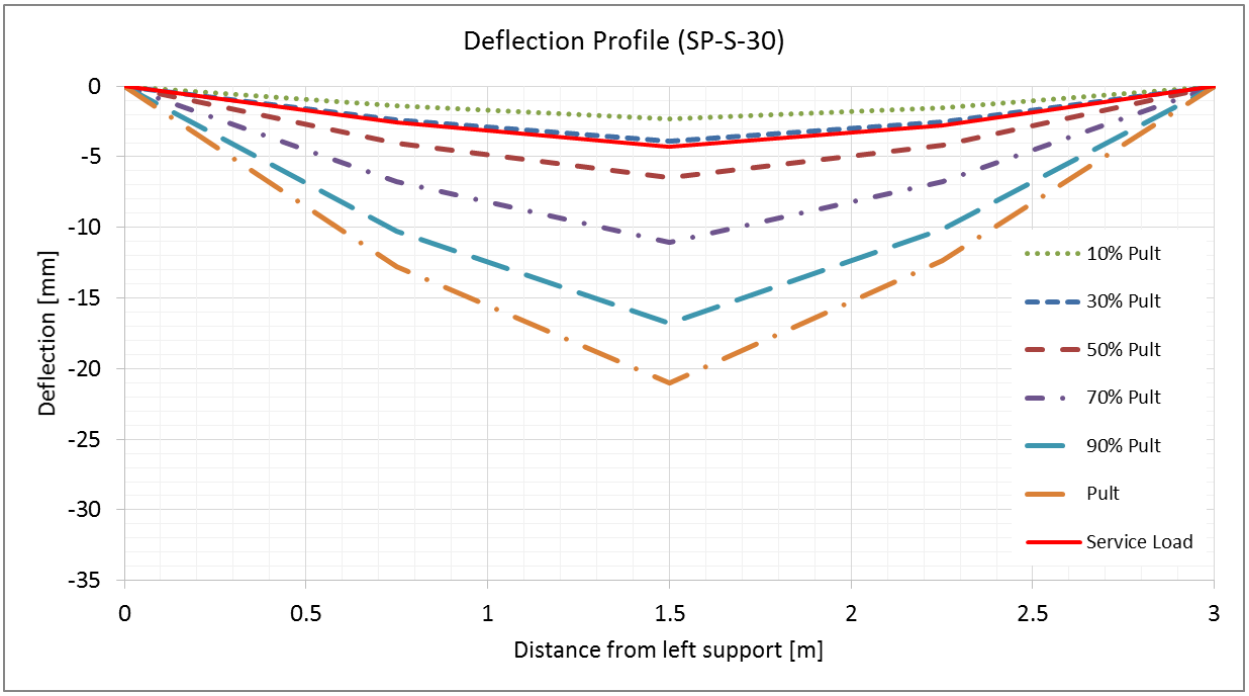

Figure 4-20 Deflection Profile of Slab SP-S-30 at Various Load Level

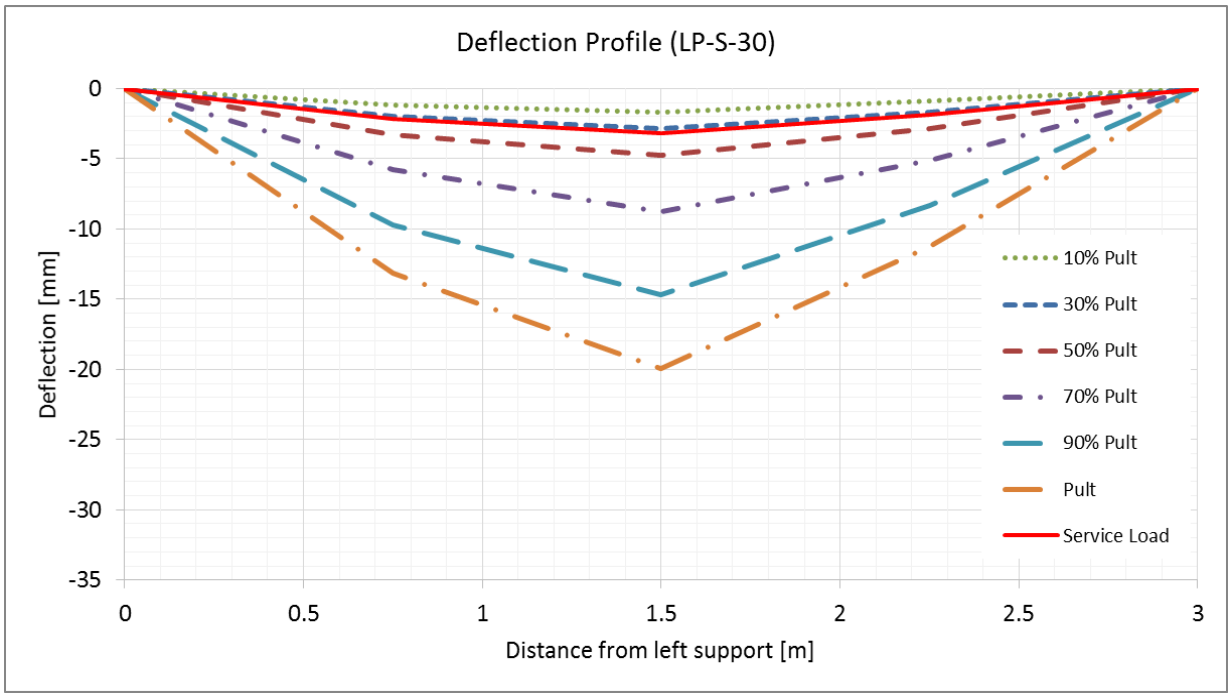

Figure 4-21 Deflection Profile of Slab LP-S-30 at Various Load Level

Deflection at any point in a simply supported slab can be calculated using the moment-area theorem. According to CSA A23.3-14 and CHBDC (CSA S16-14) the deflection of one-way reinforced concrete flexural members is calculated using effective moment of inertia (I_e) (Eq. 9.1, CSA A23.3-14). Table 4-3 tabulates deflection at mid span at different load levels in all PCP rehabilitated slabs. The larger deflection of slabs SP-S-20 and SP-S-25 at service and ultimate loads comply with higher strain values of these two slabs up to the failure. On the other hand, slabs LP-S-30 and LP-S-25 presented the least deflection at service load (15% of the ultimate deflection). Experimental and theoretical values of deflection at service load are within the permissible range of 4.8 mm (based on CSA A23.3-14) while as applied load increased a slight difference was observed between the two values. These variations could be due to the inelastic behavior of concrete after cracking and mild steel reinforcement after yielding whereas immediate deflections were computed by formulas for elastic deflection.

Load level	LP-S-20		LP-S-25		LP-S-30		SP-S-20		SP-S-25		SP-S-30	
	Deflection at mid span (mm)		Deflection at mid span (mm)		Deflection at mid span (mm)		Deflection at mid span (mm)		Deflection at mid span (mm)		Deflection at mid span (mm)	
	Theo	Exp	Theo	Exp	Theo	Exp	Theo	Exp	Theo	Exp	Theo	Exp
0.1 Pult	0.11	2.41	0.06	1.63	0.05	1.58	0.06	2.11	0.1	2.57	0.09	2.32
Service Load	4.60	4.35	4.60	3.06	4.60	3.07	4.60	4.63	4.60	4.87	4.60	4.28
0.3 Pult	4.53	3.72	4.64	2.66	4.69	2.88	4.79	4.05	5.04	4.43	5.05	3.9
0.5 Pult	11.90	6.7	12.06	4.56	12.14	4.65	12.3	7.33	12.70	7.58	12.72	6.5
0.7 Pult	18.52	10.76	18.72	8.33	18.82	8.76	19.02	13.16	19.53	12.87	19.56	11.16
0.9 Pult	24.64	17.46	24.90	13.82	25.02	14.84	25.25	21.24	25.89	19.87	25.92	16.8
Pult	27.61	23.76	27.90	19.23	28.03	19.94	28.29	30.78	28.98	25.96	29.02	21

Table 4-3 Calculated and Experimental Deflection at Mid-Span at Different Load Levels

4.4.5 Moment-Curvature Relationship

Figure 4-22 represents moment-curvature diagrams at mid span for all tested slabs until failure load. It was obtained using PI-gauges and strain gauges installed on the surface of concrete and steel reinforcement. A trend line representing strain compatibility was fitted to the strain values at different heights in the same cross-section. The slope of this strain profile represents the magnitude of curvature at the specified section and load level.

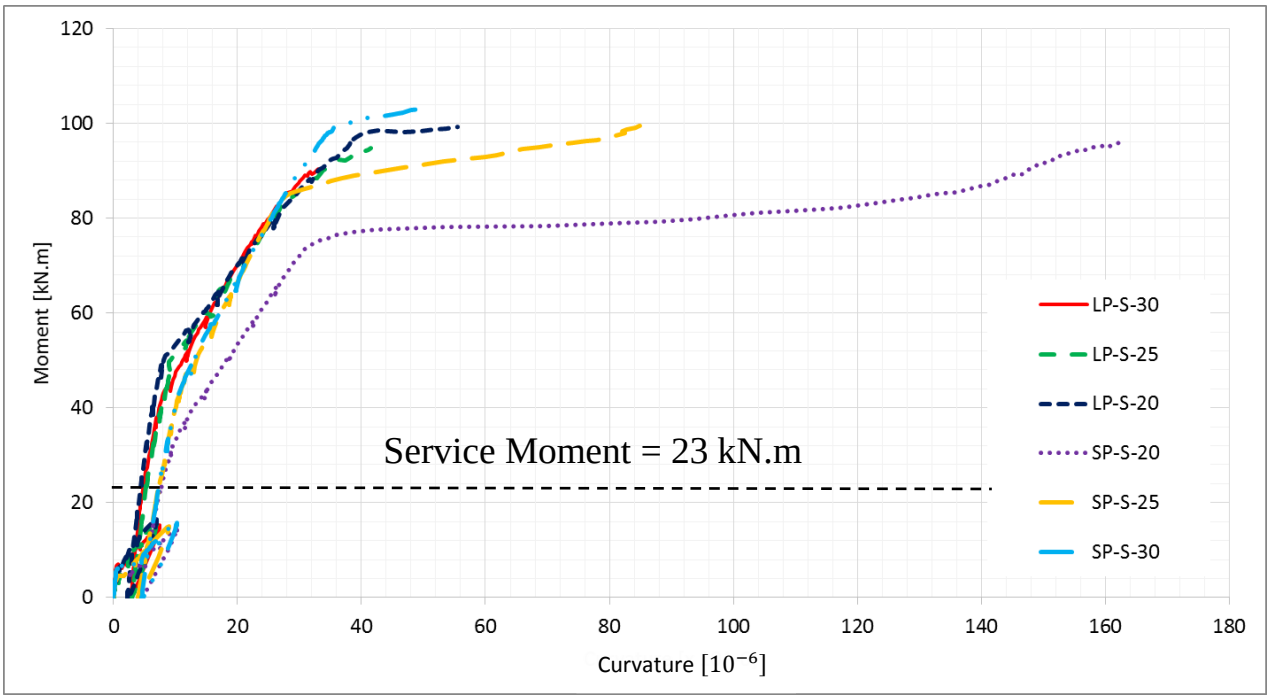

Figure 4-22 Moment-Curvature at Mid Span

As can be seen, moment-curvature for all slabs is trilinear after installation of PCPs with a change of slope at prism cracking and yielding of steel reinforcement. After cracking of concrete and installation of PCPs, the stiffness in all slabs increased slightly due to the presence of pre-stressing forces. Therefore, the moment of inertia remained close to that of an un-cracked slab. Nevertheless, after PCPs cracked in slab, stiffness was considerably reduced and effect of tension stiffening for

the PCPs diminished with increment in load. Furthermore, prior to failure, slabs LP-S-20 and SP-S-30 indicated moderate plateau while SP-S-25 and SP-S-20 experienced large plateau as a result of yielding and strain hardening phase in steel reinforcement before failure. On the other hand, slabs LP-S-30 and LP-S-25 showed stiffer behavior and lower curvature values due to higher pre-stress in PCP, which led to smaller deflection and narrower crack widths.

Figure 4-23 illustrates a comparison between theoretical and experimental moment-curvature relationships of all slabs. The theoretical values were obtained through the cross-sectional analysis using strain compatibility approach as discussed above while experimental results were extracted from experimental strain profile. It can be seen that good agreement exists between the theoretical and experimental test results.

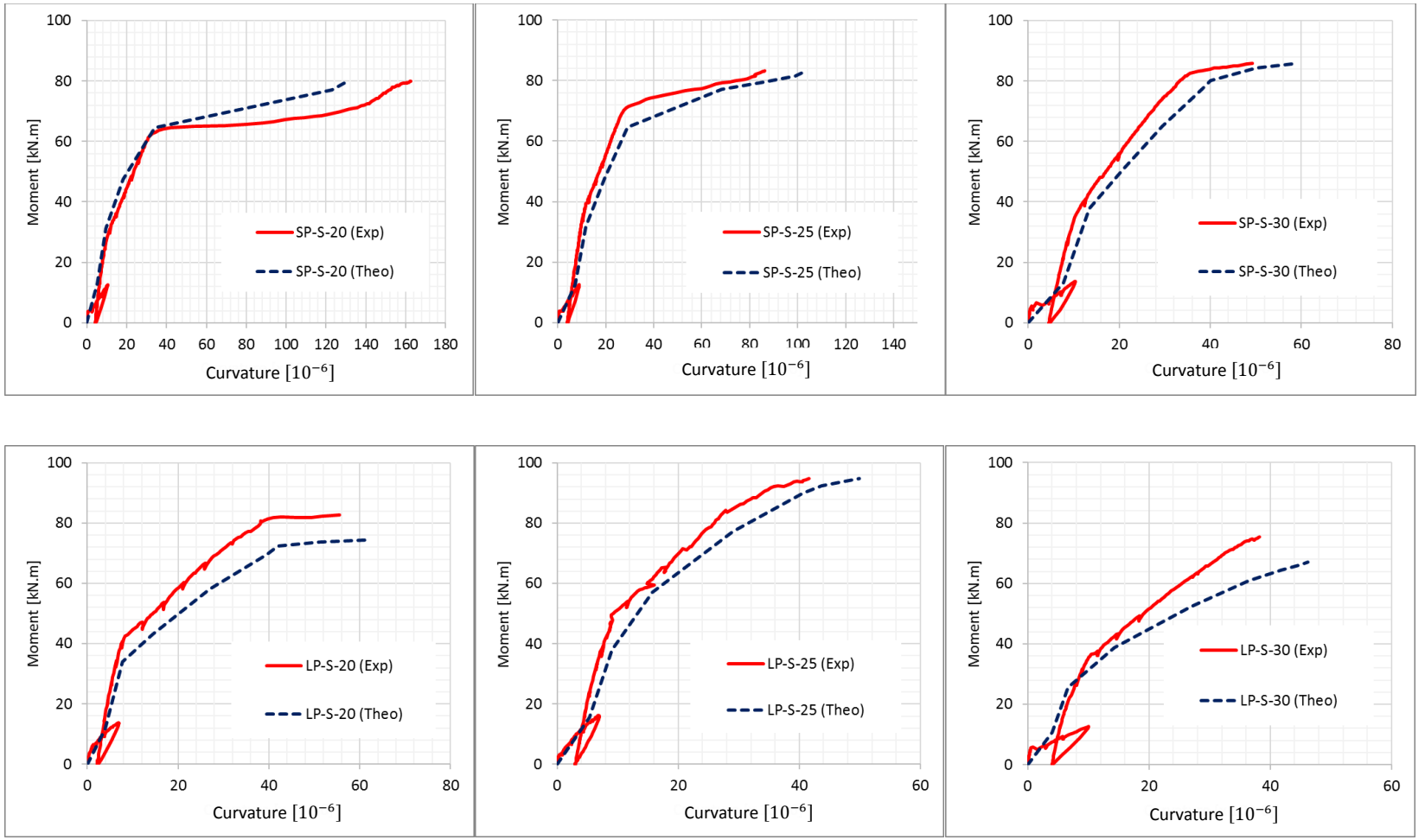

Figure 4-23 Experimental and Theoretical Moment-Curvature Comparison at Mid Span

4.4.6 Cracking Behaviour

Cracking started with the development of a few very fine vertical flexural cracks at the mid span. After increase in load, cracks initiated at quarter span and close to supports. Cracks were narrow and hairline before cracking of PCPs. After the prims cracked, cracks propagated in a faster rate and moved towards the compression zone. The initiation of wide cracks could be interpreted as an indication of excessive applied load on the slabs, if they are used in practice. As load increased, flexural vertical cracks turned to inclined cracks at location close to the end supports. These were locations where the cross section was reduced due to the fact that the embedded prisms were shorter than the opening that was created in the slab. The cracks then propagated towards load point and compression zone at top of the cross section. This was followed by the destruction of the bond between the PCPs and surrounding concrete at zones close to supports. Subsequently, several inclined cracks widened in the area close to the section where PCPs started, and slabs failed.

At ultimate load, slabs LP-S-30 and SP-S-30 presented the least numbers of cracks after failure due to the higher pre-stressing force provided by the presence of the PCPs in the cross section.

Crack spacing was measured using a tape measure with accuracy of ±1 mm in all tested slabs over the cracked zone. Table 4-4 provides the average crack spacing and numbers of formed cracks along the length of all slabs.

Table 4-4 Average Crack Spacing in All Slabs

Slab	**Number of Cracks**	**Average crack spacing [mm]**
SP-S-20	15	128
SP-S-25	14	132
SP-S-30	11	141
LP-S-20	14	130
LP-S-25	14	135
LP-S-30	12	148

Generally crack spacing is directly related to transfer length of the reinforcement while inversely related to the bond strength. In other words, longer crack spacing means longer transfer length and weaker bond mechanism between reinforcement surface and concrete. Based on the experimental values in Table 4-4, all slabs showed roughly similar crack spacing and a number of cracks which demonstrates the same transfer length and bond mechanism for all of them. However, slabs reinforced with higher pre-stressed PCPs showed fewer numbers of cracks and longer average crack spacing. Higher pre-stressing force provides more axial compression to the slab and consequently reduced number of cracks in slabs LP-S-30 and SP-S-30 compared to other tested specimens.

Steel reinforcement typically provides excellent contact surface area with concrete and proportionally sufficient bond strength due to its deformed shapes and mechanical interlock with concrete. On the contrary, prisms have smooth surface area, although their large cross-section area compared to the other types of reinforcements, compensates for their smooth surface and provides satisfactory bond with concrete.

Figure 4-24 illustrates development of maximum crack width at mid span with an increase in load for all six tested slabs. LP-S-30 had the narrowest crack both prior to the cracking of PCPs at 50% of ultimate load and afterwards. SP-S-20 showed the widest crack through the entire test among all other tested slabs with maximum crack width of 2.3 mm. The load-crack width behavior for slab LP-S-20 is not available due to an error during installation of Pi-gauges. Figure 4-25 shows maximum crack width for all six slabs after rehabilitation. The largest crack width were in slabs SP-S-20, SP-S-25 and the smallest in slab LP-S-30. This indicates that larger pre-stressing load and prism size was corresponding to smaller final crack width.

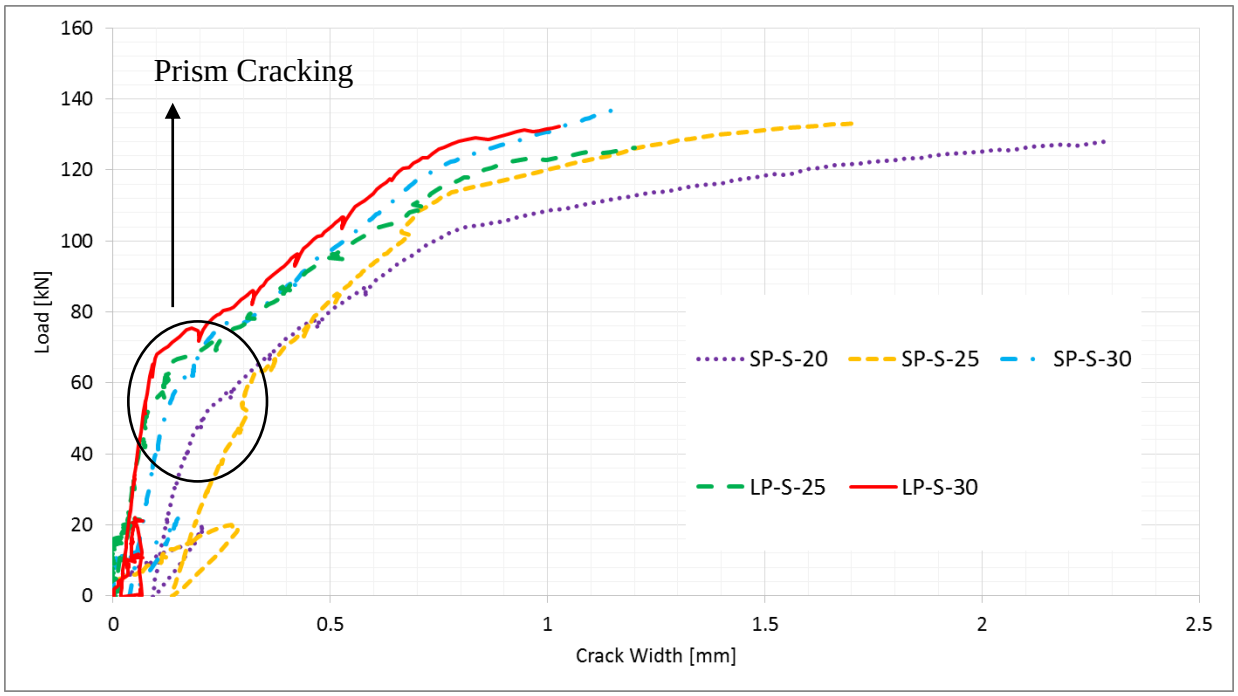

Figure 4-24 Maximum Crack Width at Mid-Span

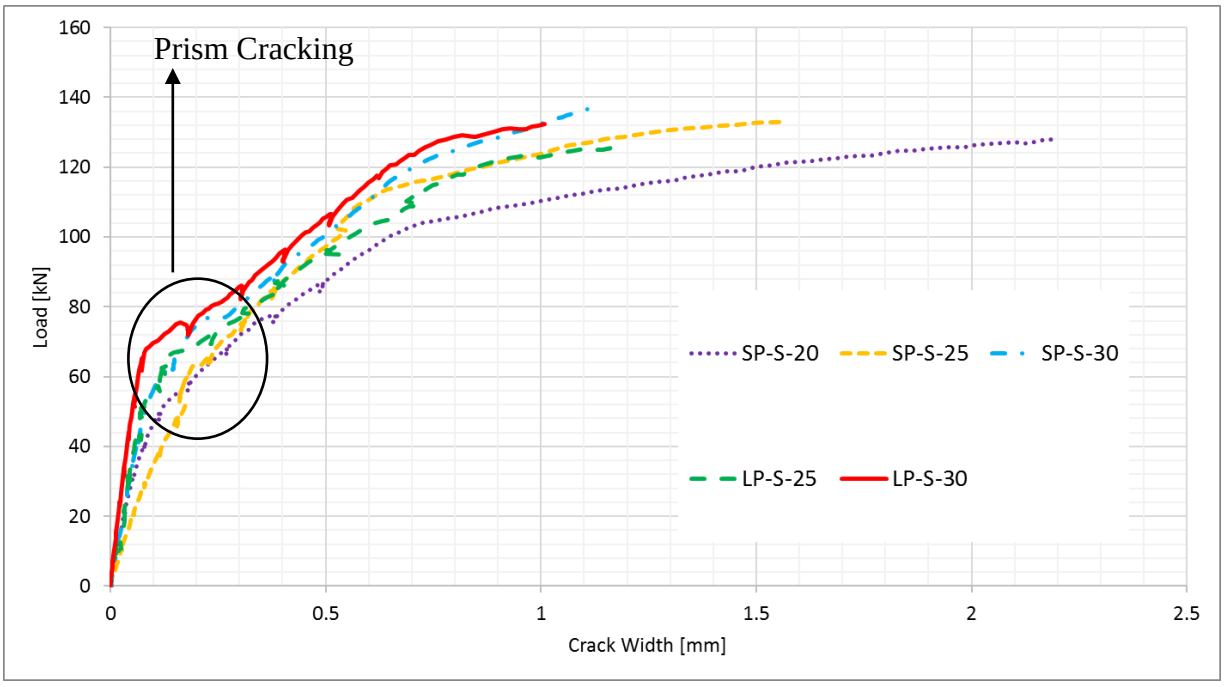

Figure 4-25 Maximum Crack Width at Mid-Span after PCPs Installation

Strain in flexural reinforcement and curvature in slabs LP repaired with 50 mm prisms were smaller compared to the slabs SP with 35 mm prisms. Hence, narrower crack widths formed in slabs LP-S-30 and LP-S-25 respectively before cracking of the PCPs. Load-cracking behavior is trilinear for all slabs with change of slope at prisms cracking and yielding of steel. Appearance of cracks in the slabs did not change stiffness considerably. In other words, cracks in the slabs were not visible, and the existing cracks in the slabs were not widening prior to the cracking of PCPs. Strain in flexural reinforcement and curvature in cross sections increased rapidly after cracking of the prisms at loads equal to 50 to 65 kN which permitted cracks to propagate and widen at a faster rate. This remarkable increment in crack widths after cracking of PCPs at load levels from 50 kN to 65 kN is shown in Figure 4-24.

Propagation of cracks in PCPs as well as increment in crack width after cracking of prisms was an indicator of failure and provided enough warning before failure. It could be considered as a significant advantage of using PCPs for rehabilitation of cracked concrete bridge decks.

Figure 4-26 and 4-27 show crack width at mid span for slabs SP-S-30 and LP-S-30 during cracking and failure phases separately. The results are tabulated for all slabs in Table 4-5. It can be seen that at cracking load level of 20 kN, cracks were wider before installation of PCPs, however after rehabilitation, at the same load level of 20 kN the cracks were narrower. In fact, after application of PCPs, the total slab stiffness increased and pre-stress force in the prisms provided sufficient axial compression for the surrounding concrete in the slabs to arrest further crack propagation until higher load levels at which the prisms themselves cracked.

Table 4-5 Comparison of Crack Width at Mid-Span Before and After Installation of PCPs

Slab	W_{cr1} **(mm)***	W_{cr2} **(mm)****	$P_{W_{cr1}}$ **(kN)**	$P^{R}_{W_{cr1}}$**(kN)*****	$(W_{cr})_{all}$ **(mm)******
SP-S-20	0.21	0.12	20.14	50.01	0.18
SP-S-25	0.27	0.19	20	44.34	
SP-S-30	0.14	0.07	21.9	57.9	
LP-S-20	N/A	N/A	N/A	N/A	
LP-S-25	0.05	0.03	21.66	35.35	
LP-S-30	0.05	0.04	22.15	33.6	

* W_{cr1} (mm): crack width before installation of prisms

** W_{cr2} (mm): crack width after installation of prisms

*** $P^{R}_{W_{cr1}}$ (kN): load during failure phase when crack width was equal to W_{cr1}

**** $(W_{cr})_{all}$ (mm): permissible crack with according to Table 2-1

Table 4-5 expresses that after installation of PCPs in slabs, stiffness for all six slabs increased and cracks propagated in a slower rate compared to the cracking phase. For instance, crack width for slab SP-S-20 at cracking phase at load level of 20 kN was 0.21 mm while after installation of PCPs the same width of cracks occurred at load level of 50 kN. The same cracking behavior and pattern was observed for other slabs. It can be seen that all crack widths are within permissible limit.

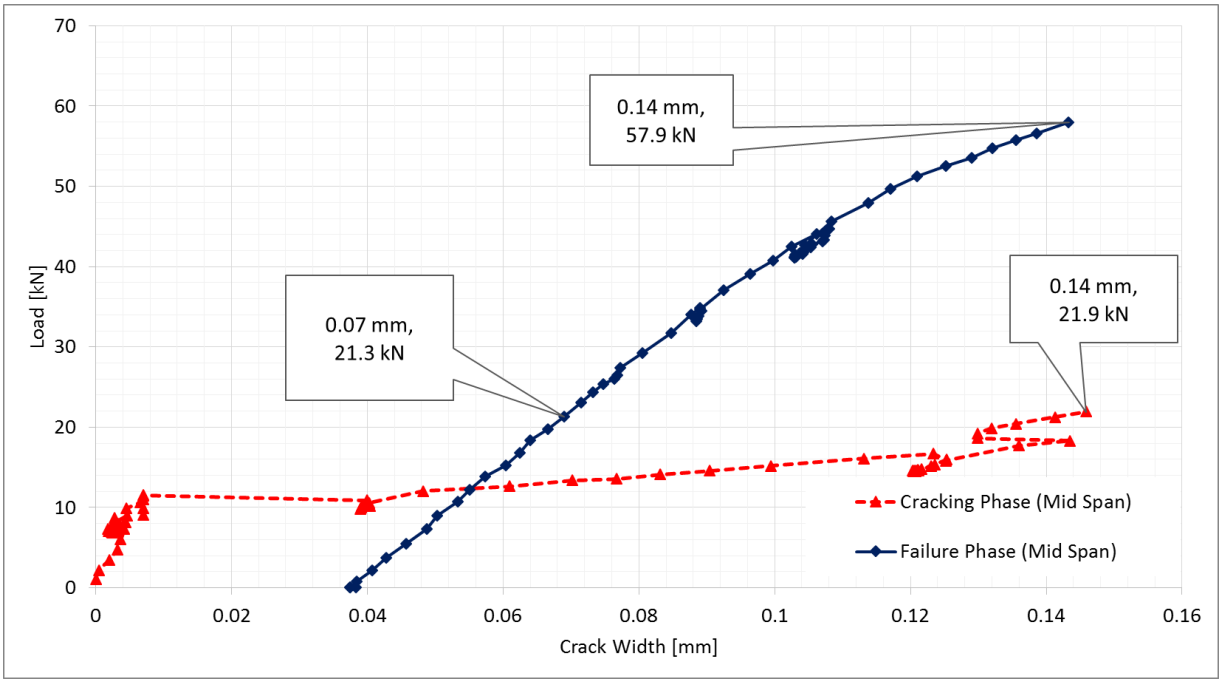

Figure 4-26 Comparison of Crack Width at Mid-Span Before and After Installation of PCPs in Slab SP-S-30

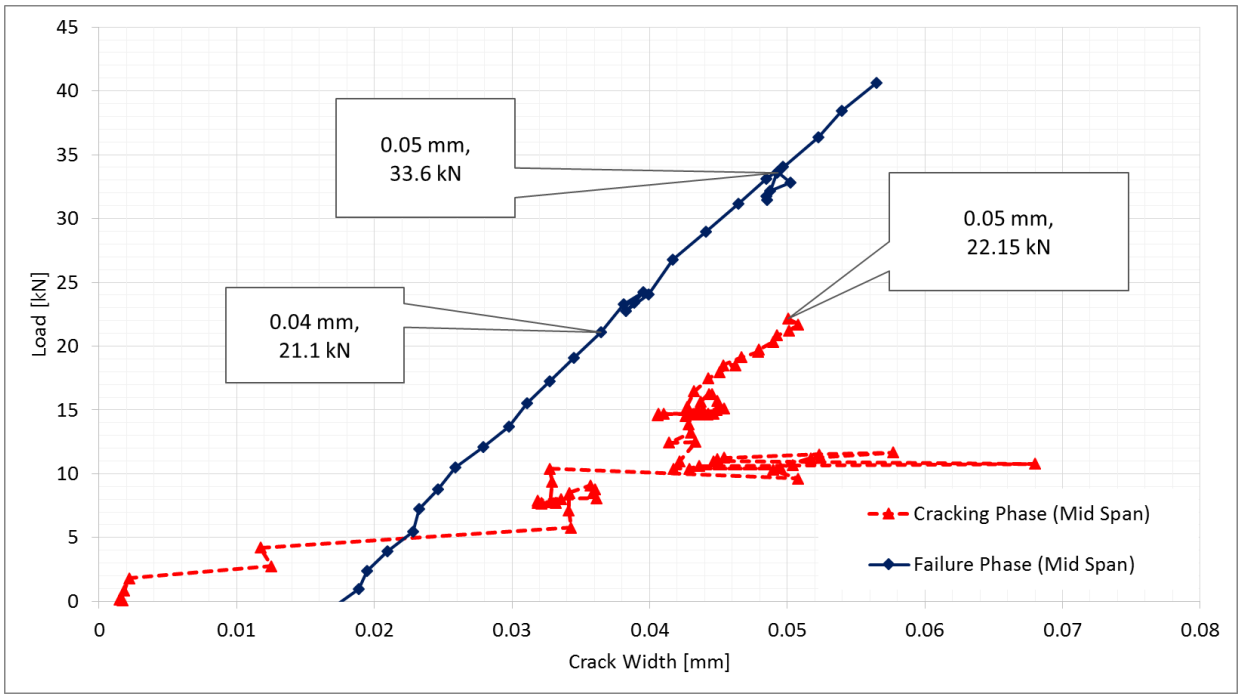

Figure 4-27 Comparison of Crack Width at Mid-Span Before and After Installation of PCPs in Slab LP-S-30

Figures 4-28 to 4-33 represent a comparison between calculated and measured crack width at mid-span where maximum bending moment occurred for all tested slabs in failure phase after installation of PCPs. For slab LP-S-20 in Figures 4-31 experimental results are missed due to malfunction of installed PI-gauges and only calculated values are demonstrated. Theoretical crack widths were computed according to CSA A23.3-14 which is based on Gergely-Lutz equation, Kaar-Mattock proposed relationship and crack-width model suggested by Frosch (Ralph J. et al. (2003)) provided in Chapter 2 in equations 2-1 to 2-3 respectively . For calculation of f_s as stress in the reinforcement at any specified load level, for cracking phase reading from strain gauges applied on mild steel reinforcements were used. After installation of PCPs in failure phase, reading from strain gauges on seven-wire steel strands inside PCPs were used to compute theoretical values.

A good agreement exists between calculated and experimental crack widths as shown in Figures 4-28 to 4-33. In all specimens, theoretical crack widths are insignificantly larger than measured results during tests due to effect of pre-stress forces provided by PCPs. On the other hand, Frosch and Gergely-Lutz equations both predicted quite similar values of crack-widths at mid span for all tested slabs as is evident in Figures 4-28 to 4-33.

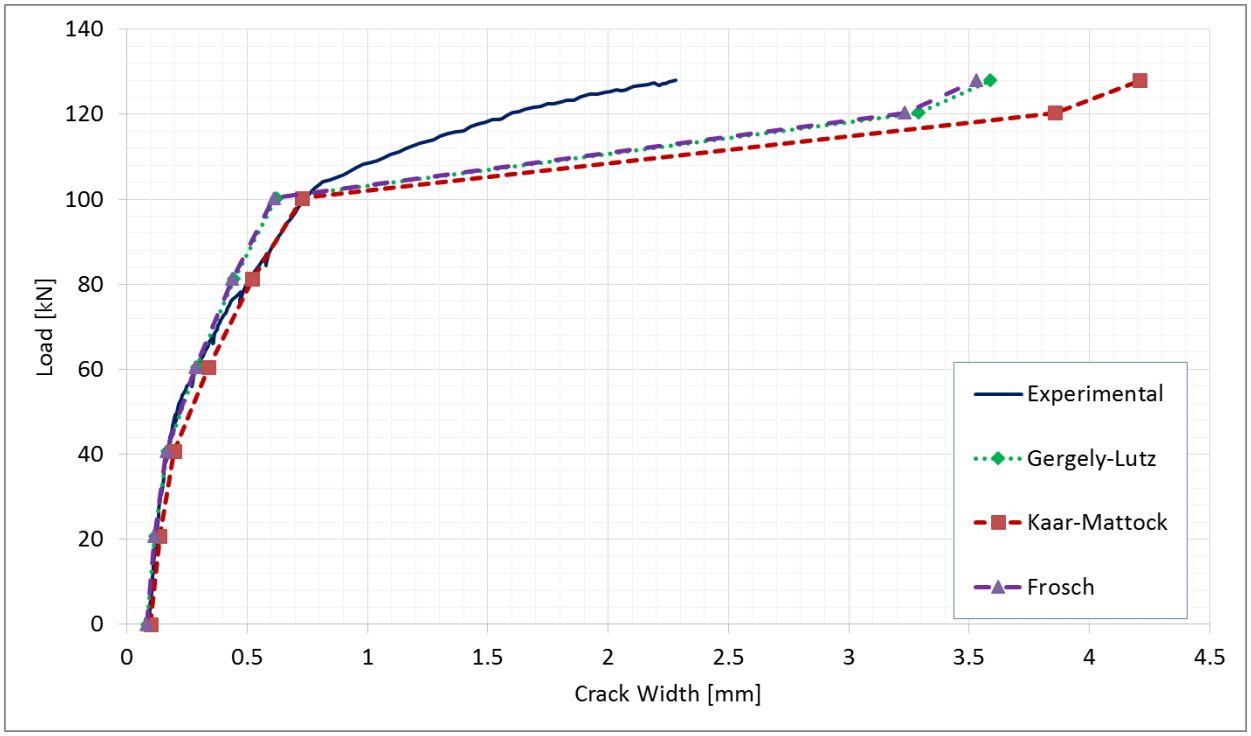

Figure 4-28 Comparison of Calculated and Measured Crack Width at Mid-Span in Slab SP-S-20 (Failure Phase)

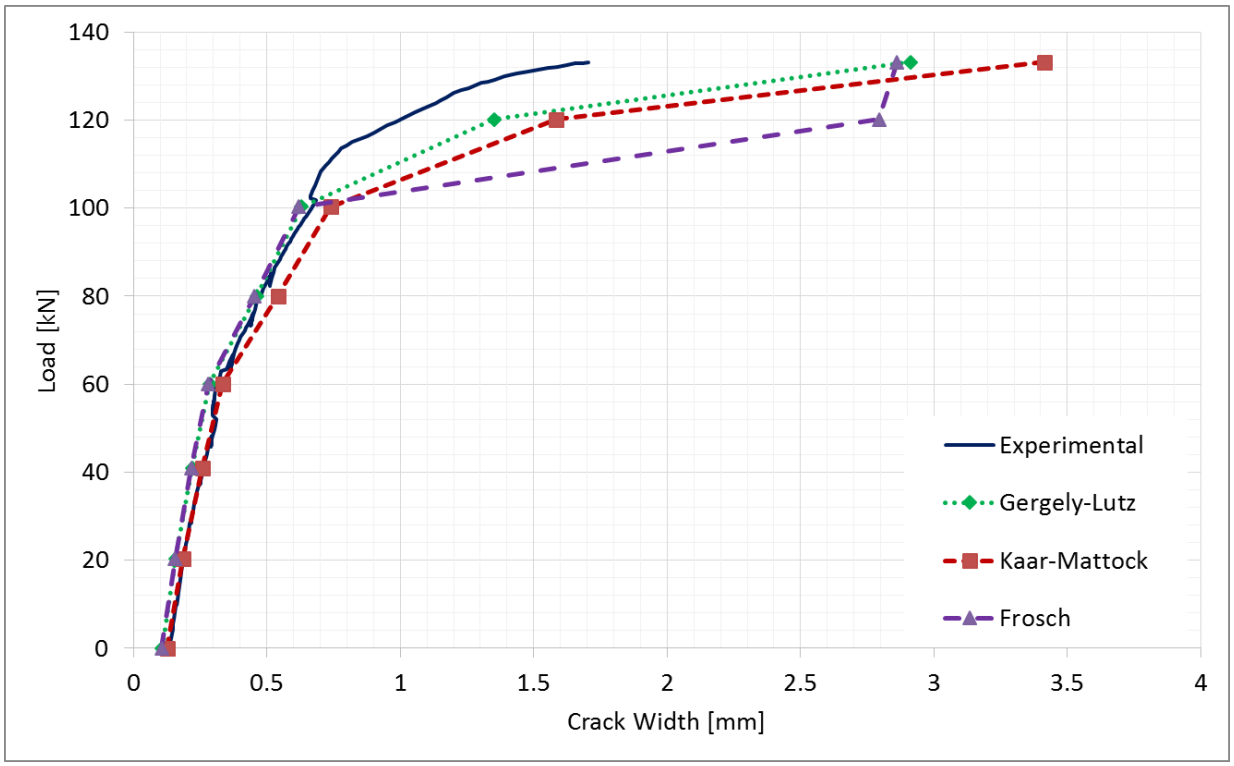

Figure 4-29 Comparison of Calculated and Measured Crack Width at Mid-Span in Slab SP-S-25 (Failure Phase)

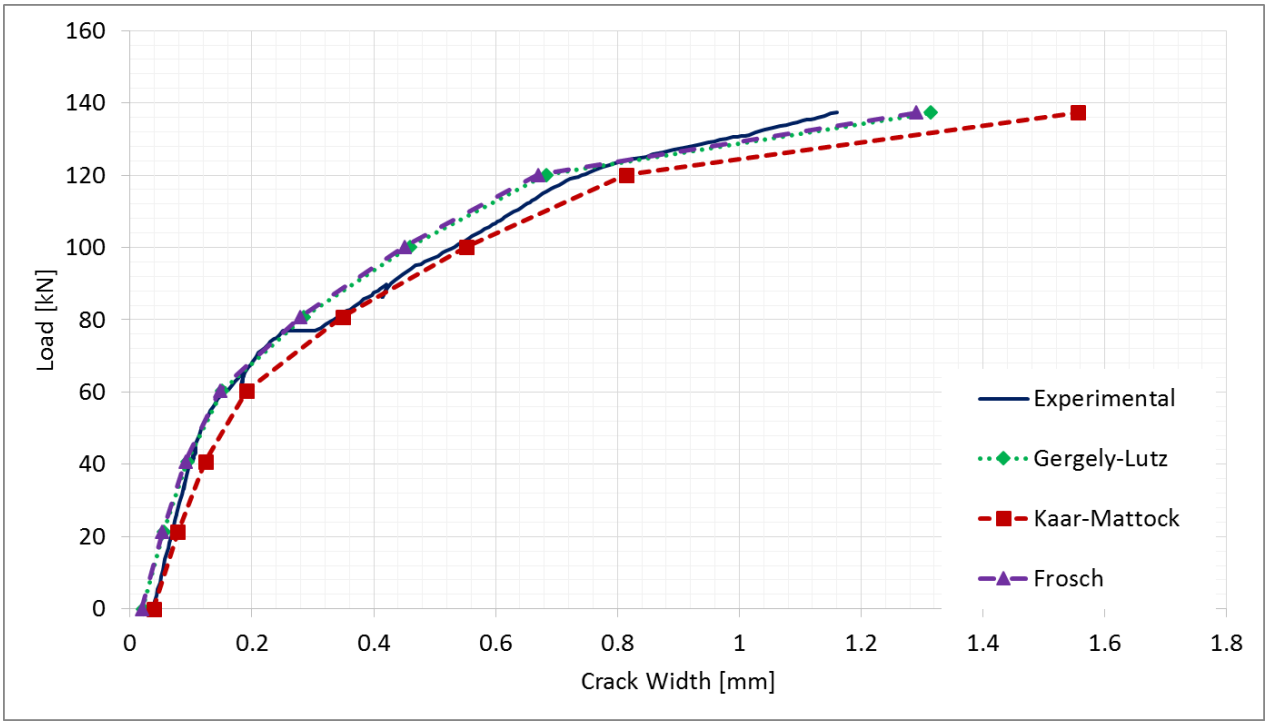

Figure 4-30 Comparison of Calculated and Measured Crack Width at Mid-Span in Slab SP-S-30 (Failure Phase)

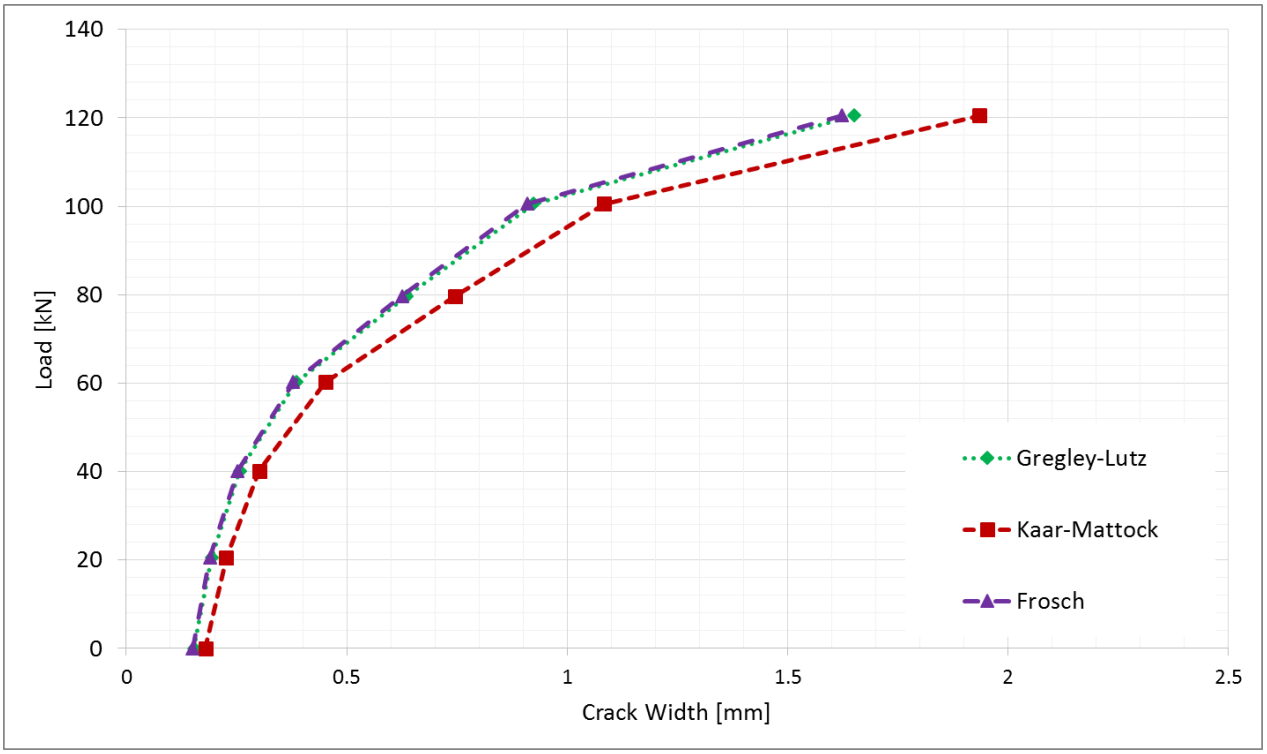

Figure 4-31 Comparison of Calculated and Measured Crack Width at Mid-Span in Slab LP-S-20 (Failure Phase)

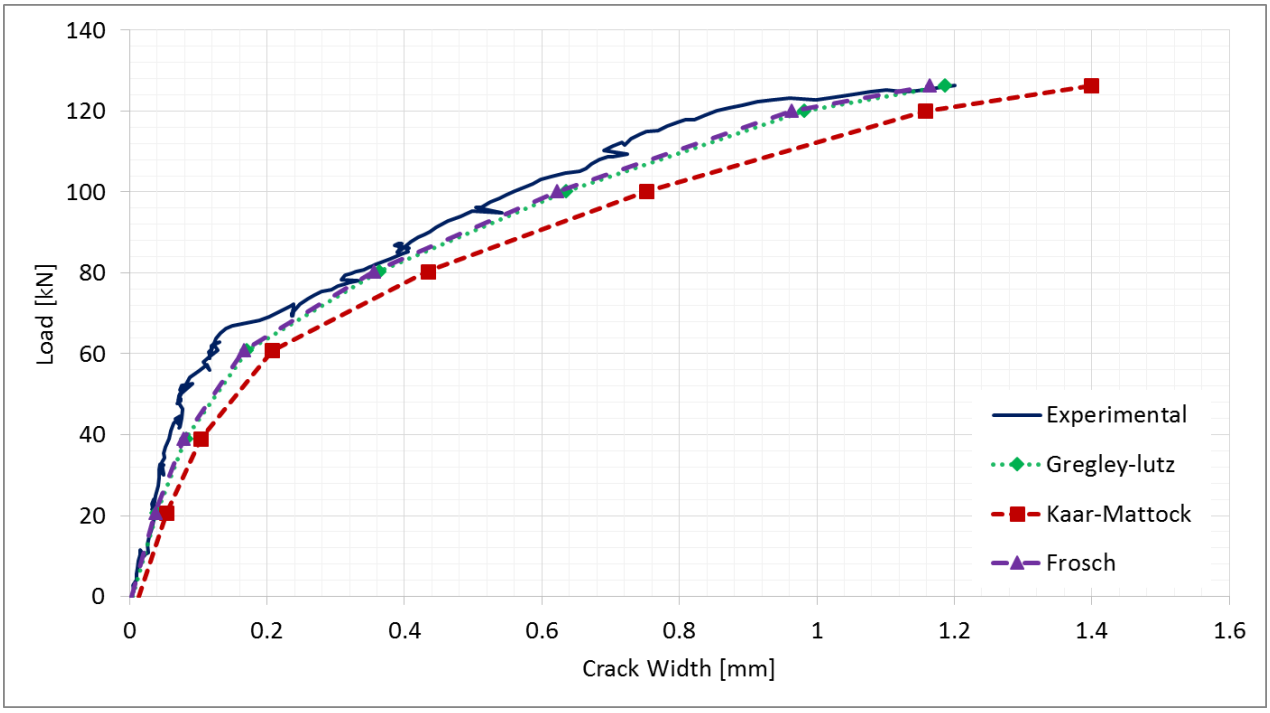

Figure 4-32 Comparison of Calculated and Measured Crack Width at Mid-Span in Slab LP-S-25 (Failure Phase)

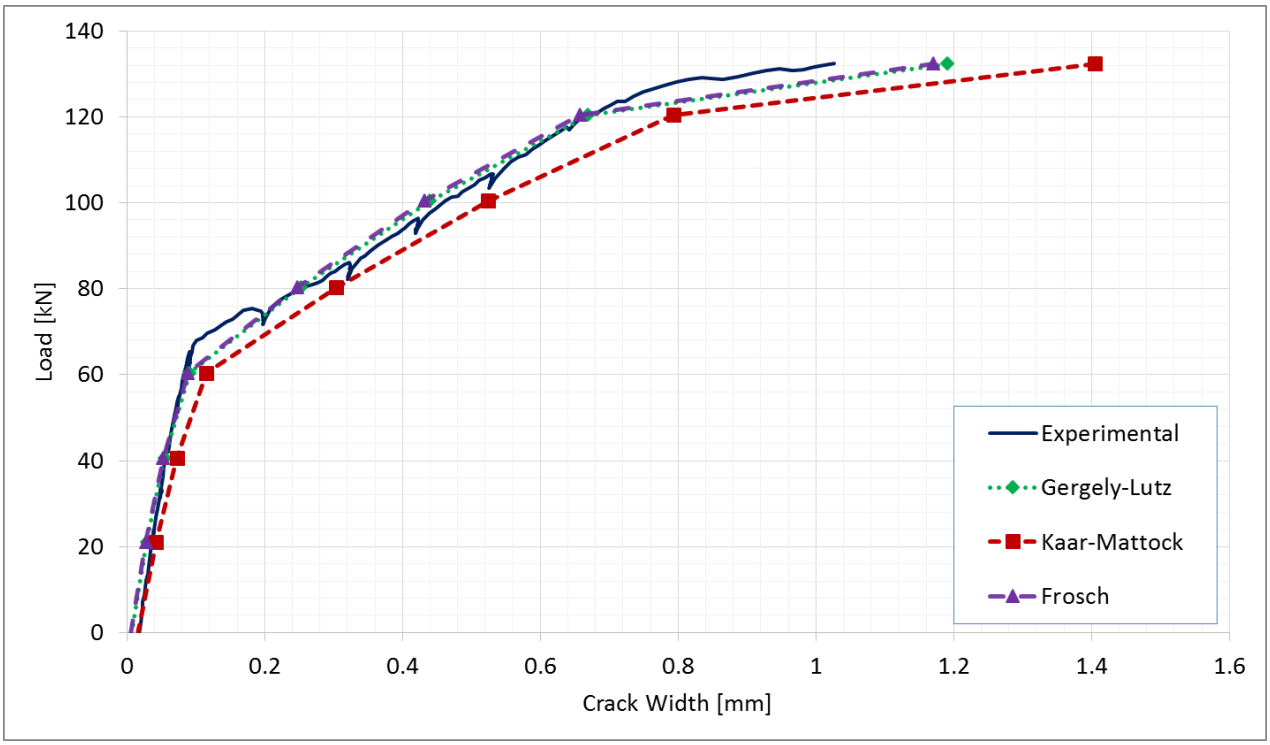

Figure 4-33 Comparison of Calculated and Measured Crack Width at Mid-Span in Slab LP-S-30 (Failure Phase)

Chapter 5

Summary, Conclusions and Recommendations

5.1 Summary

This section summarizes the experimental program followed by conclusions and recommendations for future works. This research program was conducted to investigate the performance and efficiency of steel PCPs as a repair technique for cracked reinforced concrete one-way slabs. Six full scale one-way slabs were tested under three-point bending until failure to inspect their deflection, crack width and flexural strength. The initial design of all six slabs was similar while each group of three slabs was strengthened via PCPs with different cross-section area and pre-stressing level. The prisms were cast with high strength concrete and had cross-sectional area of 50 x 50 or 35 x 35 mm. PCPs were all pre-stressed concentrically by 9 mm diameter seven-wire strands with effective pre-stressing load in the range of 20 kN to 30 kN. Table 5-1 provides a summary of all tests and number of specimens for each test.

Table 5-1 Summary of All Tests and Number of Specimens

Sample Type	**HSC Cylinders**		**Slabs**		**PCPs**
Test/Sample Type	Uniaxial Compression	Tension Splitting	LP	SP	Prism
Number of Samples	72	36	3	3	48
Total number of Samples	108		6		48

5.2 Conclusions

The following section summarizes conclusions of this research program.

1. High strength concrete developed most of its compressive and tensile strength during the first week after casting. For current research study, concrete compressive strength reached almost 80% of its strength after 7 days. The same behaviour was observed for tensile strength development of high strength concrete.
2. The maximum applicable pre-stress force for PCPs at jacking is governed by the size of prisms and the properties of concrete.
3. Higher pre-stressing levels in PCPs increase the prism cracking load and improve behavior of slabs reinforced with these PCPs at service load.
4. No slip was observed between seven wire steel strands in the prism and between the PCPs and slabs.
5. There was no appearance of bond failure between slabs and all twenty four embedded PCPs along the length of the slabs throughout testing however, some bond cracks were created at failure at the level of PCPs.
6. The moment-curvature relationship for all slabs rehabilitated with PCPs showed a trilinear behavior.
7. Moment-curvatures calculated using strain compatibility analysis represented good compliance with experimental data.
8. After installation of PCPs, stiffness in all slabs increased slightly due to the presence of pre-stressing forces. Following PCPs cracking, stiffness reduced considerably.

9. The load-deflection behavior of all slabs in failure phase was bilinear with a change of stiffness at prism cracking. It can be seen that all slabs followed a general linear trend of load-deflection prior to cracking of concrete.
10. After cracking of concrete and installation of PCPs, compared with cracking phase, initial stiffness before cracking load of 20 kN increased due to the pre-stressing force and adding of PCPs. Load-deflection behavior remained linear after cracking of concrete without significant change of slope until cracking of prisms.
11. Slabs strengthened with larger prisms and higher pre-stressing level experienced smaller values of deflection.
12. After prism installation, concrete cracks were hairline before initiation of cracking in prisms and did not grow to pass the prisms level. The crack width decreased as the pre-stressing level increased in PCP.
13. The commencement and propagation of cracks in prisms could be considered as an indication of excessive loads on structural members which could be sign of approaching failure.

5.3 Recommendations for Future Research

1. The behaviour of slabs strengthened with PCPs under cyclic loading should be investigated to predict their response if they were used in structures that are subjected to cyclic loading such as bridges.
2. The behaviour of PCP rehabilitated slabs with various types of PCP cross section, pre-stressing level and reinforcement ratio needs to be explored further.

References

1. "AASHTO LRFD Bridge Design Specifications," 2nd Edition. (1998). (pp. 5-40). Washington, D.C: American Association of State Highway and Transportation Officials.

2. (DOT), U. D. (1997). *Bureau of Transportation Statistics.* Transportation Statistics Annual Report.

3. ACI 318-02. (2002). *Building Code Requirements for Reinforced Concrete.* ACI, Detroit, Michigan, U.S.A.

4. ACI Committee 363 . (1984). *State-of-the Art Report on High-Strength Concrete* (pp. 364-411). ACI Structural Journal.

5. Ahmad, S, & Shah, S.P. (1985). Structural Properties of High Strength Concrete and its implications for precast Prestressed Concrete. *PCI Structural Journal, 30,* 92-119.

6. Akter Hosen, Mohd Zamin Jumaat, Mahfuz Ud Darain, Obaydullah, & Saiful Islam. (2014). Flexural Strengthening of RC Beams with NSM Steel Bars. *nternational Conference on Food, Agriculture and Biology (FAB-2014).* Kuala Lumpur (Malaysia).

7. Almusallam, T. e. (2013). Experimental and numerical investigation for the flexural strengthening of RC beams using near-surface mounted steel or GFRP bars. *Construction and Building Materials, 40,* 145-161.

8. Al-Obaidi, S. (2015). *Behavior of Reinforced Concrete Beams Retrofitd in Flexure Using CFRP-NSM Technique.* Phd thesis, Portland State University.

9. Asplund, S. (1949). Strengthening bridge slabs with grouted reinforcement. *in ACI Journal Proceedings*.

10. Attard, M.M, & Setunge, S. (1996). Stress-strain Relationship of Confined and Unconfined Concrete. *ACI Materials Journal, 93,* 432-442.

11. Banthia, V. M. (2003). Transverse Confinement of Deck Slabs by Concrete Straps. *Proceedings of the 6'h International Symposium on 2t9 Fiber-Reinforced Polymer Reinforcement for Concrete Structures, FRPRCS-6,* 945-954.

12. Beber, A. J, Filho, A. C, & Campagnolo. (n.d.). CFRP in the strengthening of reinforced concrete beams. *Proceedings of the International Conference on FRP Composites in Civil Engineering,* (pp. 391-398). Hong Kong, China.

13. Benmokrane, B., & Wang, P. (2001). *Durability of FRP composites in civil engineering infrastructure applications.* American Concrete Institute.

14. Berg, R.G, & Ost, B.W. (1994). Engineering Properties of Commercially Available High-Strength Concrete. *PCA R&D Serial No.1914*.

15. BioLzi, L, Guerrini, G.L, & Rosati, G. (1997). Overall Structural Behaviour of High Strength Concrete Specimens. *Construction and Building Materials, 11*, 57-63.

16. Bishara, 4. M. (1971). Continuous Beams with Prestressed Reinforcement. *ASCE Structural Journal, 97*, 2261-2275.

17. Bishara, A, Mason, G.E, & Almeida, F.N. (1971). Continuous Beams with Prestressed Reinforcement. *ASCE Structural Journal, 97*, 2261-2275.

18. Bishara, A., & Almeida, F. (1970). Concrete Beams with Prestressed Reinforcement. *ASCE Structural Journal, 96*, 1445-1460.

19. Brosens, K, & Van Gemert, D. (2001). Anchorage of externally bonded reinforcements subjected to combined shear/bending action. *Proceedings of the International Conference on FRP Composites in Civil Engineering*, (pp. 589-596). Hong Kong, China.

20. Burns, N. (1966). Development of Continuity between Precast Prestressed Concrete Beams. *PCI Journal, 11*, 23-36.

21. Canasquillo, R.L, Nilson, A.H, & Slate, F.O. (1981). Properties of High-Strength Concrete Subject to Short-term Load. *ACI Structural Journal, 78*, 171-178.

22. Caneira, D.J, & Chu, K.H. (1986). Stress-Strain Relationship for Reinforced Concrete in Tension. *ACI Structural Journal, 83*, 21-28.

23. Carolin, A. (2003). *Carbon Fiber Reinforced Polymers for Strengthening of Structural.* Sweden: Doctoral Thesis, Lulea University of Technology, .

24. CEB-FIP. (1990). *CEB-FIP Model Code (MC-90), Design Code.* Comite EuroInternational de Beton (CEB), Thomas Telford Services LTD., London.

25. Chen, B, & Nawy, E.G. (1994). Structural Behaviour Evaluation of High-Strength Concrete Beams Reinforced with Prestressed Prisms Using Fibre Optic Sensors. *ACI Structural Journal, 91*, 708-718.

26. Chen, B. a. (1994). Structural Behaviour Evaluation of High-Strength Concrete Beams Reinforced with Prestressed Prisms Using Fibre Optic Sensors. *ACI Structural Journal, 91*, 708-718.

27. *CSA Standard A23.3-14, Design of Concrete Structures.* (2014). Canadian Standards Association, Rexdale, Toronto, Ontario, Canada.

28. Damjanic, F, & Owen, D.R. (1984). Practical Consideration for Modeling of PostCracking Behavior for Finite Element Analysis of Reinforced Concrete Structures. *Proceedings of the International Conference on Computer-Aided Analysis and Design of Concrete Structures, Pineridge Press, Swansea, Wales, U.K.*

29. Davoudi, S. (2008). *CFRP Prestressed Concrete Prisms as Reinforcement in Continuous Concrete T-Beams.* Winnipeg, Manitoba, Canada: University of Manitoba.

30. De Schutter, G, Matthys, S, & Taerwe, L. (1997). Two Dimensional Analysis of Thermal Incompatibility between FRP Reinforcement and Concrete. *Diana World, 2*, 4-6.

31. De Sitter, W.R, & Tolman, F. (1995). Uni-directional Fibre Prestressed Concrete Elements, Proceedings of Non-metallic (FRP) Reinforcement for Concrete Structures. *RILEM Proceedings 29*, (pp. 49-56). Ghent, Belgium.

32. De Sitter, W.R, & Vonk, R.A. (1993). Splitting Forces in FRPR Pre-tensioned Concrete. *International Symposium on Fibre-Reinforced-Plastic Reinforcement for Concrete Structures, ACI SP 138-1*, (pp. 1-14).

33. DeStefano, R., Evans, J., Tadros, M., & Sun, C. (2003). FLEXURAL CRACK CONTROL IN CONCRETE BRIDGE STRUCTURES. *High Performance Computing, 5th International Symposium, ISHPC 2003.* Tokyo-Odaiba, Japan.

34. Dycherhoff, & Widman. (1963). Concrete Pavement with Prestressed Concrete Bars as Reinforcement. *PCA Foreign Literature Study*.

35. Evans, R.H, & Kong, F.K. (1964). The Extensibility and Micro-cracking of the InSitu Concrete in Composite Prestressed Concrete Beams. *Structural Engineer, 42*, 181-189.

36. Evans, R.H, & Parker, A.S. (1955). Behaviour of Prestressed Concrete Composite Beams. *ACI Structural Journal, 26*, 861-878.

37. Fields, F, & Bischoff, P.H. (2004). Tension Stiffening and Cracking of HighStrength Reinforced Concrete Tension Members. *ACI Structural Journal, 101*, 447-456.

38. Frosch, R. J. (1999). Another Look at Cracking and Crack Control in Reinforced Concrete. *ACI Structural Journal*, 437-442.

39. Frosch, R. J. (2001). Flexural Crack Control in Reinforced Concrete. *Design and Construction Practices to Mitigate Cracking* (pp. 135-154). American Concrete Institute.

40. Garrity, S. (2001). Near-surface reinforcement of masonry arch highway bridges. *in Proceedings 9 th Canadian Masonry Symposium, Fredericton*.

41. Gergely, P, & Lutz, L. A. (n.d.). Maximum Crack Width in Reinforced Concrete Flexural Members. *Causes, Mechanism, and Control of Cracking in Concrete, SP-20* (pp. 87-117). American Concrete Institute.

42. Hanson, N. (1969). Prestressed Concrete Prisms as Reinforcement for Crack Control. *PCI Journal, 14*, 14-31.

43. Hawileh, R. e. (2014). *Behavior of reinforced concrete beams strengthened with externally bonded hybrid fiber reinforced polymer systems* (Vol. 53). Materials & Design.

44. Hoppe, A. (1963). The mass production of Prestressed Auxiliary Members. *PCI Journal*, 44-46.

45. Jones, R, Swamy, R.N, & Charif, A. (1988). Plate separation and anchorage of reinforced concrete beams strengthened by epoxy-bonded steel plates. *Structural Engineering*, 85-94.

46. Kaar, P, & Mattock, A. (1962). High-Strength Bars as Concrete Reinforcement — Part 4: Control of Cracking. *Journal, PCA Research and Development Laboratories, 4*, 46-65.

47. Kaiser, H. (1989). *Strengthening of reinforced concrete with epoxy-bonded carbon fibre plastics.* Doctoral Thesis, Switzerland.

48. Kajfasz, S, & Rowe, R.E. (1961). *An Investigation of the Behaviour of Composite Prestressed Concrete Beams.* Composite Rectangular Beams, London, C and CA Technical Report TRA/345.

49. Kelly, P.L, Brainerd, M.L, & Vatovec, M. (2000). Design philosophy for structural strengthening with FRP. *Concrete International Magazine, 22*, 77-82.

50. Klaiber, F.W, Dunker, K.F, Wipf, T.J, & Sanders, W.W. (1987). *Methods of strengthening existing highway bridges.* Technical Report, Transportation Research Board, NCHRP Research Report No. 293.

51. L'Hermite, R.L, & Bresson, J. (1967). Beton arme par collage des armateures . *RILEM International Symposium, Synthetic Resins in Building Construction*, (pp. 175-203). Paris.

52. Ladner, M. (1983). Reinforced concrete members with subsequently bonded steel plates. *printed in Strengthening of Building Structures, Iabse Symposium*, 203-210.

53. Lercehntal, C. (1967). Bonded steel reinforcement for concrete slabs. *Materials and Structures, 37*, 263-269.

54. Li, Q, & Ansari, F. (2000). High Strength Concrete in Uniaxial Tension. *ACI Materials Journal, 97*, 49-57.

55. Marzuk, H, & Chen, Z.W. (1995). Fracture Energy and Tension Properties of HighStrength Concrete. *Journal of Materials in Civil Engineering, 7*, 108-116.

56. Mawal, B. (1979). Concrete Beams with Prestressed Elements. *ASCE Structural, 105*, 617-633.

57. Meier, U. (1992). Carbon fibre-reinforced polymers: Modern materials in bridge engineering. *Structural Engineering International, 2*, 7-12.

58. Mikhailov, O. (1958). Recent Research on the Action of Unstressed Concrete in Composite Structures. *Third Congress of FIP*, 51-65.

59. Mirza, J.F, Zia, P, & Bhargava, J.R. (1971). *Static and Fatigue Strengths of Beams Containing Prestressed Concrete Tension Elements.* Highway Research record.

60. Mohamed, T. K. (2002). *FLEXURAL PERFORMANCE AND BOND CHARACTERISTICS OF FRP STRENGTHENING TECHNIQUES FOR CONCRETE STRUCTURES.* PhD thesis University of Manitoba.

61. Nawy, E.G, & Chen, B. (1998). Deformational Behaviour of High Strength Concrete Continuous Composite Beams Reinforced with Prestressed Prisms and Instrumented with Bragg Grating Fibre Optic Sensors. *ACI Structural Journal, 95*, 51-60.

62. Ozell, A. (1957). Behaviour of Simple-Span and Continuous Composite Prestressed Concrete Beams. *PCI Journal, 2*, 41-74.

63. Popovics, S. (1970). A review of Stress-Strain Relationships for Concrete. *ACI Journal, 67*, 243-248.

64. Raithby, K. (1980). External strengthening of concrete bridges with bonded steel plates. Transport and Road research Laboratory.

65. Sika Canada Inc. (n.d.). *Technical specification, http://www.Sika.ca*.

66. Svecova, D. (1998). *Behaviour of Concrete Beams Reinforced with FRP Prestressed Concrete Prisms.* Ph.D. Thesis, Carleton University, Ottawa, Canada.

67. Svecova, D. a. (n.d.). Flexural Behaviour of Concrete Beams Reinforced with Carbon Fibre-Reinforced Polymer (CFRP) Prestressed Prisms. *ACI Structural Journal, 97*, 731-738.

68. Taerwe, L, & Pallemans, I. (n.d.). Force Transfer of AFRP Bars in Concrete Prisms, Proceedings of Non-metallic (FRP) Reinforcement for Concrete Structures. *RILEM Proceedings 29*, (pp. 154-163). Ghent, Belgium.

69. Taerwe, L. (1993). Fiber-Reinforced-Plastic (FRP) Developments and Applications in Europe. *FRP Reinforced for Concrete Structures, A. Nanni (Editor)*, 99-112.

70. Taljsten, B. (1994). *Strengthening of existing concrete structures with externally bonded steel or fibre reinforced plastics.* Doctoral Thesis, Lule, University of Technology.

71. Täljsten, B. C. (2003). Concrete structures strengthened with near surface mounted reinforcement of CFRP. *Advances in structural engineering*, 201-213.

72. Tann, D., & Delpark, R. (1999). Experimental investigation of concrete beams reinforced with narrow carbon strips. *Proc. Int. Conf. Structural Faults & Repair*.

73. Teng, J.G, Chen, J.F, Smith, S.T, & Lam, L. (2002). FRP strengthened RC structures. *John Wiley & Sons Ltd, England*.

74. Thorenfeldt, E, Tomaszewicz, A, & Jensen, J.J. (1987). Structural Properties of High-Strength Concrete and Application in Design. *Proceedings of the Symposium "Utilization of High Strength Concrete" Stavanger, Norway, Tapir, Trondheim,*, (pp. 149-159).

75. Van Gemert, D. (1980). Force transfer in epoxy bonded steel-concrete joints. *International Journal of Adhesion and Adhesive, 2*, 67-72.

76. Vogel, H. (2005). *Thermal Compatibility of FRP in Prestressed Concrete Beams, M.Sc. Thesis.* University of Manitoba, Winnipeg, Canada.

77. Vogel, H. M. (2011). *Serviceability of Concrete Beams Reinforced with FRP and Concrete Prisms Prestressed with CFRP*. Winnipeg, Manitoba, Canada: University of Manitoba.

78. Zia,P, Mirza, J.F, & Rizkalla, S.H. (1976). Static and Fatigue Tests of Composite T Beams Containing Prestressed Concrete Tension Elements. *PCI Journal, 21*, 76-93.

APPENDIX A

DESIGN OF ONE-WAY SLABS

Mechanical Properties of materials:

- **Concrete Properties:**

$f'_c = 40\ MPa$

$\varepsilon_{cu} = 0.0035$

$f_t = 0.6\lambda\sqrt{f'_c} = 0.6\sqrt{40} = 3.79\ MPa$

$E_c = 4500\sqrt{f'_c} = 4500\sqrt{40} = 28460\ MPa$

$\alpha_1 = 0.85 - 0.0015 * (f'c) = 0.85 - 0.0015 * (40) = 0.79$

$\beta_1 = 0.97 - 0.0025 * (f'c) = 0.97 - 0.0025 * (40) = 0.87$

$Concrete\ Cover = 60\ mm$

- **Steel Reinforcement Properties:**

$f_y = 400\ MPa$

$E_s = 200\ GPa$

$\varepsilon_y = \frac{f_y}{E} = 200000 = 0.002$

- **Cross Section Properties**

$b = 600\ mm \qquad h = 200\ mm$

$l_t = 3000\ mm$ Total length

$l_c = 2500\ mm$ Center to center length

$A_g = 600 * 200 = 120000\ mm^2$

$\mathrm{I_g} = \frac{\mathrm{bh}^3}{12} = \frac{600 * 200^3}{12} = 4 * 10^8\ mm^4$

$Designed\ Bending\ Moment:\ M_f = 30\ kN.m/m$

For a simply supported slab:

$$M_{max} = \frac{PL}{4} \rightarrow P_{max} = \frac{4M}{l_c} = \frac{4*30}{2.5} = 48\ kN$$

Design Procedure:

1. Estimate the slab thickness (h):

$l_n = 2250\ mm \quad clear\ span$

Table 9.2 (CSA A23.3-04)→ for simply supported slab:

$$h \geq \frac{l_n}{20} = \frac{2250\ mm}{20} = 112.5\ mm \rightarrow h = 200\ mm$$

2. Effective slab depth (d):

Using 15M as a Tension reinforcement

15M details:

Diameter = 16 mm, Area = 200 mm^2

$$\text{d} = \text{h} - \text{cover} - \frac{d_b}{2} = 200 - 60 - \frac{16}{2} = 132\ mm$$

3. Calculate the required area of tension reinforcement (A_s):

$M_f = 30\ kN.m/m$

b) Calculate the required area of tension reinforcement using the direct procedure:

$$M_r = T_r\left(d - \frac{a}{2}\right) = f_y A_s\left(d - \frac{a}{2}\right)$$

$$a = \frac{f_y A_s}{\alpha_1 f'_c\, b}$$

$$A_s = \frac{\alpha_1 f'_c\, b}{f_y}\left(d - \sqrt{d^2 - \frac{2M_r}{\alpha_1 f'_c\, b}}\right)$$

For:

$f_y = 400\ MPa$

$\alpha_1 = 0.79$

$$A_s = 0.001975 f'_c\ b \left(d - \sqrt{d^2 - \frac{2.53\ M_r}{f'_c\ b}} \right) mm^2$$

The following units should be used in the above equation:

$$M_r\ [N.mm]$$

$$b\ [mm]$$

$$d\ [mm]$$

$$f'_c\ [MPa]$$

$$A_s = 0.001975 * 40 * 600 * \left(132 - \sqrt{132^2 - \frac{2.53 * (30 * 10^6)}{40 * 600}} \right) = 596.2 \cong 597\ \frac{mm^2}{mm}$$

Choose 4# 15M:

$$4 * 200 = 800\ \frac{mm^2}{mm}$$

c) Determine the required bar spacing:

15M for tension steel:

$$A_b = 200\ mm^2$$

The required bar spacing can be determined as:

$$s \leq A_b \frac{600}{A_s}$$

$$s \leq 200 * \frac{600}{597} = 201\ mm\ = 20.1\ cm$$

Provided bar spacing:

$$s = 200 * \frac{600}{800} = 150\ mm = 15\ cm$$

Assumed bar spacing = 120 mm = 12 cm

d) Check whether the provided area of reinforcement is greater than or equal to the required amount of reinforcement:

$$800\frac{mm^2}{mm} > 597\frac{mm^2}{mm}$$

So for tension reinforcement:

15M@120 → 4#15M

4. Confirm that the maximum tension reinforcement requirement is satisfied (A23.3 Cl.10.5.2)

Check the reinforcement ratio

$$\rho = \frac{A_s}{bd} = \frac{800}{600 * 132} = 0.0101$$

Balanced reinforcement ratio for $f'_c = 40\ MPa\ and\ f_y = 400\ MPa$: → Table A.4

$$\rho_b = 0.034$$

$$\rho = 0.0101\ < \rho_b = 0.034$$

5. Determine the actual effective depth:

Same as step 2:

d = 132 mm

6. Confirm that the minimum reinforcement requirement is satisfied (A23.3 Cl.7.8.1)

a) Calculate the gross cross-sectional area:

$$A_g = b * h = 600 * 200 = 120000\ mm^2$$

b) Determine the minimum reinforcement area:

$$A_{smin} = 0.002\, A_g$$

$$= 0.002 * 120000 = \ 240\ \frac{mm^2}{m}$$

c) Check whether the provided reinforcement area (A_s) is adequate:

$$A_s = 800\ \frac{mm^2}{mm} > A_{smin} = 240\ \frac{mm^2}{m}$$

7. Confirm that the maximum bar spacing requirement is satisfied (A23.3 Cl.7.4.1.2)

a) Calculate the maximum bar spacing (s_{max}) as the **lesser** of:

$$3 * h = 3 * 200 = 600\ mm$$

$$and$$

$$500\ mm$$

The smaller value governs, so:

$$s_{max} = 500\ mm$$

b) Compare the actual bar spacing with the maximum bar spacing:

$$s = 120\ mm < 500\ mm$$

8. Calculate M_r:

a) Calculate the depth of the compression stress block:

$$a = \frac{f_y A_s}{\alpha_1 f'_c\, b}$$

$$a = \frac{400 * 800}{0.79 * 40 * 600} = 16.87\ mm$$

b) Calculate the moment resistance:

$$M_r = T_r \left(d - \frac{a}{2}\right) = f_y A_s \left(d - \frac{a}{2}\right)$$

$$M_r = 400 * 800 * \left(132 - \frac{16.87}{2}\right) = 39.5 \ \frac{kN.m}{m}$$

9. Confirm that the strength requirement is satisfied (A23.3 Cl.8.1.3):

$$\boldsymbol{M_r = 39.5 \frac{kN.m}{m} \geq M_f = 30 \frac{kN.m}{m}}$$

$$\boldsymbol{M_{max} = \frac{PL}{4} \ \rightarrow P_u = \frac{4M}{l_c} = \frac{4*39.5}{2.5} = 63.2\ kN}$$

10. Design the shrinkage and temperature reinforcement (A23.3 Cl.7.8.1 and Cl.7.8.3)

a) The minimum area of shrinkage and temperature reinforcement is the same as for the tension steel:

$$A_{smin} = 0.002\ A_g$$

$$= 0.002 * 120000 = \ 240 \ \frac{mm^2}{m}$$

b) The maximum bar spacing (s_{max}) is the **lesser** of

$$5 * h = 5 * 200 = 1000\ mm$$

$$and$$

$$500\ mm$$

The smaller value governs, so:

$$s_{max} = 500\ mm$$

c) Determine the required bar spacing:

15M:

$$A_b = 200\ mm^2$$

The required bar spacing can be determined as:

$$s \leq A_b \frac{600}{A_s}$$

$$s = 200 * \frac{600}{240} = 500\ mm = 50\ cm$$

$$s = 400 \leq s_{max} = 500\ mm$$

So,

$$s = 400\ mm$$

d) Check whether the provided area of reinforcement is greater than or equal to the required amount of reinforcement:

$$A_s = A_b \frac{600}{s}$$

$$A_s = 200 * \frac{600}{400} = 300\ \frac{mm^2}{m}$$

$$A_s = 300\ \frac{mm^2}{m} \geq\ A_{smin} = 240 \frac{mm^2}{m}$$

So for shrinkage and temperature reinforcement:

15M@400 → **8 #15M**

Shear Control

1. Calculate the design shear force (V_f)

a) $l_n = 2250\ mm$ $\quad clear\ span$

b) The factored load:

$$M_{max} = \frac{PL}{4} \rightarrow P_f = \frac{4M}{l_c} = \frac{4*39.5}{2.5} = 63.2\ kN$$

c) Maximum shear force at the face of support for simply supported one-way slab:

$$V_f = \frac{P_f}{2} = \frac{63.2}{2} = 31.6\frac{kN}{m}$$

2. Determine the concrete shear resistance (V_c) (A23.3 Cl.11.3.4)

$$d = 132\ mm$$

a) Find the effective shear depth (d_v)

The effective shear depth is taken as the greater of

$$0.9d = 0.9 * 132 = 118.8\ mm$$
$$0.72h.\ 0.72 * 200 = 144\ mm$$

$$\boldsymbol{d_v = 144\ mm}$$

b) Determine the β value. Since:

$$h = 200\ mm < 300\ mm$$

According to A23.3 cl.11.3.6.2, for slab with an overall thickness not greater than 350 mm, $\beta = 0.21$ can be used.

c) Finally, the V_c can be determined as:

$$V_c = \lambda\beta\sqrt{f'_c}b_w d_v$$

$$V_c = 1.0 * 0.21 * \sqrt{40} * 600 * 144 = 114.75\ \frac{kN}{m}$$

3. Determine whether shear reinforcement is required (A23.3 Cl.11.2.8.1)

If $V_f < V_c$, then shear reinforcement is not required:

$$V_f = 31.6\frac{kN}{m} < V_c = 114.75\ \frac{kN}{m}$$

No shear reinforcement is required

APPENDIX B

EXPERIMENTAL RESULTS

LOAD-DEFLECTION AT MID-SPAN DURING CRACKING PHASE

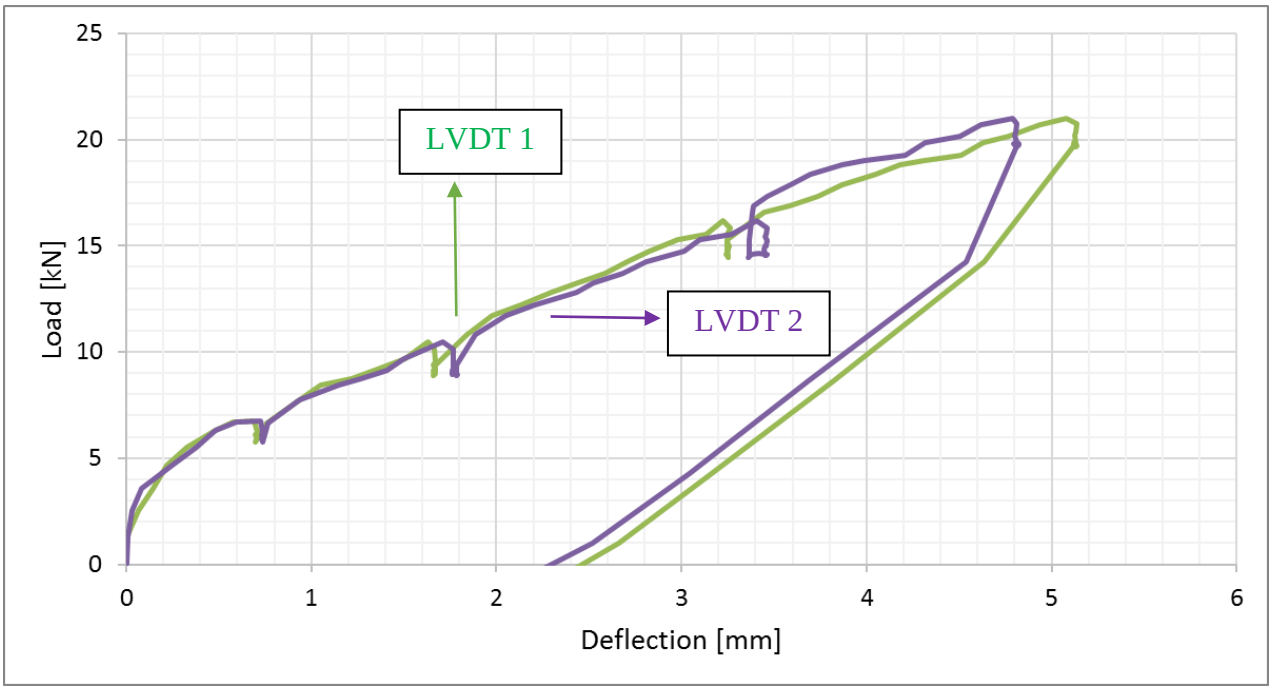

Slab SP-S-20

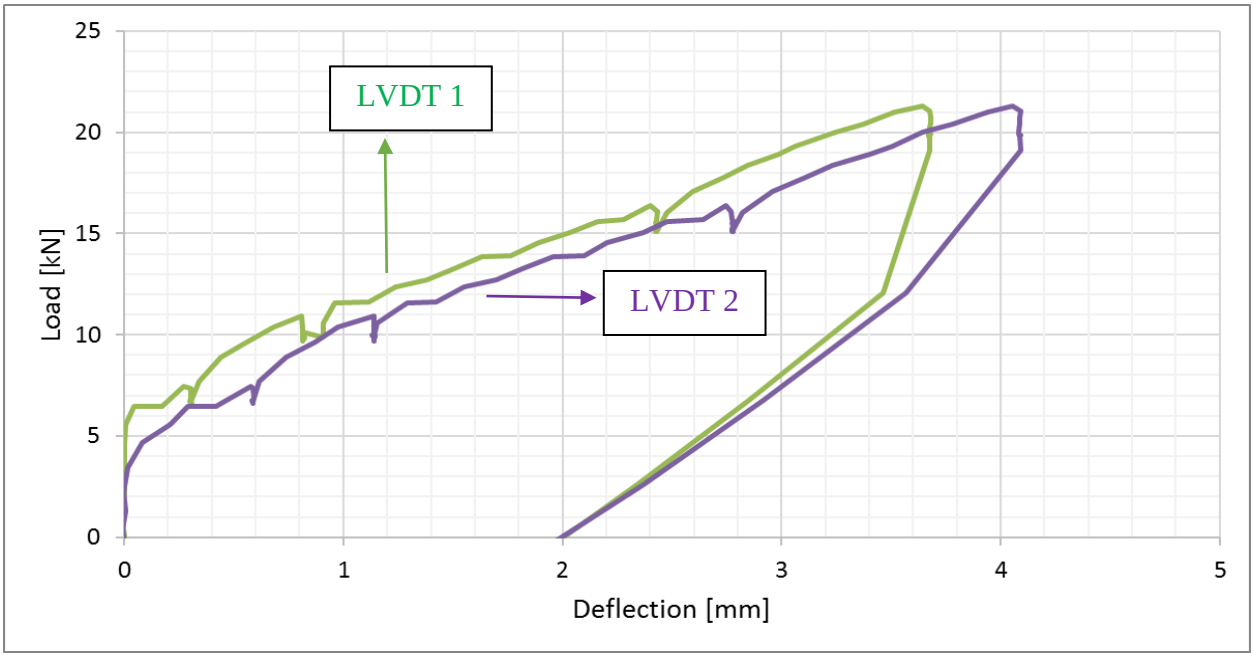

Slab SP-S-25

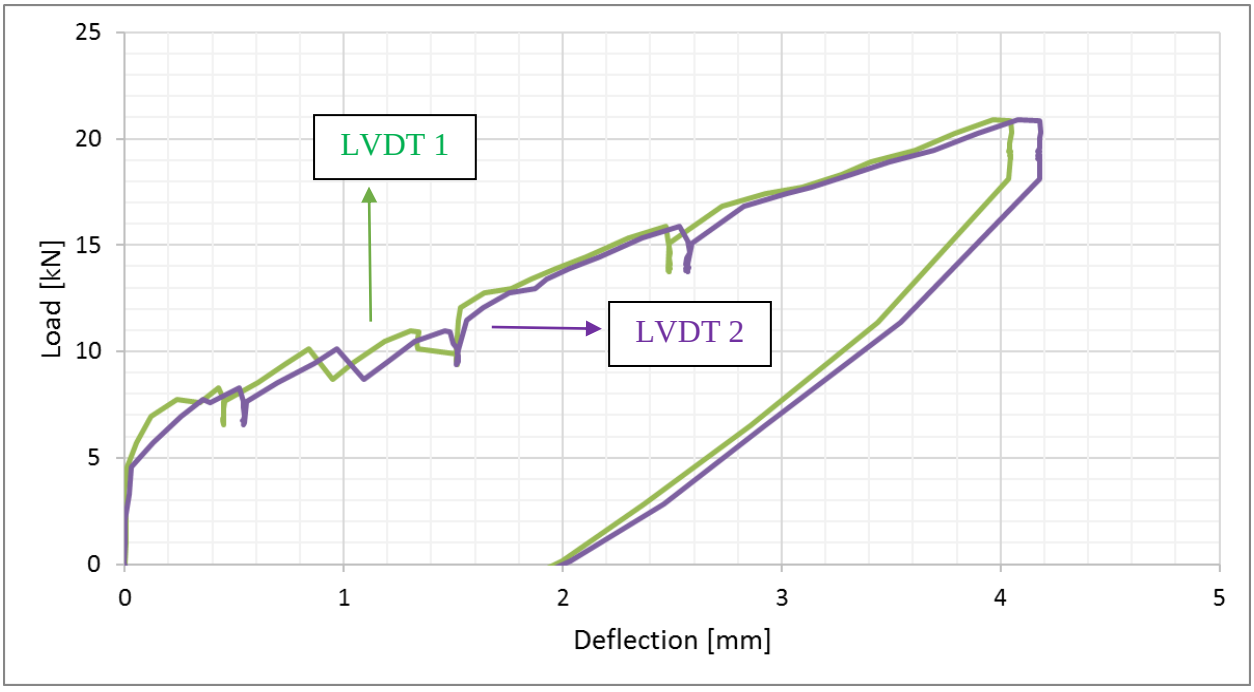

Slab SP-S-30

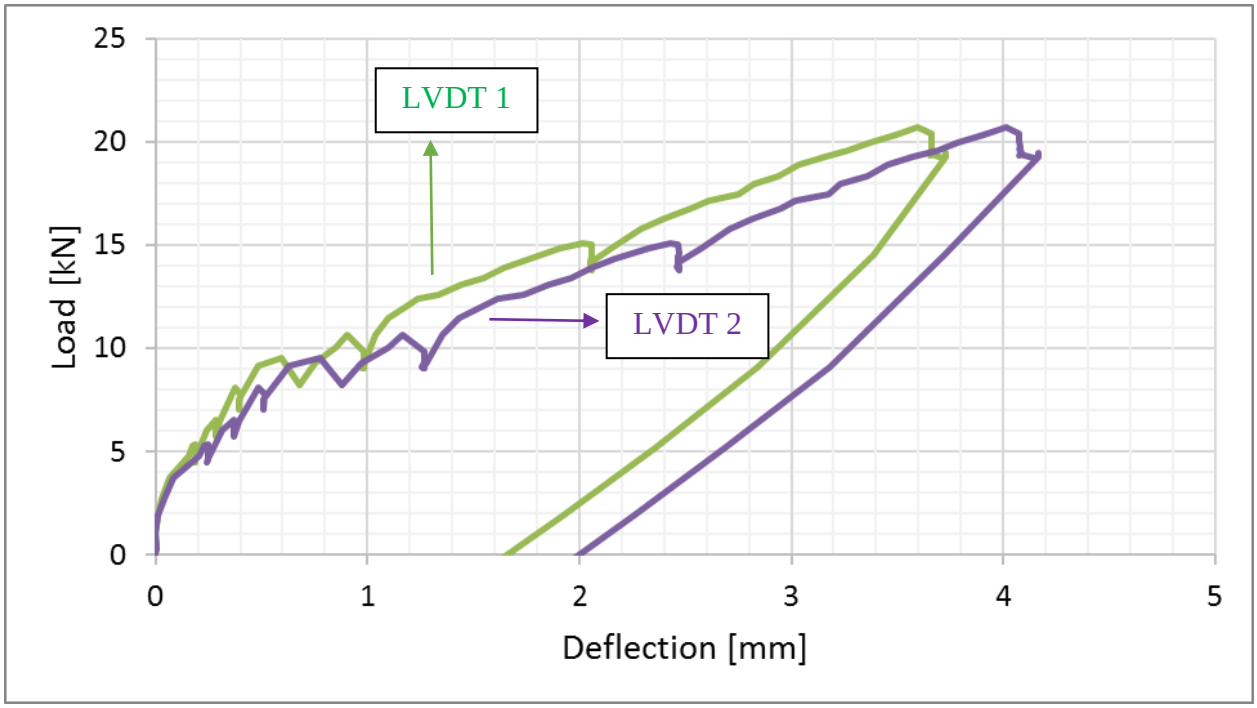

Slab LP-S-20

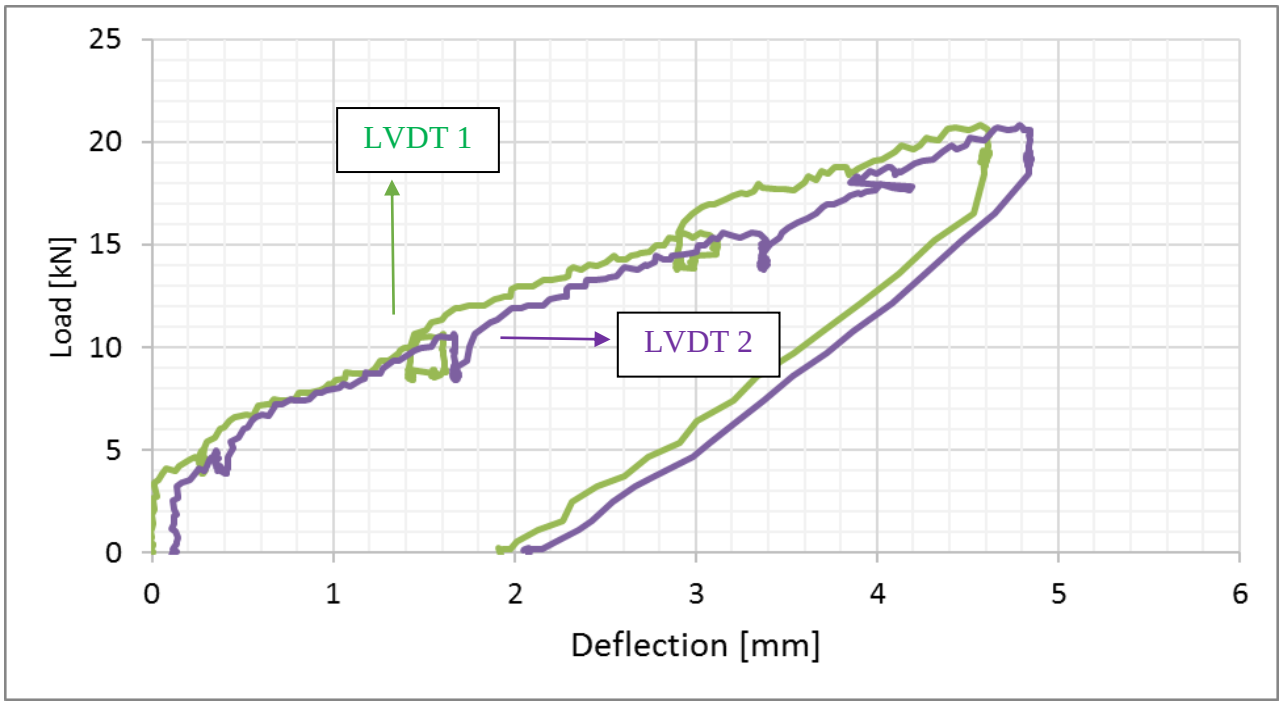

Slab LP-S-25

MOMENT-CURVATURE AT MID-SPAN DURING CRACKING PHASE

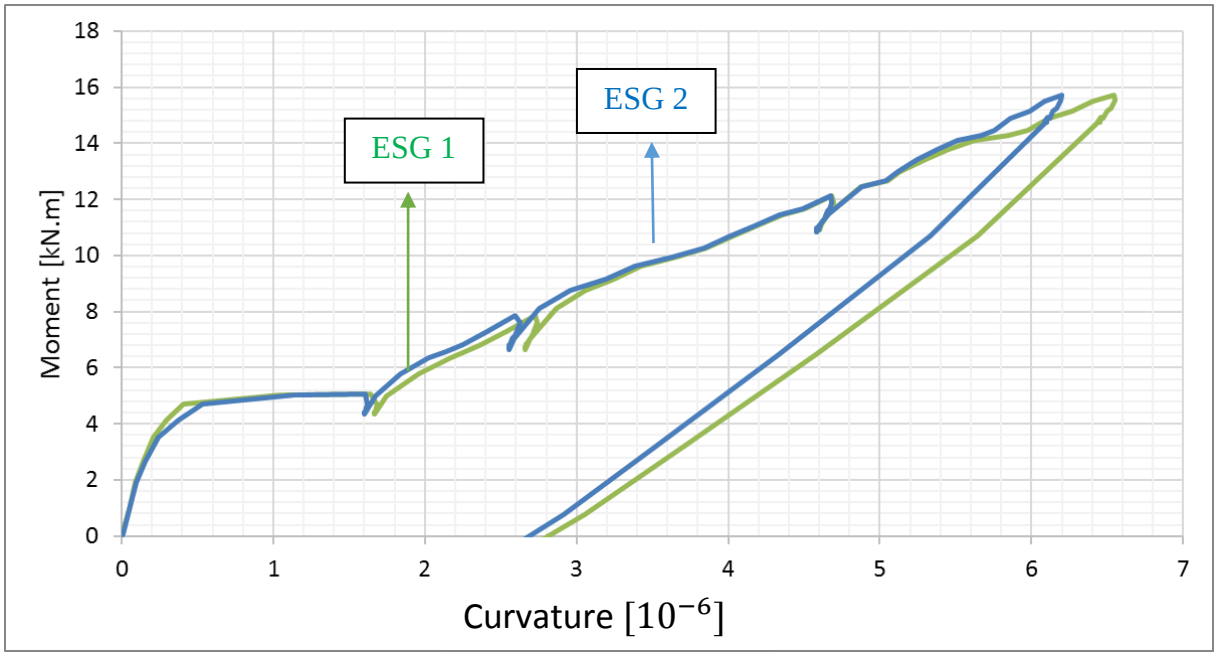

Slab SP-S-20

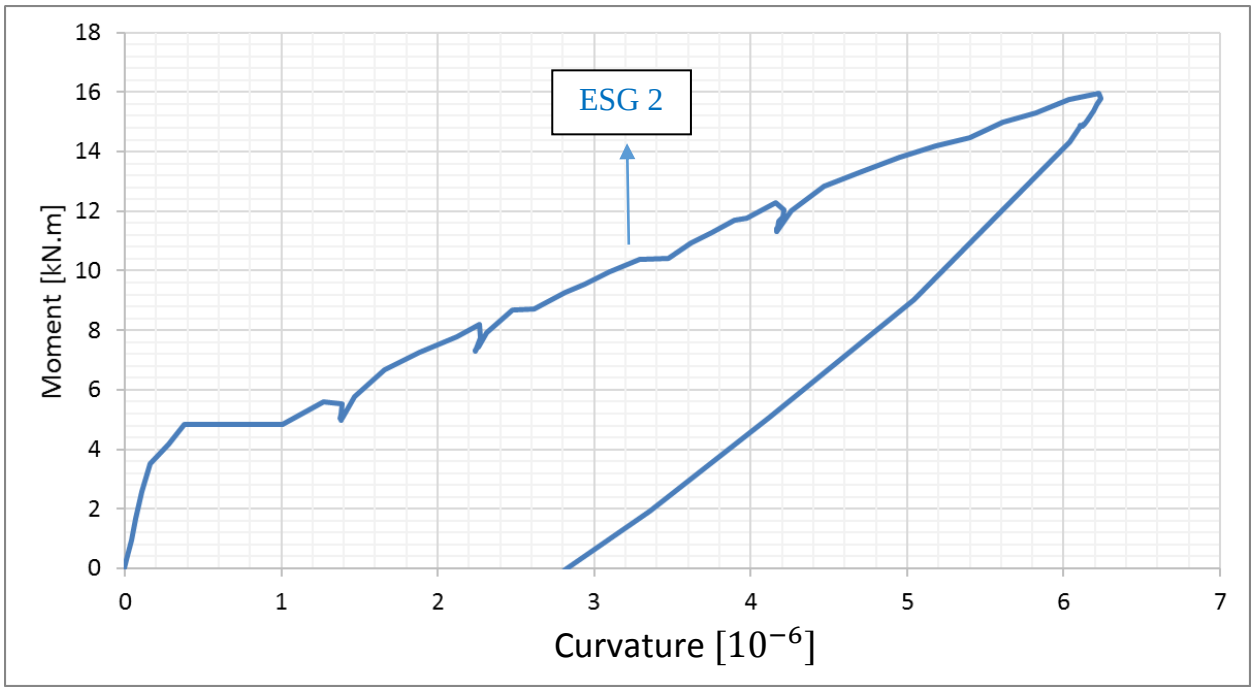

Slab SP-S-25

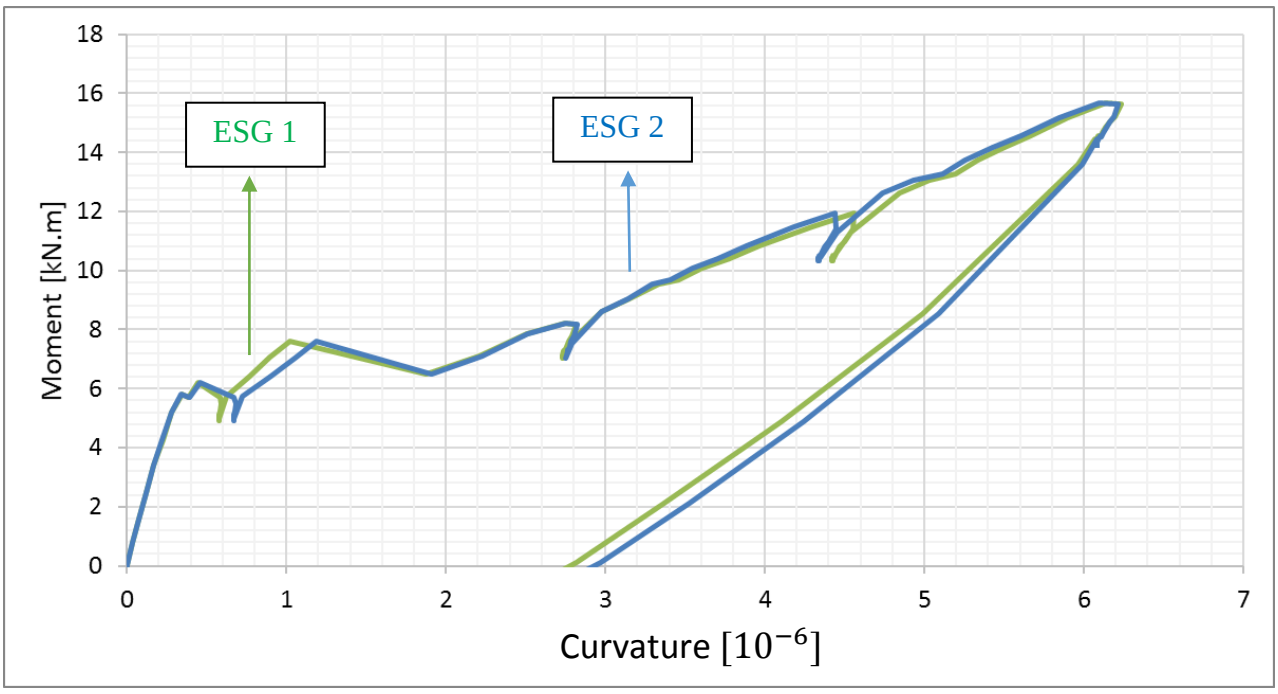

Slab SP-S-30

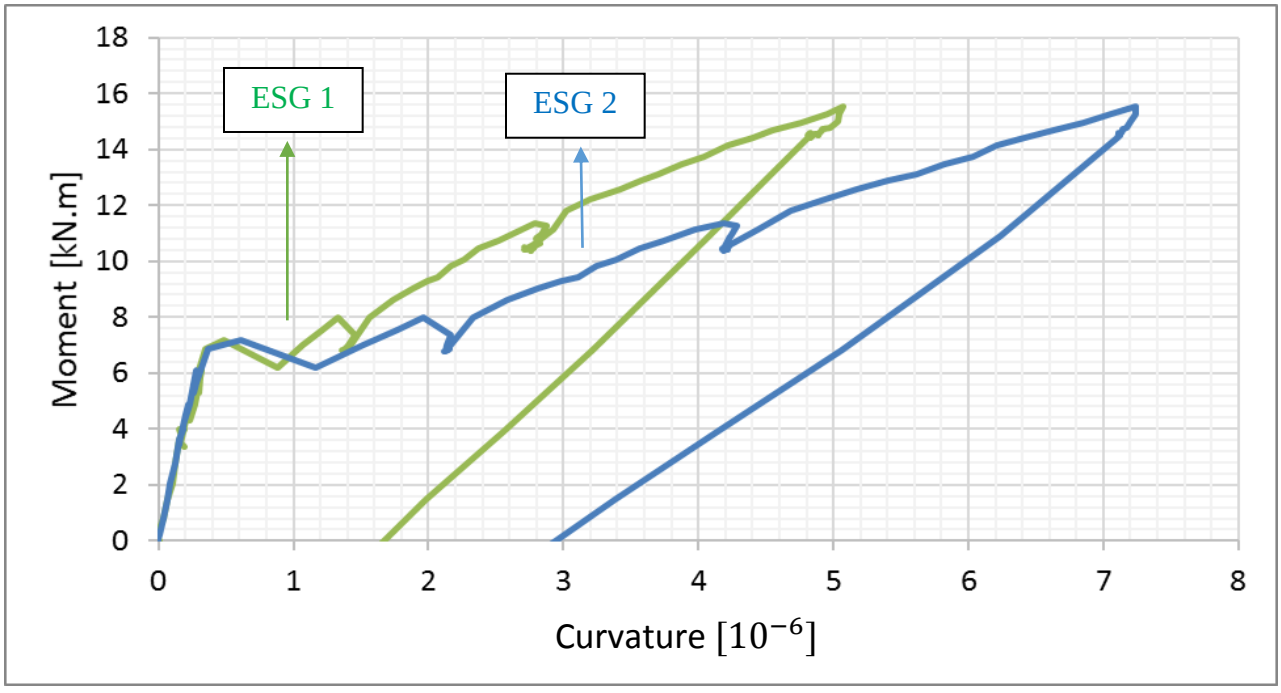

Slab LP-S-20

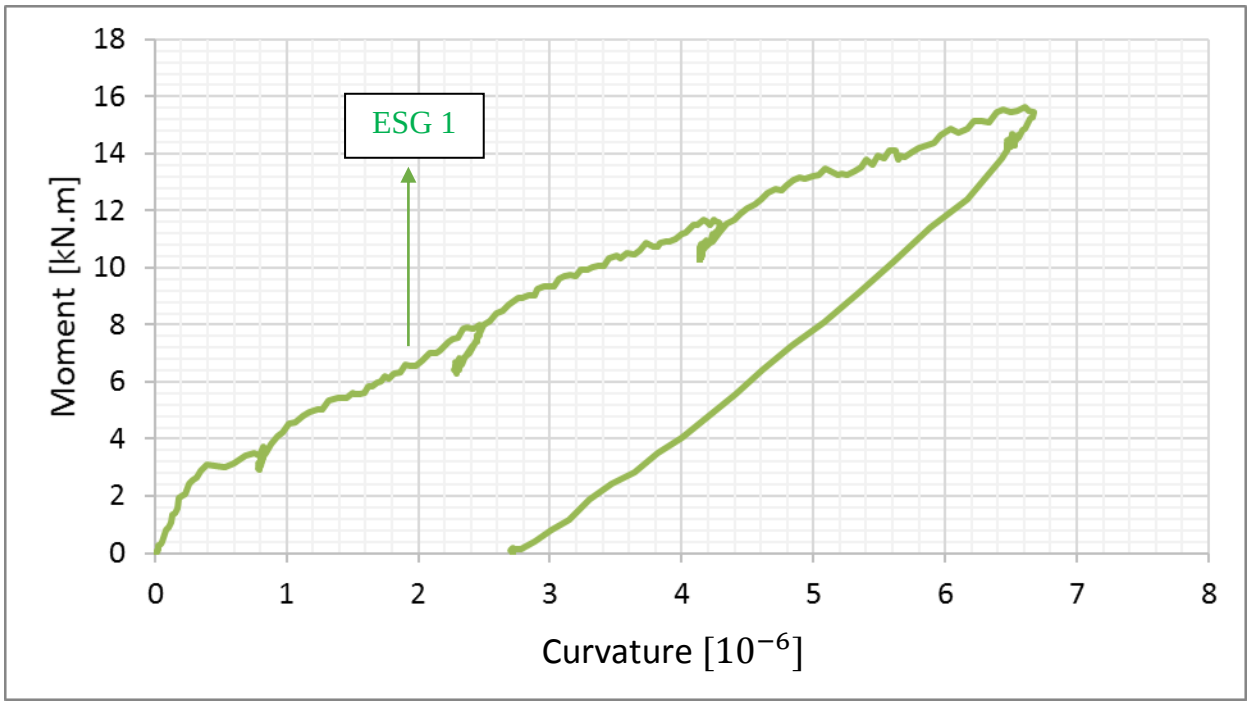

Slab LP-S-25

NEUTRAL AXIS CALCULATIONS

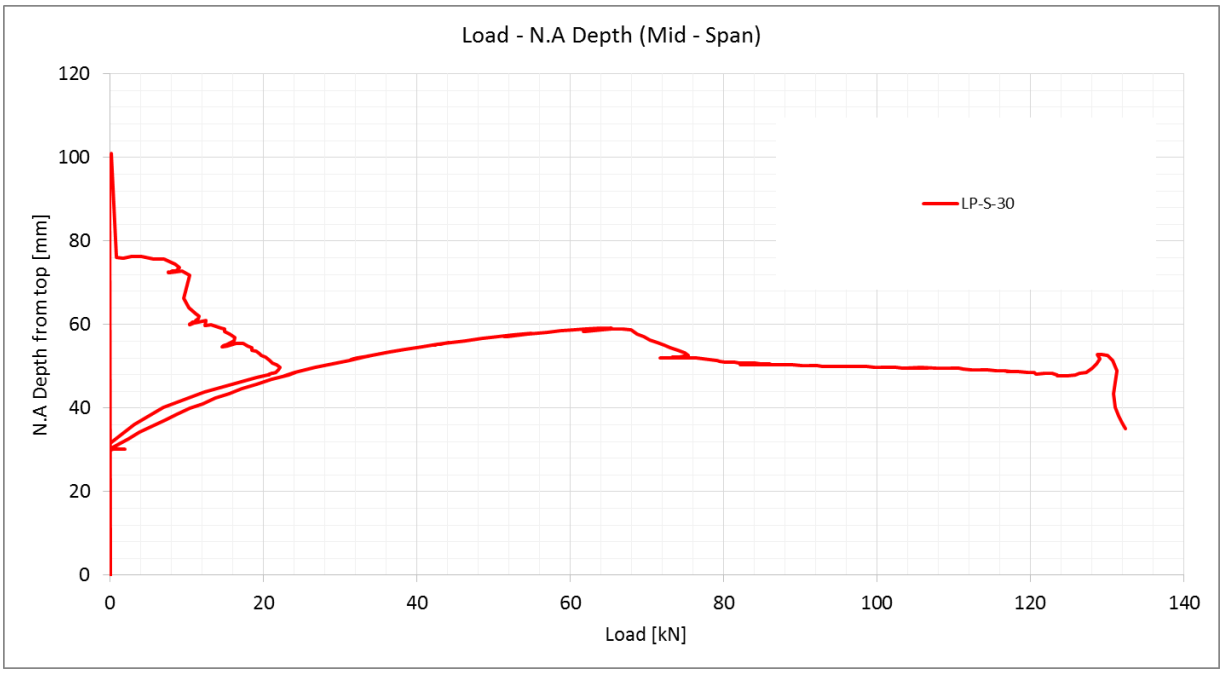

Change of neutral axis with load in slab LP-S-30

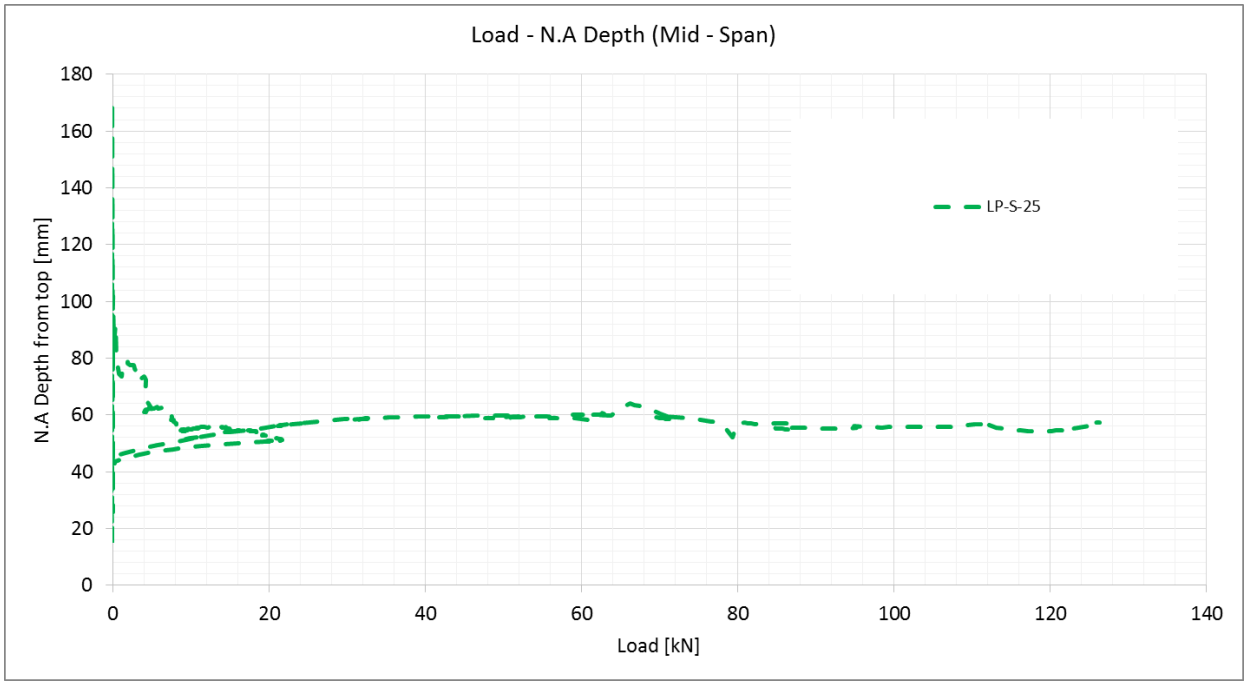

Change of neutral axis with load in slab LP-S-25

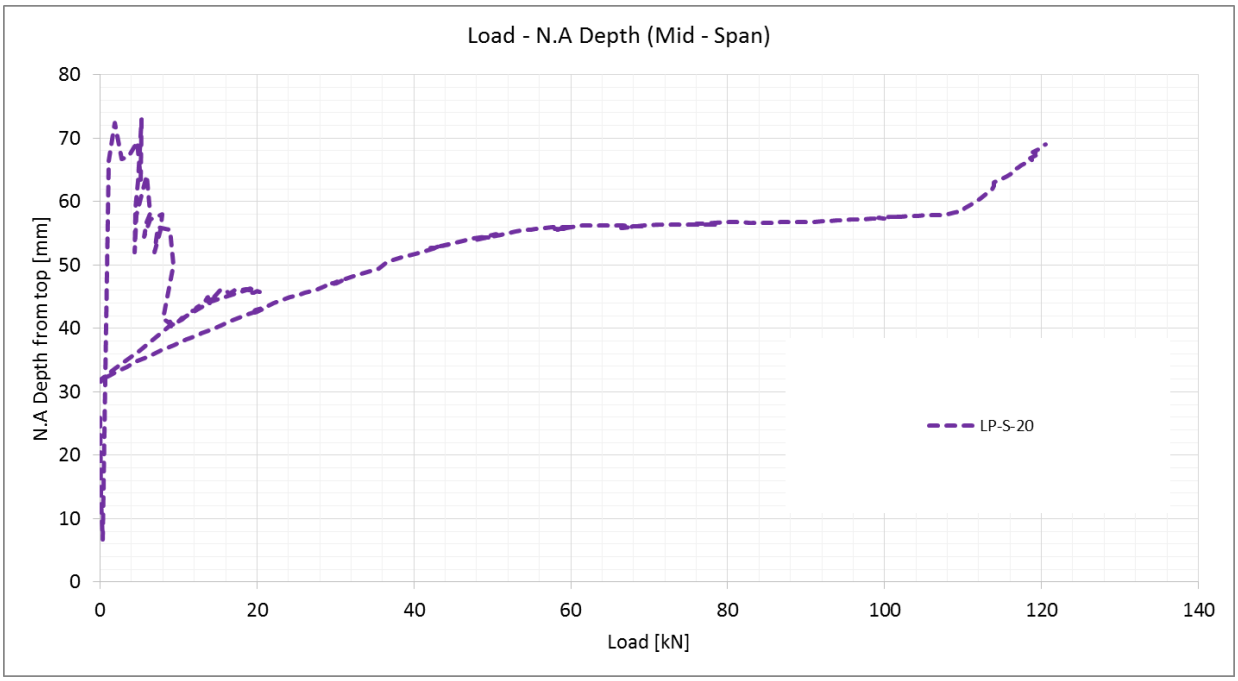

Change of neutral axis with load in slab LP-S-20

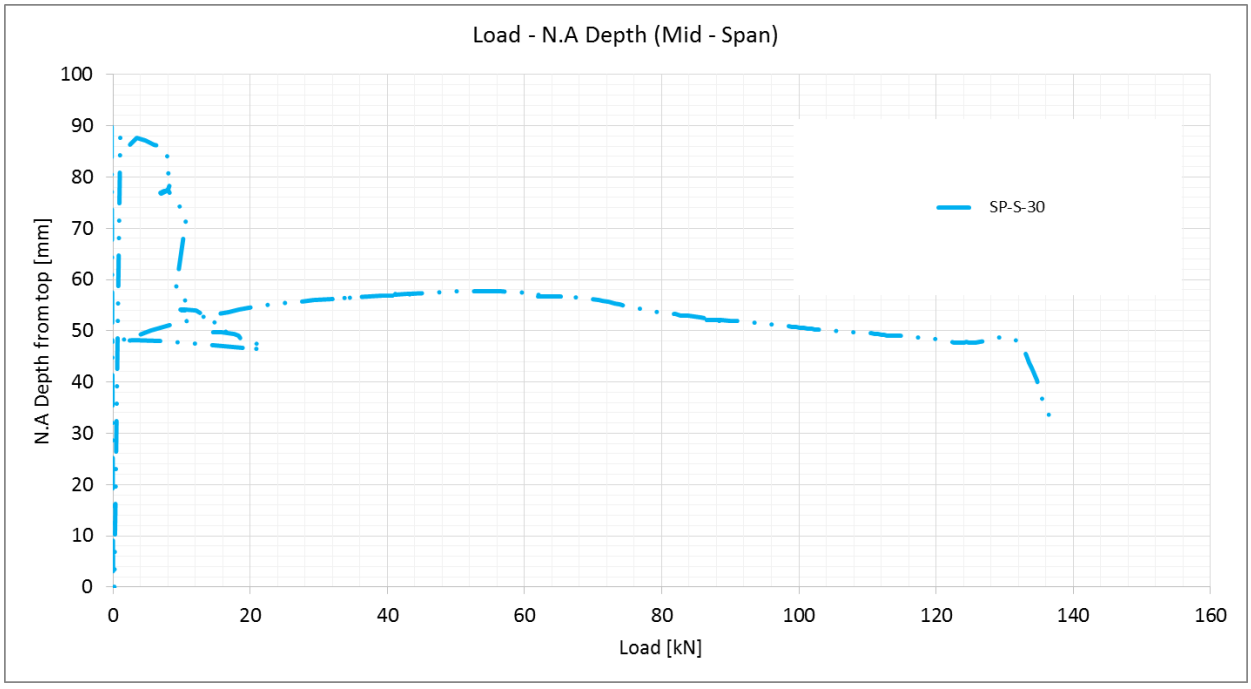

Change of neutral axis with load in slab SP-S-30

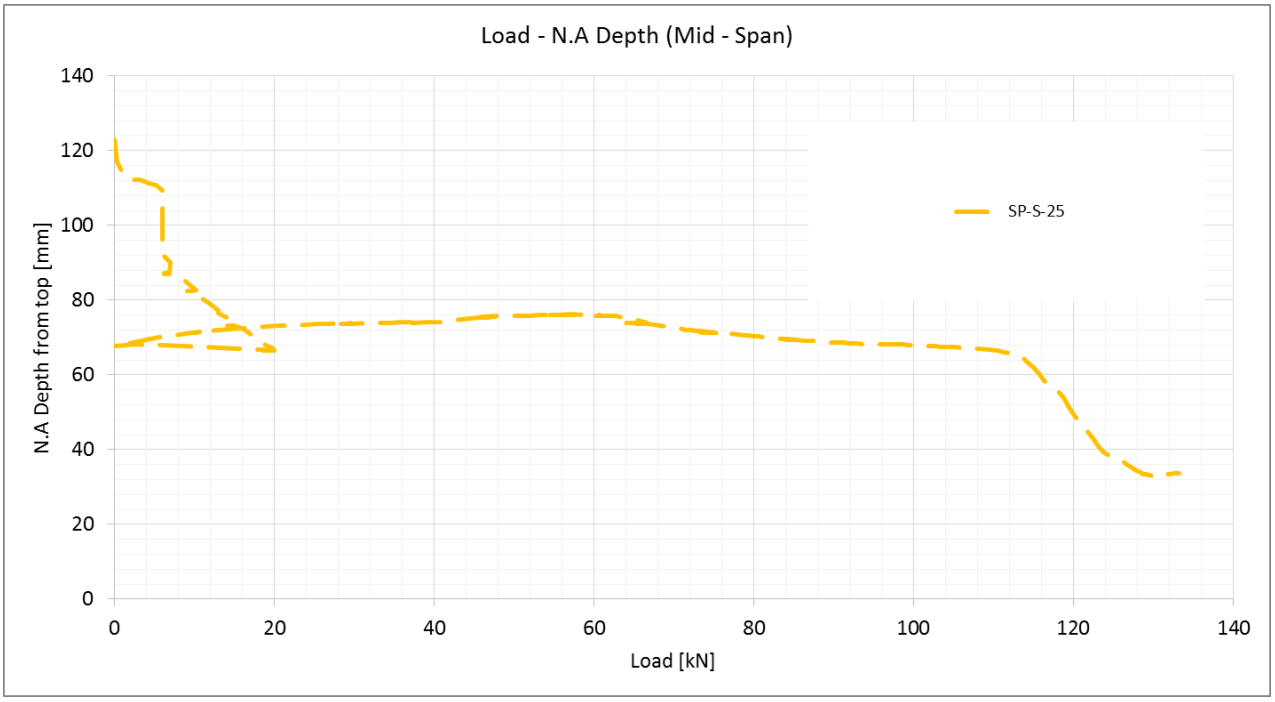

Change of neutral axis with load in slab SP-S-25

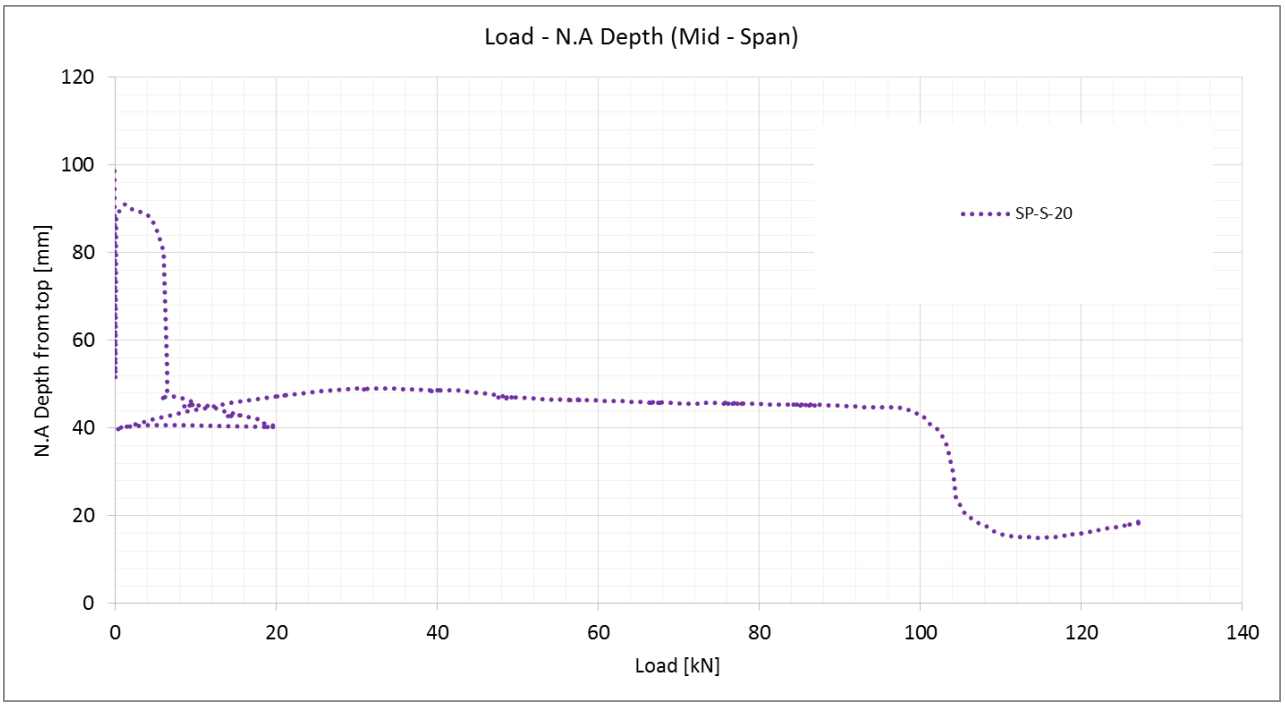

Change of neutral axis with load in slab SP-S-20

DEFLECTION PROFILE RESULTS

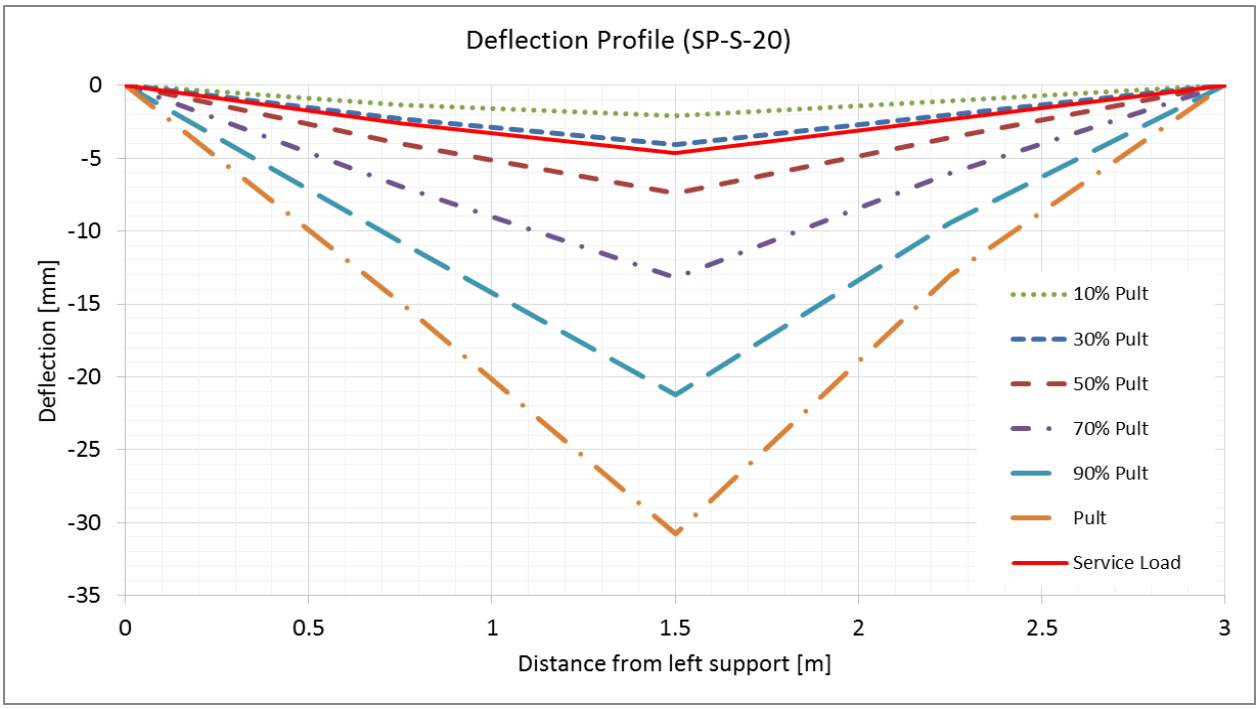

Deflection profile of slab SP-S-20 at various load level

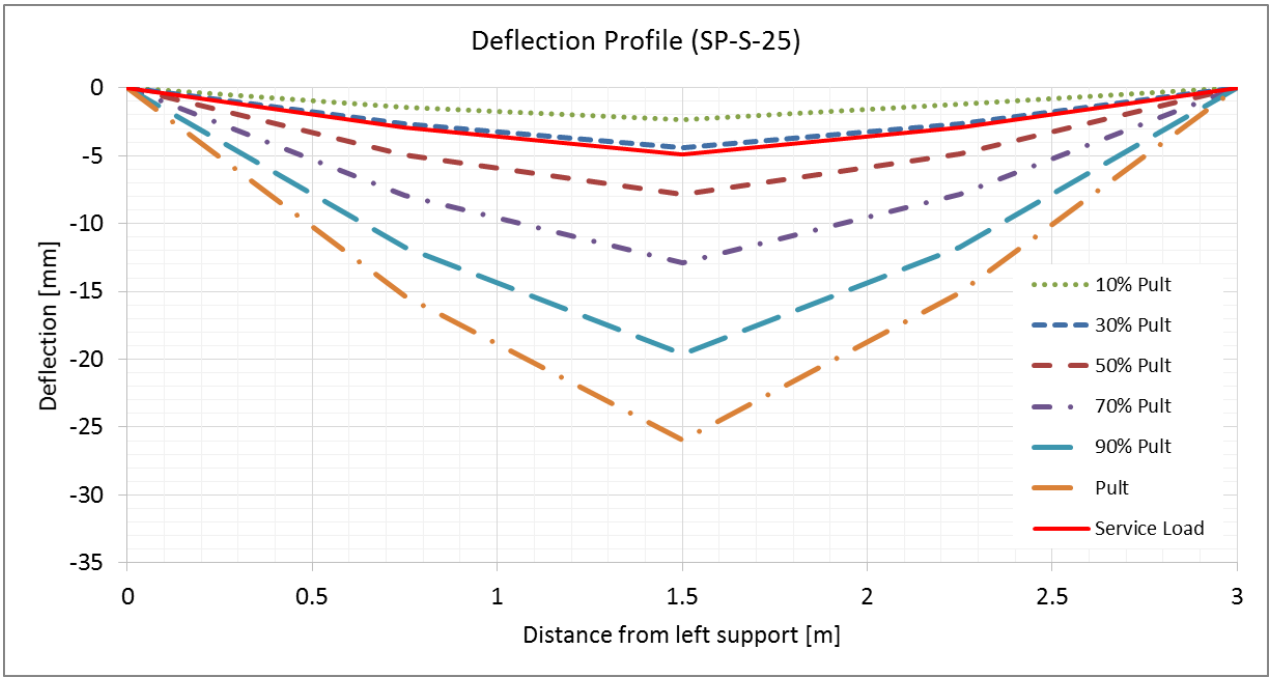

Deflection profile of slab SP-S-25 at various load level

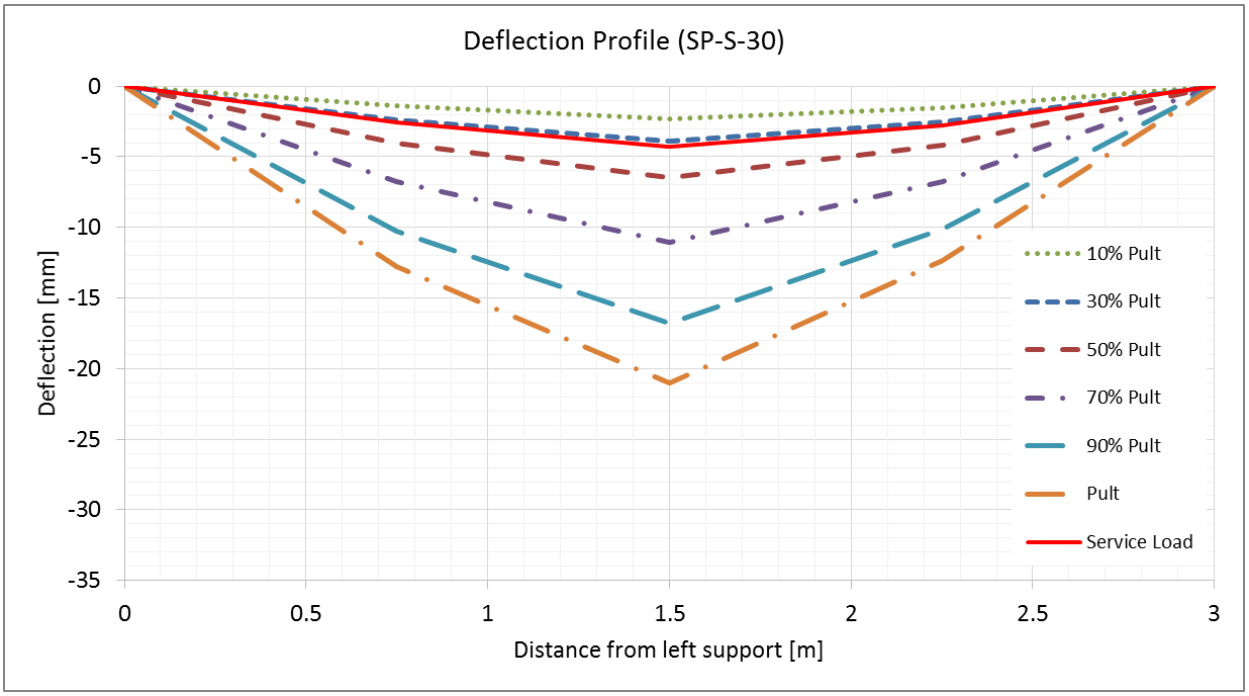

Deflection profile of slab SP-S-30 at various load level

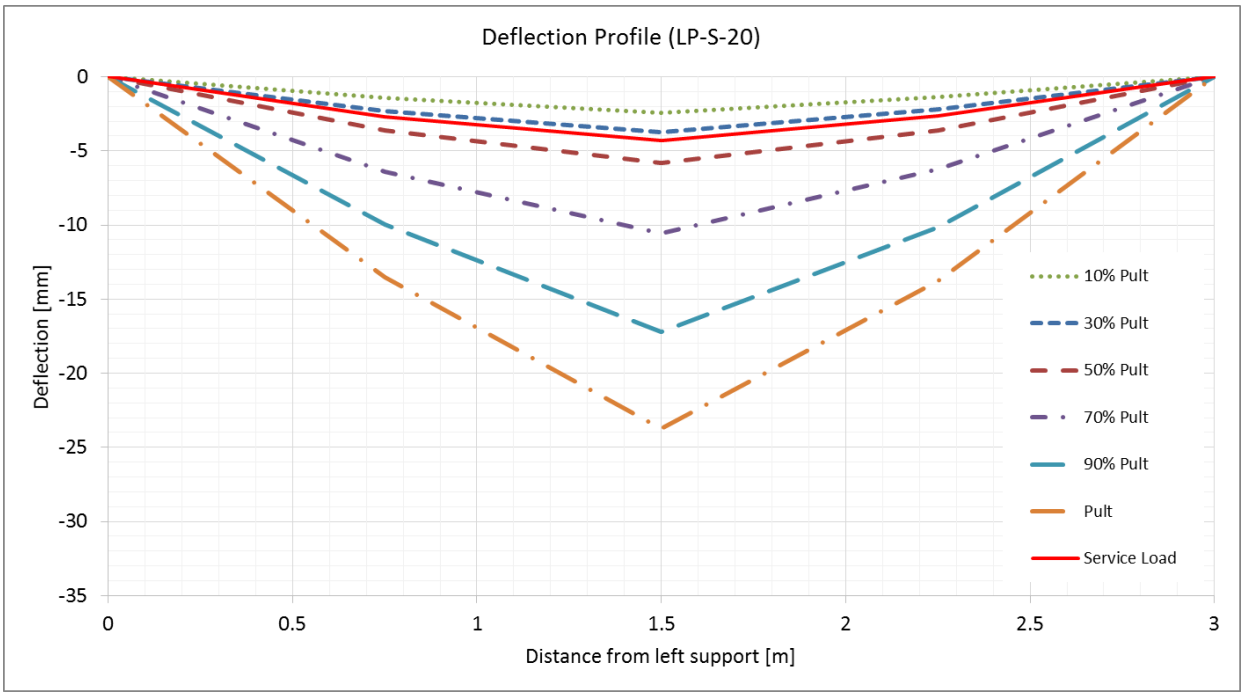

Deflection profile of slab LP-S-20 at various load level

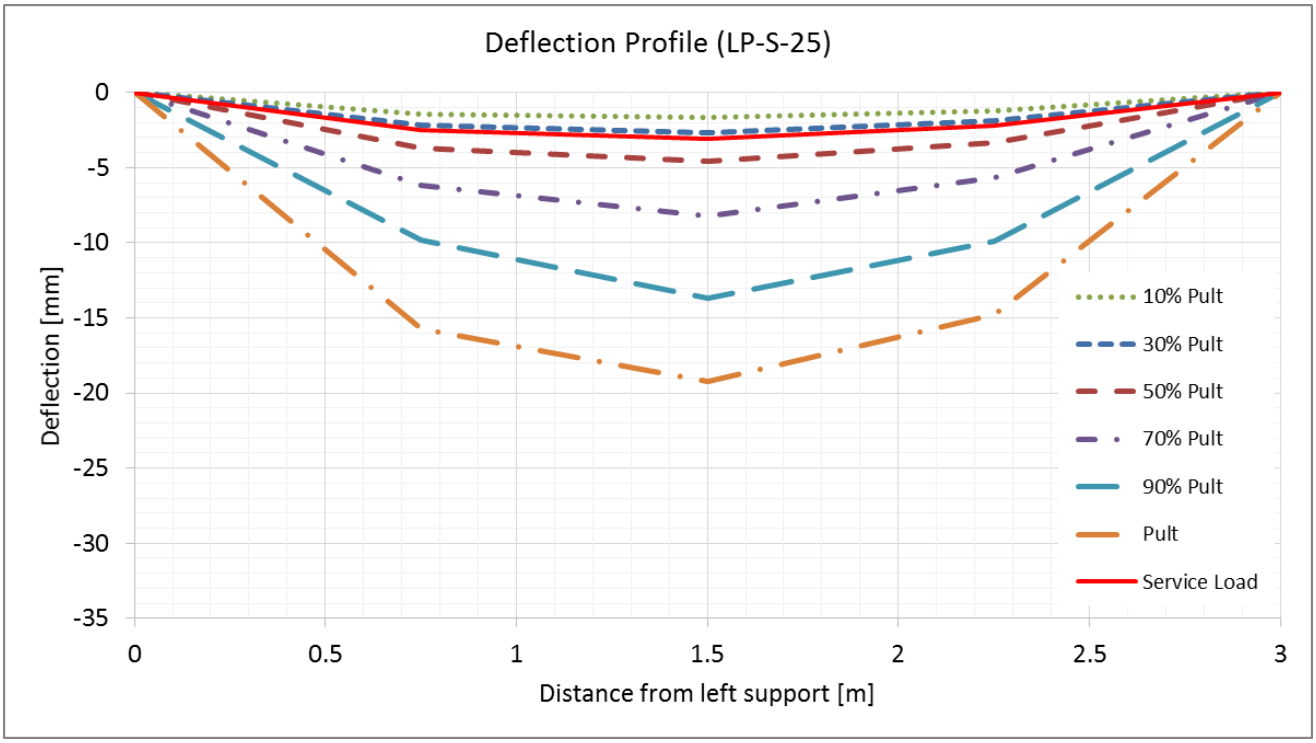

Deflection profile of slab LP-S-25 at various load level

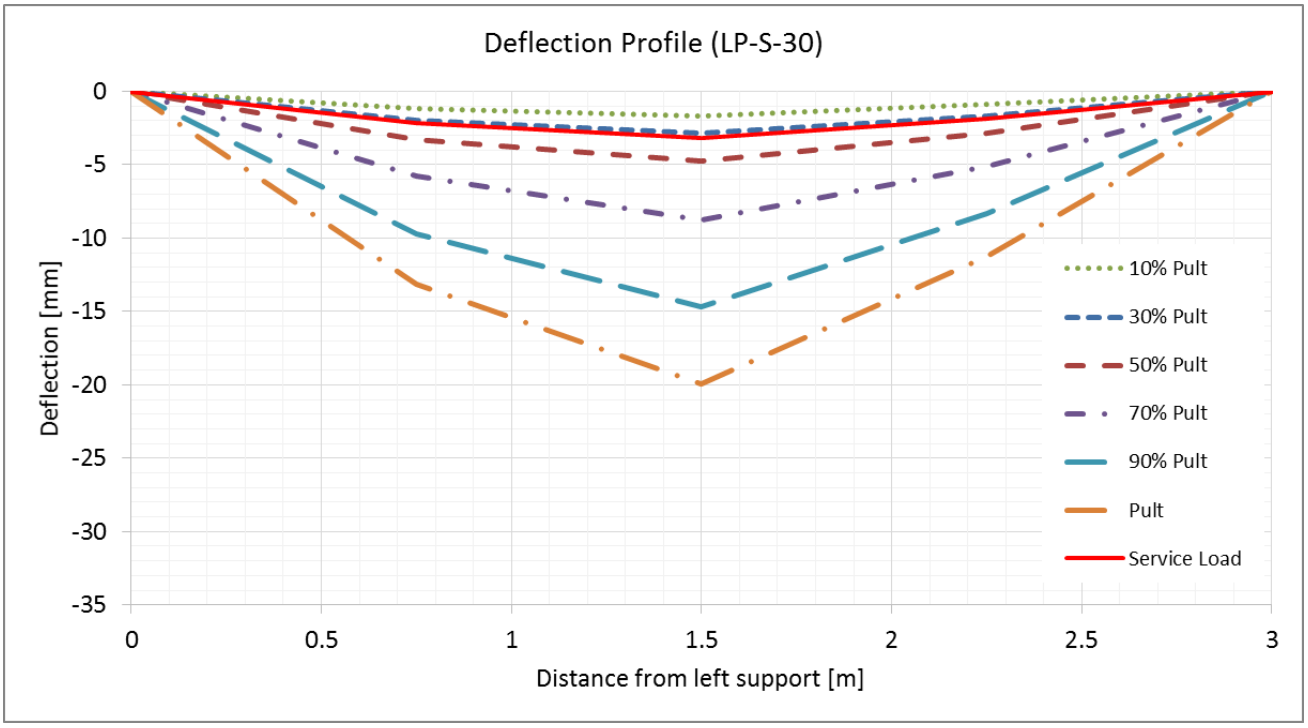

Deflection profile of slab LP-S-30 at various load level

COMPARISON OF CRACK WIDTH AT MID SPAN BEFORE AND AFTER INSTALLATION OF PCPS IN SLABS

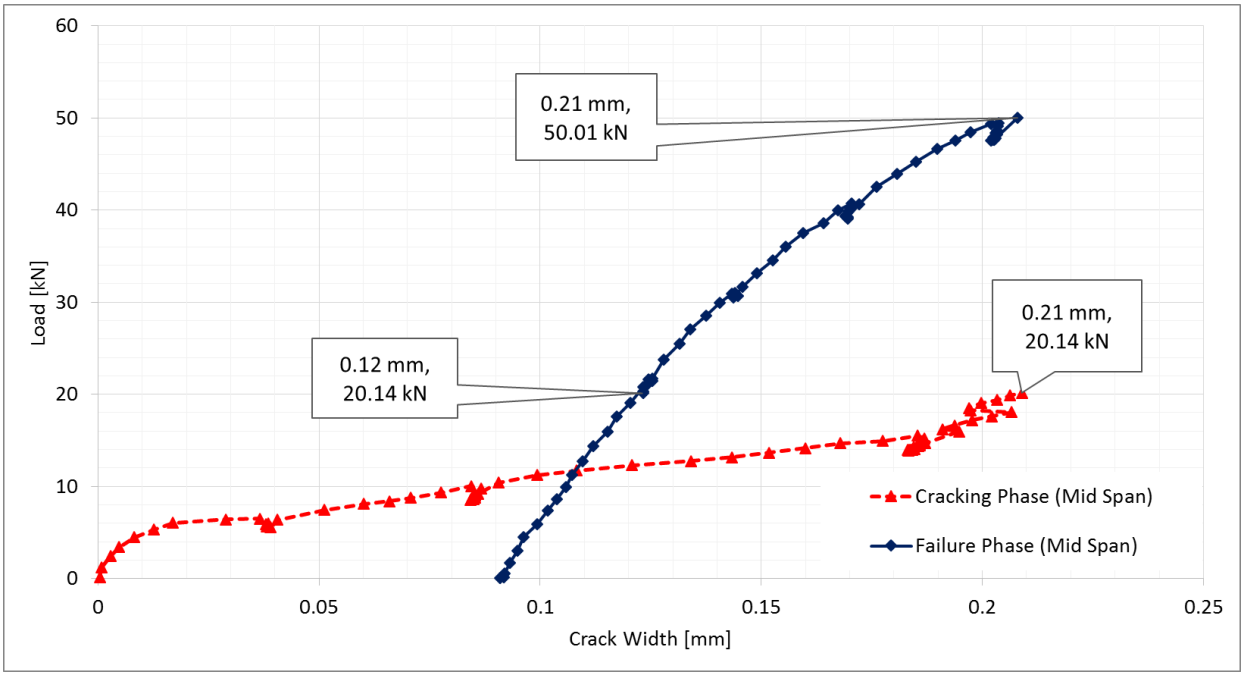

Comparison of crack width at mid span before and after installation of PCPs in slab SP-S-20

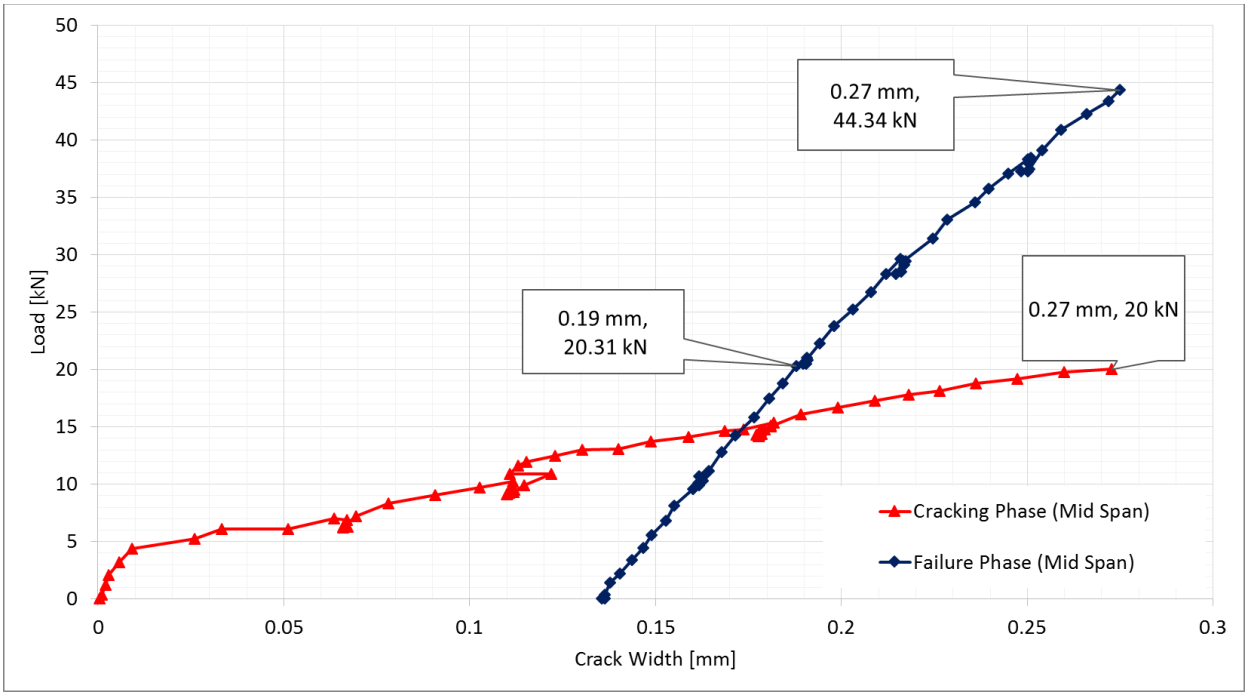

Comparison of crack width at mid span before and after installation of PCPs in slab SP-S-25

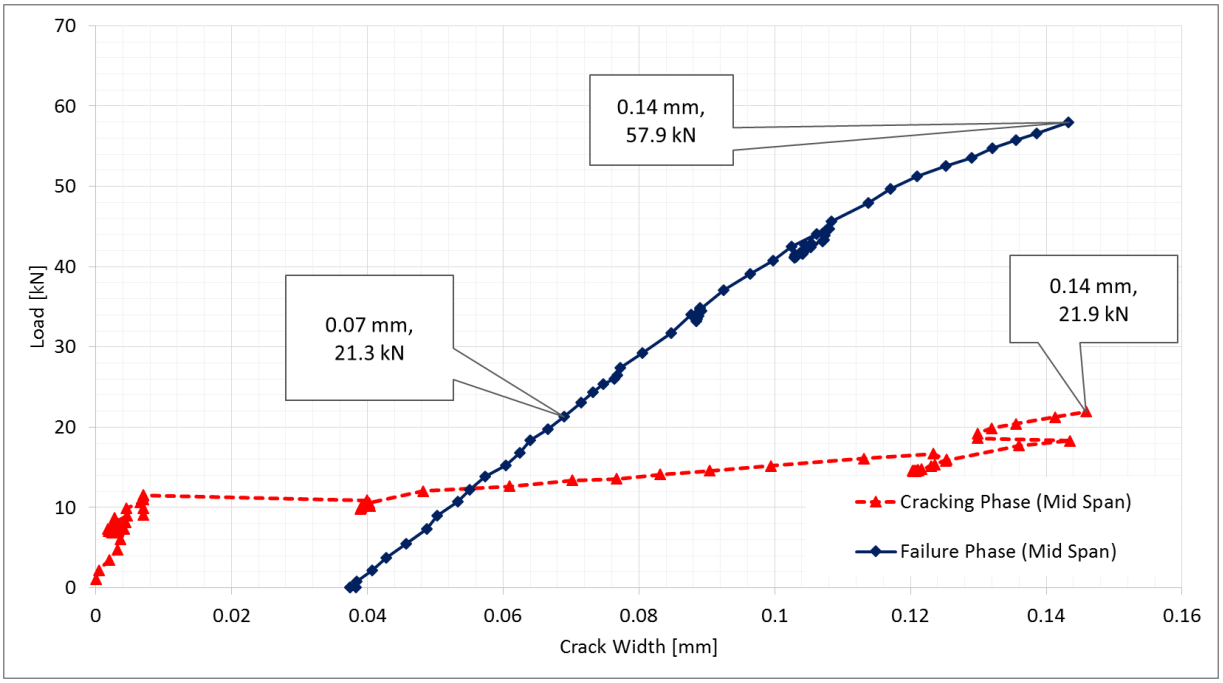

Comparison of crack width at mid span before and after installation of PCPs in slab SP-S-30

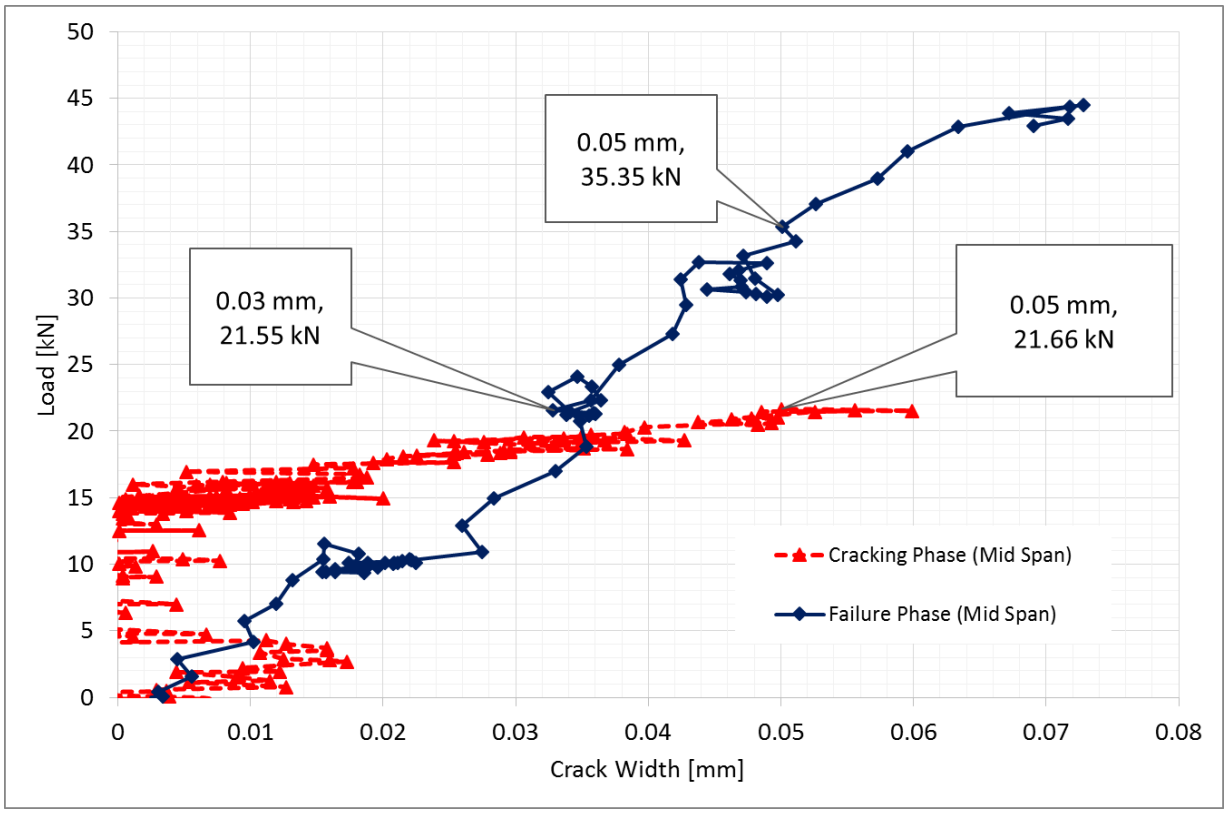

Comparison of crack width at mid span before and after installation of PCPs in slab LP-S-25

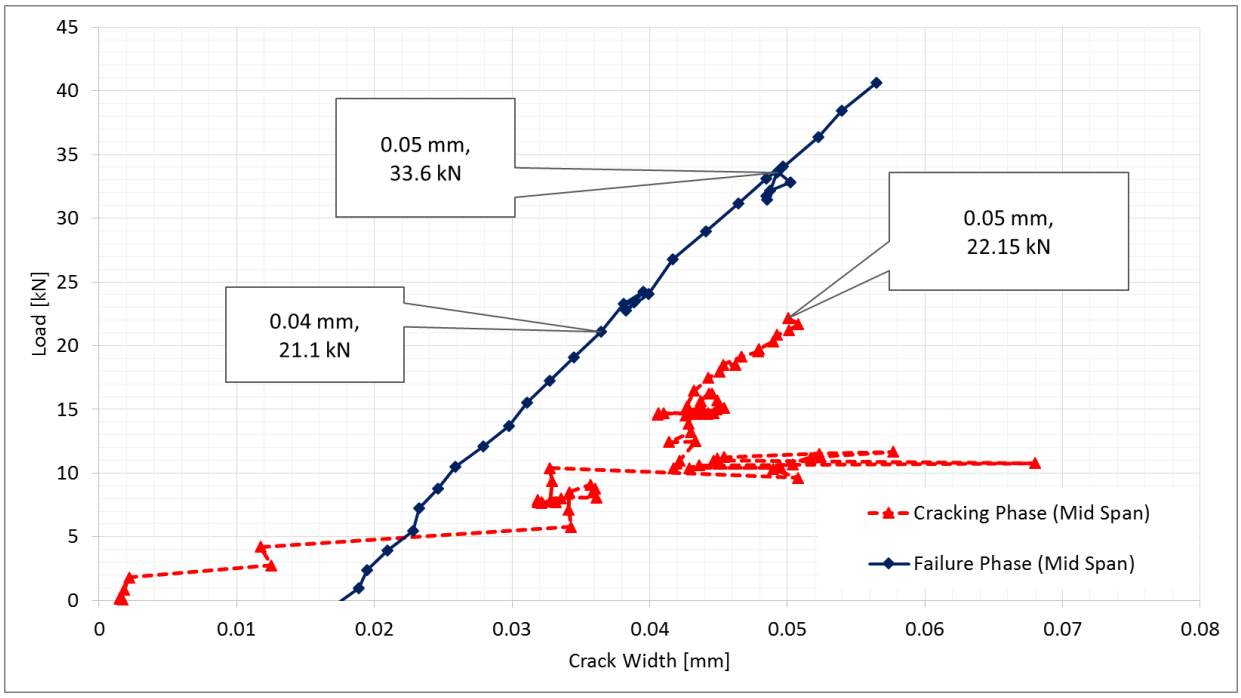

Comparison of crack width at mid span before and after installation of PCPs in slab LP-S-30

COMPARISON OF CALCULATED AND MEASURED CRACK WIDTH AT MID SPAN IN SLABS IN CRACKING PHASE

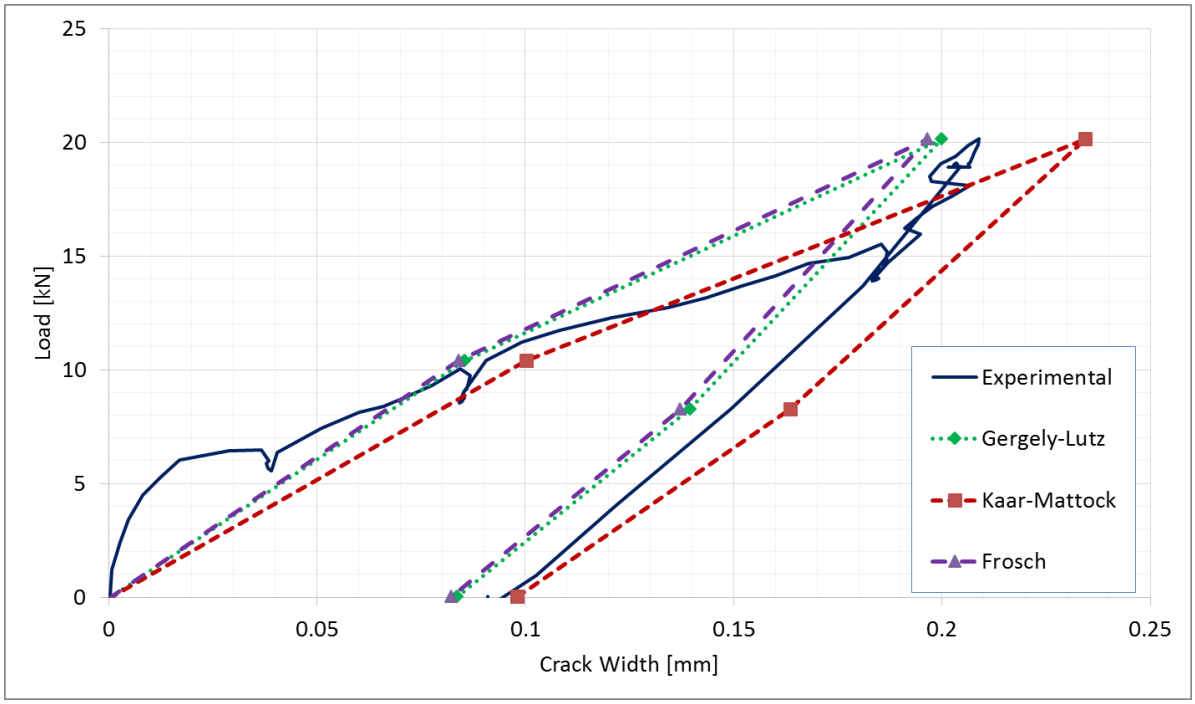

Comparison of calculated and measured crack width at mid span in slab SP-S-20 (cracking phase)

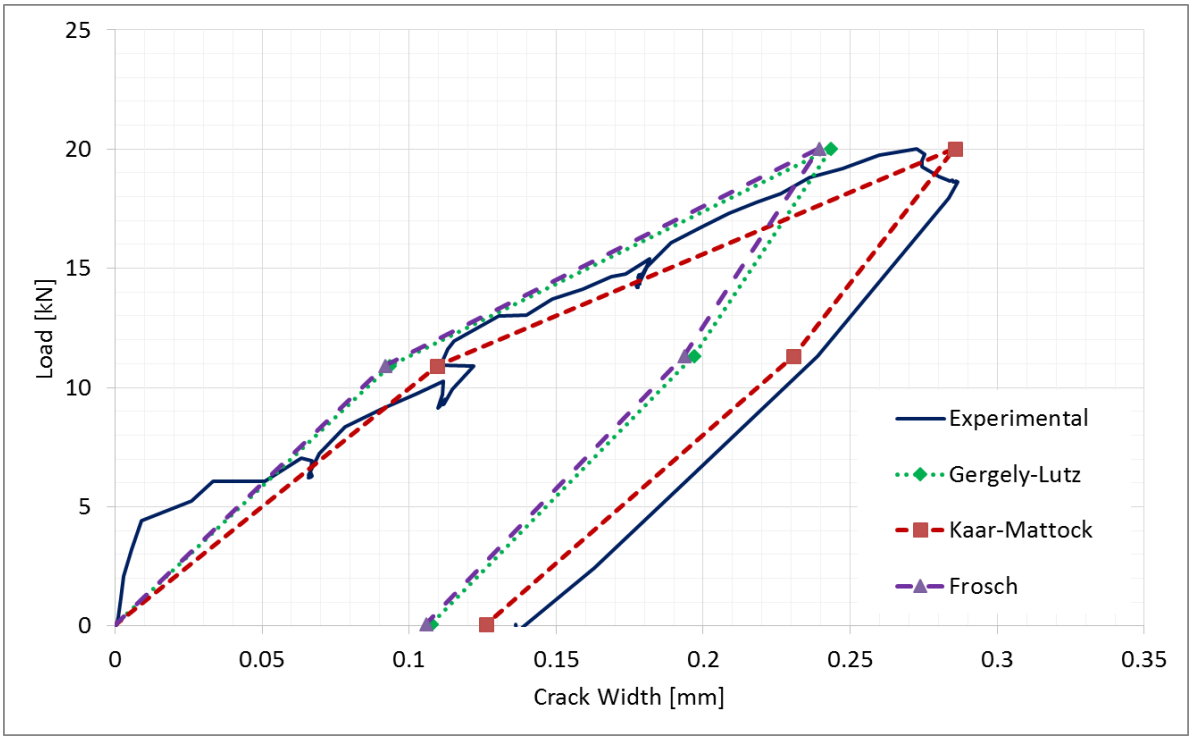

Comparison of calculated and measured crack width at mid span in slab SP-S-25 (cracking phase)

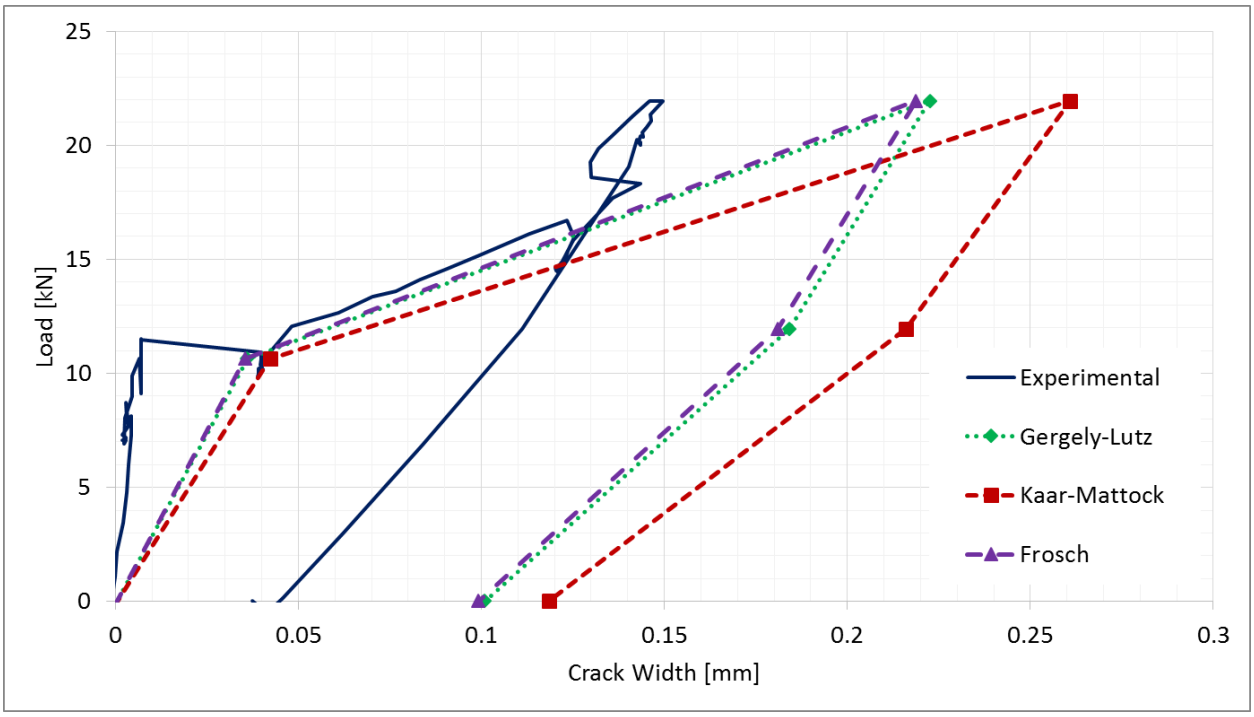

Comparison of calculated and measured crack width at mid span in slab SP-S-30 (cracking phase)

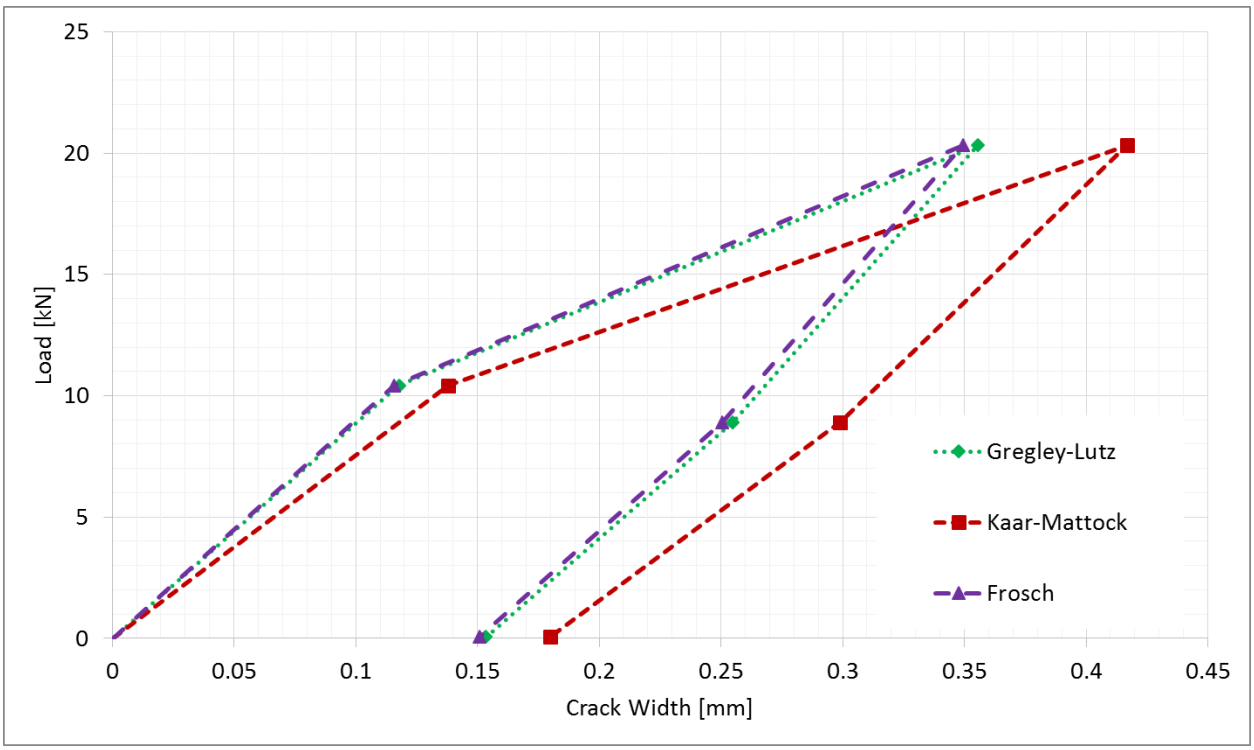

Comparison of calculated and measured crack width at mid span in slab LP-S-20 (cracking phase)

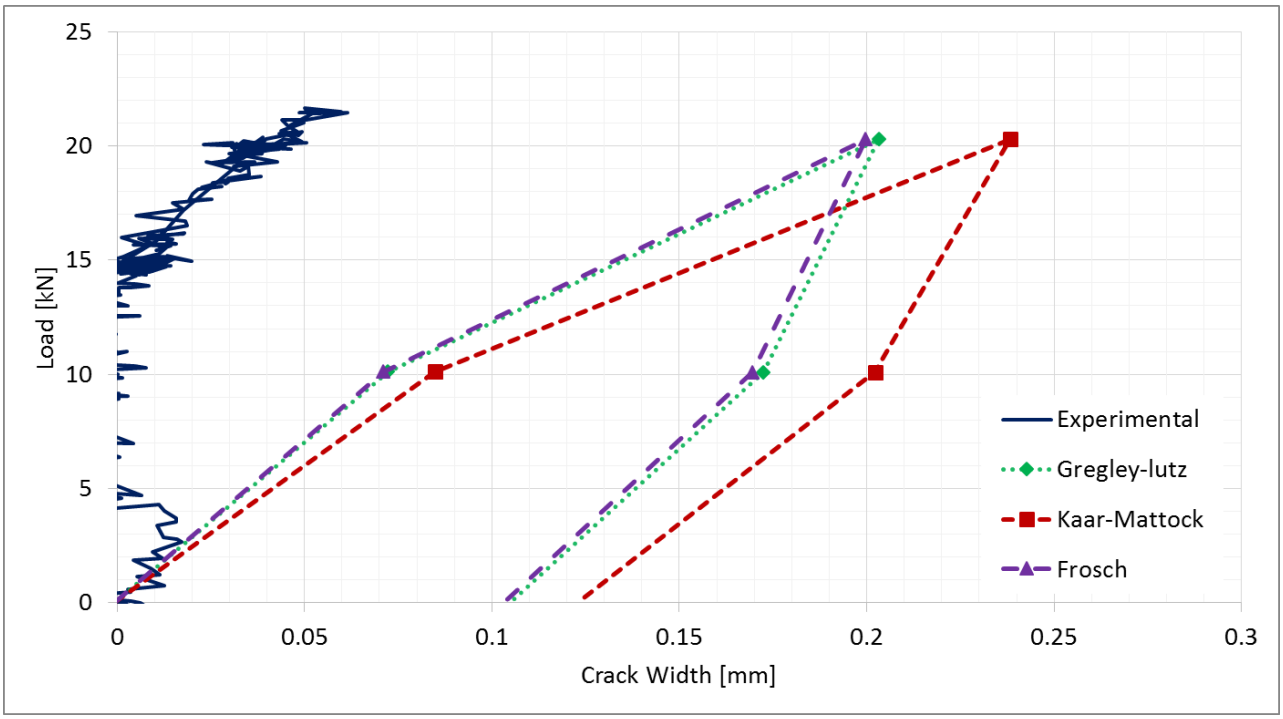

Comparison of calculated and measured crack width at mid span in slab LP-S-25 (cracking phase)

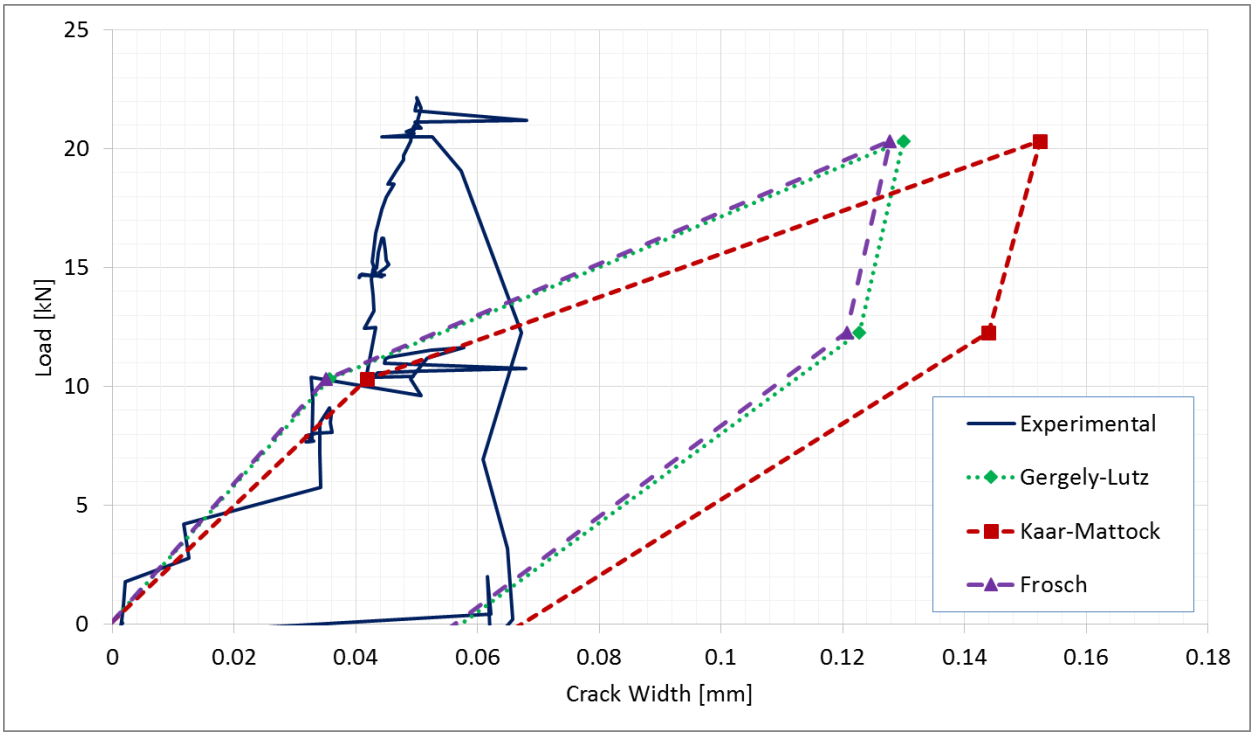

Comparison of calculated and measured crack width at mid span in slab LP-S-30 (cracking phase)

APPENDIX C

DURAL FAST SET GEL TECHNICAL SPECIFICATIONS SHEET

DURAL FAST SET GEL

Rapid-Setting, High Modulus Epoxy Adhesive

EUCLID CHEMICAL

Description

DURAL FAST SET GEL is a two-component, 100% solids, moisture insensitive, rapid-setting epoxy adhesive and binder for numerous applications. This high modulus, structural gel is perfect for bonding applications that require a quick turn-around. DURAL FAST SET GEL can be used in temperatures as low as 35°F (2°C) and rising.

Primary Applications

- Bonding of concrete, masonry, steel, or wood
- Anchoring bolts, dowels, or pins
- Rapidly seal cracks and set ports prior to injection
- Mix with sand to create a repair mortar

Features/Benefits

- Exceptional adhesion to construction materials
- Perfect for vertical and overhead bonding
- Easy to use 1:1 mix ratio
- DOT Not Regulated (non-corrosive)
- Moisture insensitive
- Rapid strength gain in a wide temperature range

Technical Information

The following information was obtained under laboratory conditions:

Property	Result
Mixed Viscosity	Consistency/Flow: 0.125 in (0.32 cm)
Pot Life, minutes AASHTO T-237	9
Compressive Strength, psi (MPa) ASTM C 109	7 days: 10,150 (70.0)
Compressive Modulus, psi (MPa) ASTM C 695	7 days: 3.02 x 10^5 (2,083)
Bond Strength, psi (MPa) ASTM C 882	14 days: 3,000 (37.1)
Tensile Strength, psi (MPa) ASTM D 638	7 days: 6,878 (47.4)
Water Absorption @ 24 hours, % ASTM D 570	< 0.4
Appearance/Color	Light Gray

Reinforcing Steel				Threaded Rod			
Rebar Diameter	Hole Diameter	Embedment Depth	Pull-Out Strength*	Rod Diameter	Hole Diameter	Embedment Depth	Pull-Out Strength*
#4: 1/2" (13 mm)	5/8" (16 mm)	4.5" (11.4 cm)	20513 lbf (91 kN)	3/8" (10 mm)	1/2" (13 mm)	3.5" (8.9 cm)	8722 lbf (39 kN)
#5: 5/8" (16 mm)	3/4" (19 mm)	5.5" (14.0 cm)	30591 lbf (136 kN)	1/2" (13 mm)	5/8" (16 mm)	4.5" (11.4 cm)	20851 lbf (93 kN)
#6: 3/4" (19 mm)	7/8" (22 mm)	6.5" (16.5 cm)	42912 lbf (191 kN)	5/8" (16 mm)	3/4" (19 mm)	5.5" (14.0 cm)	33072 lbf (147 kN)
#7: 7/8" (22 mm)	1" (25 mm)	7.5" (19.1 cm)	55180 lbf (245 kN)	3/4" (19 mm)	7/8" (22 mm)	6.5" (16.5 cm)	42092 lbf (187 kN)
#8: 1" (25 mm)	1 1/8" (29 mm)	9" (22.9 cm)	67395 lbf (300 kN)	7/8" (22 mm)	1" (25 mm)	7.5" (19.1 cm)	59520 lbf (265 kN)
--	--	--	--	1" (25 mm)	1 1/8" (29 mm)	9.5" (24.1 cm)	71117 lbf (316 kN)

*Direct tension pull-out strengths were obtained at 7 days, in accordance with ASTM E 488-10.

19215 Redwood Road • Cleveland, OH 44110
800-321-7628 t • 216-531-9596 f
www.euclidchemical.com

Packaging

DURAL FAST SET GEL is packaged in 4 gal (15 L) and 10 gal (38 L) units, in cases of 22 oz. (650 ml) cartridges (12 per case), and in 10 oz. (300 ml) cartridges (24 per case). The mix ratio is 1:1 by volume.

Shelf Life

2 years in original, unopened containers

Specifications/Compliances

Complies with ASTM C 881-10 Types I and IV, Grade 3, Classes A, B, and C

Canadian MTQ

DOT Not Regulated (non-corrosive)

Coverage/Yield

For anchoring, 1 neat gal (3.8 L) yields 231 in^3 (3,785 cm^3) of epoxy. 1 gal (3.8 L) of neat DURAL FAST SET GEL epoxy mixed with 1 gal (3.8 L) of dry 20/40 mesh silica sand will yield approximately 368 in^3 (6,030 cm^3) of mortar.

Note: Coverage rates are approximate. Actual coverage depends on temperature, texture, and substrate porosity.

Directions for Use

Surface Preparation: The surface must be structurally sound, dry, clean and free of grease, oil, curing compounds, soil, dust and other contaminants. Surface laitance must be removed. Concrete surfaces must be roughened and made absorptive, preferably by mechanical means, and then thoroughly cleaned of all dust and debris. If the surface was prepared by chemical means (acid etching), a water/baking soda or water/ammonia mixture, followed by a clean water rinse, must be used for cleaning, in order to neutralize the substrate. Allow substrate to dry before application. Route cracks and blow dust/debris from them with oil-free compressed air. Following surface preparation, the strength of the surface can be tested if quantitative results are required by project specifications. An elcometer or similar tensile pull tester may be used in accordance with ASTM D 4541, and the tensile pull-off strength should be at least 250 psi (1.7 MPa).

When coating steel, all contamination should be removed and the steel surface prepared to a "near white" finish (SSPC SP10) using clean, dry blasting media.

Mixing: Mix bulk units of DURAL FAST SET GEL using a low-speed drill and a mixing paddle. Pre-mix Part A and Part B separately for approximately 1 minute each. Combine Part A and Part B in a 1 to 1 ratio by volume, then mix thoroughly for 3 minutes.

To make DURAL FAST SET GEL mortar, gradually add clean, dry, 20/40 mesh silica sand to previously mixed DURAL FAST SET GEL epoxy and mix thoroughly for 1 to 2 minutes. The mix ratio of aggregate to mixed epoxy is approximately 1 to 1 by volume, but can be modified depending on the desired consistency of the mortar.

Scrape the bottom and sides of the containers at least once during mixing. Do not scrape bottom or sides of the container once mixing operations have ceased; doing so may result in unmixed resin or hardener being applied to the substrate. Unmixed resin or hardener will not cure properly. Do not aerate the material during mixing. The mixing paddle types recommended to keep aeration at a minimum are drill mixing paddle #P3 and #P12, as found in Guideline 320.5R-2014, published by ICRI.

Application: Bonding hardened concrete to hardened concrete: Apply by spatula, brush, or trowel. Ensure the surfaces to be joined have uniform coatings of DURAL FAST SET GEL. For optimum results, the bond line should not exceed 1/8" (3.2 mm). Join surfaces and hold or clamp firmly until the epoxy gels. Ideally, a small amount of adhesive should exude from the joint. Surfaces must be mated while the adhesive is still tacky. **Anchoring bolts, dowels, pins:** DURAL FAST SET GEL can be used neat or as a mortar to grout vertically-aligned anchors (into a horizontal substrate) or horizontally-aligned anchors (into a vertical substrate). The anchor hole should be free of all debris before grouting. The optimum hole size is 1/16" (1.6 mm) annular space (1/8" (3.2 mm) larger diameter than anchor diameter). Depth of embedment is typically 10 to 15 times anchor diameter. **Patching and repairs:** Apply DURAL FAST SET GEL neat as a primer coat to the prepared concrete surface. Mix the DURAL FAST SET GEL into an epoxy mortar and apply to the area by trowel or spatula in lifts of 1" to 1-1/2" (25 to 38 mm) before the neat primer coat becomes tack free. Allow each lift to reach initial set before applying subsequent lifts. **Setting ports & sealing cracks:** Place a small amount of mixed DURAL FAST SET GEL on the back of the port and carefully place it centered over the crack. Be careful to not fill the hole of the injection port. Place neat DURAL FAST SET GEL over the face of the cracks to be pressure injected, and around each injection port. Allow DURAL FAST SET GEL to sufficiently harden before injecting, to prevent blowouts. **Pick-proof sealant:** Apply a bead of DURAL FAST SET GEL to the joints and areas being sealed. Strike off the epoxy with a rounded spatula, or similarly rounded tool, to finish.

Clean-Up

Clean tools and application equipment immediately with acetone, xylene, or MEK. Clean spills or drips with the same solvents while still wet. Hardened DURAL FAST SET GEL will require mechanical abrasion for removal.

PRECAUTIONS/LIMITATIONS

- Store DURAL FAST SET GEL indoors, protected from moisture, at temperatures between 50°F and 90°F (10°C and 32°C)
- Surface and ambient temperature during applications should be between 35°F and 90°F (2°C and 32°C)
- Material temperatures should be at least 35°F (2°C) and rising
- Working time and cure time will decrease as the temperature increases, and will increase as the temperature decreases
- Do not thin DURAL FAST SET GEL
- DURAL FAST SET GEL will discolor upon prolonged exposure to ultraviolet light and high-intensity artificial lighting.
- DURAL FAST SET GEL is not to be used as a finished/aesthetic coating
- Do not use DURAL FAST SET GEL for overhead anchoring
- In all cases, consult the product Safety Data Sheet before use

Rev. 05.16